

The Journal of **Gemmology**

Volume 35 / No. 6 / 2017



Silver, Freiberg, Erzgebirge,
Saxony, Germany
Specimen courtesy of
Collector's Edge
Minerals, Inc.



Now Available
The Sisk Gemology Reference
by JERRY SISK

463 Editorial

COLUMNS

464 What's New

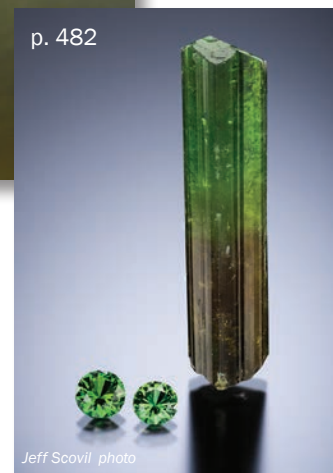
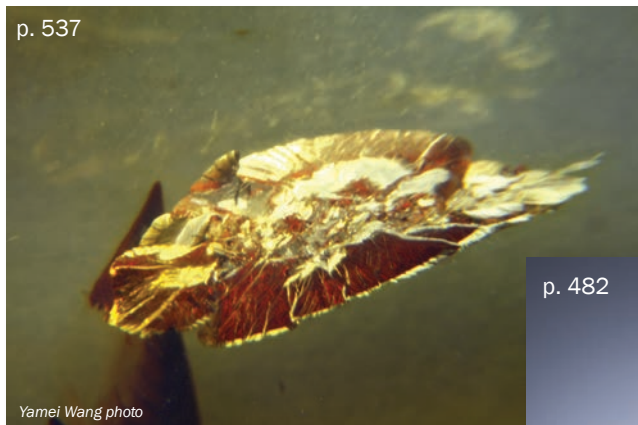
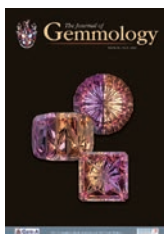
Gemchrom EOS diamond colorimeter | GoSpectro smartphone-based spectrometer | DiaTrue mobile | SSEF PearlScan | CIBJO Blue Books | Gemmological Society of Japan abstracts | GIA News from Research on sapphires from Madagascar, Myanmar and Thailand | GIT Lab Update on grandierite from Madagascar | Goldsmiths' Company *Technical Journal* | PDAC diamond abstracts | SSEF *Facette* | SSEF Trade Alert on Kashmir-like sapphires from Madagascar | World Bank report on Ethiopia's coloured stone industry | Gemstone Knowledge Hub

468 Gem Notes

Amethyst from Brazil | Beryl-lonite from Pakistan | Apache Blue Stone from Arizona, USA | Yellow Tianhuang stone | Cuck-stained quartzite from Afghanistan | Sapphires from Canada and northern Ethiopia | Tourmaline from Mwajanga and Simanjiro District, Tanzania | Alluvial diamond mining in South Africa | Quartz from Brazil with hematite/goethite, pyrite and rhodochrosite inclusions | Quartz from Pakistan with biotite and actinolite inclusions | HPHT synthetic diamond research in The Netherlands | Borosilicate glass | Synthetic ruby resembling Burmese ruby | 'Sea Sediment Jasper' | Blue synthetic star spinel | Gems at the Natural History Museum, London

Cover Photo:

A new approach for microscopically distinguishing natural from synthetic ametrine is described on pp. 506–529 of this issue. Shown in this composite photo are three custom-faceted natural ametrines: a 19.87 ct round StarBrite cut, a 20.35 ct cushion ZigZag cut and a 13.69 ct square StarBrite cut. Courtesy of John Dyer Gems, Edina, Minnesota, USA; photos by Ozzie Campos.



ARTICLES

Feature Articles

- 506 **Distinction of Natural and Synthetic Ametrine by Microscopic Examination—A Practical Approach**
By Karl Schmetzer

- 530 **Gemmological and Spectroscopic Features of Untreated vs. Heated Amber**
By Yamei Wang, Mingxing Yang, Shufang Nie and Fen Liu

Gemmological Brief

- 544 **Sassolite- and CO₂-H₂O-bearing Fluid Inclusions in Yellow Danburite from Luc Yen, Vietnam**
By Le Thi-Thu Huong, Kurt Krenn and Christoph Hauzenberger

551 Conferences

Sinkankas Symposium—Sapphire | Presentations in Tucson, Arizona, USA

554 Gem-A Notices

556 Learning Opportunities

559 New Media

565 Literature of Interest

The Journal is published by Gem-A in collaboration with SSEF and with the support of AGL and GIT.





Editor-in-Chief

Brendan M. Laurs
brendan.laurs@gem-a.com

Production Editor

Mary A. Burland
mary.burland@gem-a.com

Marketing Consultant

Ya'akov Almor
advertising@gem-a.com

Editorial Assistants

Carol M. Stockton
Angharad Kolator Baldwin

Editor Emeritus

Roger R. Harding

Executive Editor

Alan D. Hart

Associate Editors

Ahmadjan Abduriyim, *Tokyo, Japan*; Raquel Alonso-Perez, *Harvard University, Cambridge, Massachusetts, USA*; Edward Boehm, *RareSource, Chattanooga, Tennessee, USA*; Maggie Campbell Pedersen, *Organic Gems, London*; Alan T. Collins, *King's College London*; John L. Emmett, *Crystal Chemistry, Brush Prairie, Washington, USA*; Emmanuel Fritsch, *University of Nantes, France*; Rui Galopim de Carvalho, *Portugal Gemas, Lisbon, Portugal*; Lee A. Groat, *University of British Columbia, Vancouver, Canada*; Thomas Hainschwang, *GGTL Laboratories, Balzers, Liechtenstein*; Henry A. Hänni, *GemExpert, Basel, Switzerland*; Jeff W. Harris, *University of Glasgow*; Alan D. Hart, *Gem-A, London*; Ulrich Henn, *German Gemmological Association, Idar-Oberstein*; Jaroslav Hyršl, *Prague, Czech Republic*; Brian Jackson, *National Museums Scotland, Edinburgh*; Stefanos Karampelas, *Basel, Switzerland*; Lore Kiefert, *Gübelin Gem Lab Ltd., Lucerne, Switzerland*; Hiroshi Kitawaki, *Central Gem Laboratory, Tokyo, Japan*; Michael S. Krzemnicki, *Swiss Gemmological Institute SSEF, Basel*; Shane F. McClure, *Gemmological Institute of America, Carlsbad, California*; Jack M. Ogden, *Striptwist Ltd., London*; Federico Pezzotta, *Natural History Museum of Milan, Italy*; Jeffrey E. Post, *Smithsonian Institution, Washington DC, USA*; Andrew H. Rankin, *Kingston University, Surrey*; Benjamin Rondeau, *University of Nantes, France*; George R. Rossman, *California Institute of Technology, Pasadena, USA*; Karl Schmetzer, *Petershausen, Germany*; Dietmar Schwarz, *Federated International GemLab, Bangkok, Thailand*; Menahem Sevdemish, *Gemewizard Ltd., Ramat Gan, Israel*; Guanghai Shi, *China University of Geosciences, Beijing*; James E. Shigley, *Gemmological Institute of America, Carlsbad, California*; Christopher P. Smith, *American Gemological Laboratories Inc., New York, New York*; Evelyne Stern, *London*; Elisabeth Strack, *Gemmologisches Institut Hamburg, Germany*; Tay Thye Sun, *Far East Gemmological Laboratory, Singapore*; Pornsawat Wathanakul, *Gem and Jewelry Institute of Thailand, Bangkok*; Chris M. Welbourn, *Reading, Berkshire*; Bert Willems, *Leica Microsystems, Wetzlar, Germany*; Bear Williams, *Stone Group Laboratories LLC, Jefferson City, Missouri, USA*; J.C. (Hanco) Zwaan, *National Museum of Natural History 'Naturalis', Leiden, The Netherlands*.

Content Submission

The Editor-in-Chief is glad to consider original articles, news items, conference/excursion reports, announcements and calendar entries on subjects of gemmological interest for publication in *The Journal of Gemmology*. A guide to the various sections and the preparation of manuscripts is given at www.gem-a.com/index.php/news-publications/publications/journal-of-gemmology/submissions, or contact the Production Editor.

Subscriptions

Gem-A members receive *The Journal* as part of their membership package, full details of which are given at www.gem-a.com/membership. Laboratories, libraries, museums and similar institutions may become direct subscribers to *The Journal*.

Advertising

Enquiries about advertising in *The Journal* should be directed to the Marketing Consultant. For more information, see www.gem-a.com/index.php/news-publications/publications/journal-of-gemmology/advertising.

Database Coverage

The Journal of Gemmology is covered by the following abstracting and indexing services: Australian Research Council academic journal list, British Library Document Supply Service, Chemical Abstracts (CA Plus), Copyright Clearance Center's RightFind application, CrossRef, EBSCO (Academic Search International, Discovery Service and TOC Premier), Gale/Cengage Learning Academic OneFile, GeoRef, Index Copernicus ICI Journals Master List, Mineralogical Abstracts, Cambridge Scientific Abstracts (ProQuest), Scopus and the Thomson Reuters' Emerging Sources Citation Index (in the Web of Science).



Copyright and Reprint Permission

For full details of copyright and reprint permission contact the Editor-in-Chief.

The Journal of Gemmology is published quarterly by Gem-A, The Gemmological Association of Great Britain. Any opinions expressed in *The Journal* are understood to be the views of the contributors and not necessarily of the publisher.

Printed by DG3 (Europe) Ltd.

© 2017 The Gemmological Association of Great Britain
ISSN: 1355-4565



21 Ely Place
London EC1N 6TD
UK

t: +44 (0)20 7404 3334
f: +44 (0)20 7404 8843
e: information@gem-a.com
w: www.gem-a.com

Registered Charity No. 1109555
A company limited by guarantee and registered in England No. 1945780
Registered office: Palladium House, 1-4 Argyll Street, London W1F 7LD

President

Maggie Campbell Pedersen

Vice Presidents

David J. Callaghan
Alan T. Collins
Noel W. Deeks
E. Alan Jobbins
Andrew H. Rankin

Honorary Fellows

Gaetano Cavalieri
Terrence S. Coldham
Emmanuel Fritsch

Honorary Diamond Member

Martin Rapaport

Chief Executive Officer

Alan D. Hart

Council

Justine L. Carmody – Chair
Kathryn L. Bonanno
Paul F. Greer
Kerry H. Gregory
J. Alan W. Hodgkinson
Nigel B. Israel
Jack M. Ogden
Richard M. Slater
Christopher P. Smith

Branch Chairmen

Midlands – Georgina E. Kettle
North East – Mark W. Houghton
South East – Veronica Wetten
South West – Richard M. Slater

Understanding Gems™

Research Tools at Your Fingertips

The core foundations of the Gemmological Association of Great Britain are gemmological knowledge and education, which are furthered through Gem-A's courses, publications, website and annual conference, as well as by the tools and books that are available through the Association's instruments division. Gem-A's leadership role in disseminating high-quality gemmological knowledge is exemplified by its flagship scholarly publication, *The Journal of Gemmology*, which has published ground-breaking technical articles from researchers worldwide since its inception in 1947.

I am pleased to announce that as of April 2017, the entire 70-year archive of *The Journal* has been posted online. This collection of PDF files (currently numbering 259 issues) is accessible by visiting *The Journal's* website at <https://gem-a.com/news-publications/publications/journal-of-gemmology>. The most recent issues continue to be accessible only to Gem-A members in the 'Latest Issues' section of the website, while the rest of the collection is freely available to anyone via 'The Journal Archive'. And there is more good news: Also available online is the full archive of Gem-A's trade publication, *Gems&Jewellery*—and its predecessor, *Gem & Jewellery News*, going back to its inception in 1991—through *G&J's* home page at <https://gem-a.com/news-publications/publications/gems-jewellery>.

While *The Journal's* archive is clearly a valuable storehouse of gemmological information, how do you go about finding what you are looking for? The answer lies in *The Journal's* cumulative index, which also can be downloaded as a PDF file from *The Journal's* website. This index was recently updated to include all issues through 2016, and it is our intention to continue to update it annually, so separate volume indexes will no longer be prepared. The index can be searched for any keyword or author that you are looking for, and the combination of this resource with access to the full archive of back issues puts all of the research published in *The Journal* at your fingertips.

For those wishing to dive even deeper into research published in *The Journal*, I invite you to visit the Data Depository, which is freely available online at <https://gem-a.com/news-publications/publications/journal-of-gemmology/data-depository>. There you will find supplemental data, diagrams, photos and videos that accompany some of the recent articles that have appeared in *The Journal*.

Gem-A is pleased to make these valuable resources available to help with your research and continuing education. Please use and enjoy them!

Brendan M. Laurs
Editor-in-Chief





THE JOURNAL ARCHIVE

The *Journal of Gemmology* archive is now available for everyone to view online. The archive goes back to 1947 when the first issue of *The Journal* was published.

Current Gem-A Members and Direct Subscribers receive free access to all available volumes of the publication, simply log in using your membership number and password.

If you are not a member and would like to gain access to all available issues of *The Journal* please visit our [membership](#) pages or contact membership@gem-a.com.

THE JOURNAL OF GEMMOLOGY 2011 - 2015

			
VOLUME 34 / NO. 5 / 2015	VOLUME 34 / NO. 6 / 2015	VOLUME 34 / NO. 7 / 2015	VOLUME 34 / NO. 8 / 2015

The full *Journal* archive is now available online. *Journal* issues that were published before 2005 (i.e. without currently accessible digital files) were scanned and processed using character-recognition software to make them fully searchable. All illustrations were scanned using settings that were optimized to maintain a good balance between file size and resolution, keeping download times as short as reasonably possible.

What's New

INSTRUMENTATION

Gemchrom EOS Diamond Colorimeter

The EOS Diamond Colorimeter from Italy-based Gemchrom was released in January 2016. The compact instrumentation determines the colour grade of unmounted polished diamonds of 0.10–20.00 ct in the D–M colour range with a clarity grade of at least VS₂. The grading time is less than 20 seconds per stone, and results can be reported according to GIA, HRD and IGI grading systems. The unit is self-calibrating, with a built-in centring device and an LED lighting system that has a lamp life of 6,000 hours. The unit weighs 4 kg and measures 17.7 × 21.2 × 29.3 cm, and comes with a separate label printer. For more information and a demonstration video, visit www.gemchrom.com. CMS



OGI Systems DiaTrue Mobile

In April 2017, OGI Systems Ltd. (Ramat Gan, Israel) launched a new synthetic diamond detector called DiaTrue Mobile. This portable device follows the development of the previous desktop models (DiaTrue and DiaTrue XL). It rapidly scans both single stones and parcels (0.001 ct or larger), and the analysis can then be shared using a mobile device via WhatsApp and email. The unit weighs 1.3 kg and measures 9.5 × 6.8 × 20.0 cm. Visit www.ogisystems.com/diatruemobile.html. BML



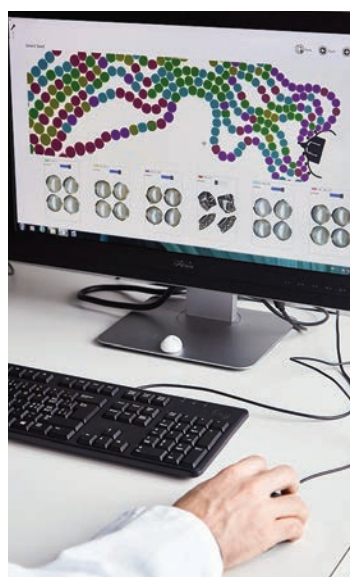
GoSpectro Smartphone-based Spectrometer

In September 2016, ALPhANOV of Talence, France, released the GoSpectro device, a visible-range (380–750 nm) spectrometer that works with a camera-equipped smartphone or tablet. Spectral resolution is 10 nm with 1 nm accuracy. Weighing just 30 g (55 × 20 × 20 mm), it is highly portable and works with Apple iOS and Android apps, enabling the user to save and email spectra. The software also can perform baseline correction and spectral subtraction, and compare spectra with external databases. The unit is priced at €300. Visit www.alphanov.com/223-news-gospectro—the-power-of-spectroscopy-at-your-fingertips.html. CMS



SSEF PearlScan

In March 2017, the Swiss Gemmological Institute SSEF released PearlScan, which is designed to quickly count and measure the dimensions of large quantities of strung pearls. The system consists of an A4 scanner, computer and software, and produces images and a detailed report of the number, diameter and roundness factor of each pearl. PearlScan is sold through SSEF's subsidiary SATT Gems in Basel, Switzerland. Visit www.sattgems.ch/pearlscan. CMS



NEWS AND PUBLICATIONS

CIBJO Blue Books Updated

In February 2017, the latest editions of several CIBJO Blue Books (Diamond, Gemstone, Pearl, Coral and Gemmological Laboratory) became available for download from www.cibjo.org/introduction-to-the-blue-books. The Blue Books provide definitive grading standards and nomenclature, and are periodically updated by CIBJO commissions that include representatives of gem trade organizations and laboratories. PDF downloads are free to CIBJO members and to those belonging to a CIBJO-member organization, and otherwise cost CHF9.90 for each Blue Book or CHF49.90 for a set of all six books (i.e. those mentioned above, as well as the 2012 Precious Metals Book). CMS



Gemmological Society of Japan 2016 Conference Abstracts

In August 2016, extended abstracts from 16 lectures given at the Annual Meeting of the Gemmological Society of Japan, held from 28 June to 2 July 2016, became available at www.jstage.jst.go.jp/browse/gsj. The documents are in Japanese with English summaries or keywords, and cover a range of topics including melee-sized synthetic diamonds, new technologies, pearls and more. CMS



GIA News from Research: Sapphires from Baw Mar, Myanmar

In February 2017, a report titled 'An in-depth gemological study of blue sapphires from the Baw Mar mine (Mogok, Myanmar)' was posted by the Gemological Institute of America at www.gia.edu/gia-news-research/blue-sapphires-baw-mar-mine-mogok-myanmar. The Baw Mar mine has recently produced a significant amount of fine blue sapphires with gemmological properties somewhat

different from those typically recovered in the Mogok area. The blue colour of stones from the northern part of the mine is medium to dark, while material from the southern portion is lighter blue. All of the sapphires have a trace-element composition similar to those from metamorphic-type deposits, such as those from Sri Lanka and some sources in Madagascar. CMS



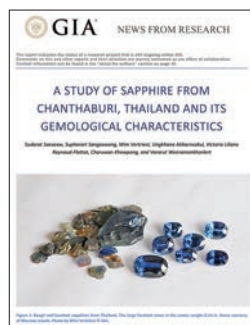
GIA News from Research: Sapphires from Bemainty, Madagascar

In February 2017, GIA posted a report titled 'Sapphires from the gem rush Bemainty area, Ambatondrazaka (Madagascar)' at www.gia.edu/gia-news-research/sapphires-gem-rush-bemainty-ambatondrazaka-madagascar. It provides a description of the Bemainty area (near Ambatondrazaka) and other gem corundum sources in north-eastern Madagascar, as well as the gemmological features of 38 sapphire samples (mostly blue but also some pinkish orange). The report concludes that these sapphires will be difficult to distinguish from those of other metamorphic-type deposits. CMS



GIA News from Research: Sapphires from Chanthaburi, Thailand

Posted online by GIA in February 2017, 'A study of sapphire from Chanthaburi, Thailand and its gemological characteristics' presents the results of research on 59 blue to greenish blue samples from the Khao Ploy Waen area of Chanthaburi. The study sam-



ples revealed features similar to those of sapphires from other basalt-related origins. Nevertheless, they are distinguishable from magmatic-type sapphires mined in Cambodia and Nigeria. Visit www.gia.edu/gia-news-research/sapphire-chanthaburi-thailand-gemological-characteristics. CMS

GIT Lab Update: Grandierite from Madagascar

In March 2017, The Gem and Jewelry Institute of Thailand in Bangkok released a report titled 'Gem-quality grandierite from Madagascar'. It describes six rough samples received in September 2016. The report suggests that the depth of their bluish green colour could be related to iron content. Download this and previous GIT reports at www.git.or.th/articles_tech_nic_en.html. BML



PDAC Diamond Abstracts

Abstracts are available from the March 2017 conference of the Prospectors & Developers Association of Canada, held in Toronto, Ontario. A session titled 'Diamonds in Africa: Part 2—The rest of the story' consisted of six presentations on diamonds from Angola, Lesotho (Letseng), West Africa (Sierra Leone, Guinea and Liberia), Zimbabwe and Namibia, as well as techniques for diamond resource evaluation. Download the abstracts at www.pdac.ca/convention/programming/technical-program/sessions/technical-program/diamonds-in-africa-part-2-the-rest-of-the-story. BML



SSEF Facette

In February 2017, the Swiss Gemmological Institute SSEF released *Facette Magazine* No. 23 at www.ssef.ch/fileadmin/Documents/PDF/640_Facette/SSEF-Facette-23.pdf. This issue covers emerald fissure filling and cleaning; rare and unusual stones (such as pezzottaite, musgravite and taaffeite) seen recently at SSEF; neutron and X-ray tomography of emeralds; a description of the historic 'Sleeping Lion Pearl'; purple garnets from Mozambique; blue sapphires from Bemainty, Madagascar; oiled rubies; time-of-flight mass spectrometry; opalized dinosaur bone; fake *Tridacna* pearls; exceptional jadeite; an eskolaite inclusion in synthetic ruby; treatment of and research on golden cultured pearls; blue colour in type IIb diamonds; an Umba ruby with a zircon spectrum; heated pink sapphire in antique jewellery; gibbsite as a coral imitation; age dating of pearls offered as a lab service; testing and sorting colourless diamond melee; SSEF news and instruments; and more. CMS



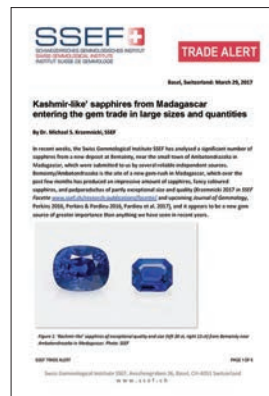
The Goldsmiths' Company Technical Journal

Issue 16 (Summer 2016) of this journal is now available at <http://technical-journal.thegoldsmiths.co.uk/wp-content/uploads/2016/07/Technical-Journal-Issue-16.pdf>. It features an update from the Assay Office; a profile of The National Association of Jewellers; an introduction to modelling, moulding, and other methods of creating precious-metal *objets d'art*; a report on the 2016 Goldsmiths' Craft & Design Council Awards; a feature on Baird & Co, UK's largest gold refiner and the sole producer of rhodium bars; a report on the 29th Santa Fe Symposium on Jewelry Manufacturing Technology; and a description of a new micro-pavé setting technique. CMS



SSEF Trade Alert: 'Kashmir-like' Sapphires from Madagascar

In early 2017, the Swiss Gem-mological Institute SSEF studied a 'significant number' of sapphires from the new deposit at Bemainty, Madagascar. This trade alert focuses on those samples with a 'Kashmir-like' appearance, including a velvety blue colour appearance, and how to distinguish them from Kashmir sapphires. Typical features of Bemainty sapphires include exceptional clarity (even in large-sized stones), narrow growth zones, and the lack of pargasite and tourmaline inclusions that are characteristic of Kashmir sapphires. In addition, the sapphires from the two localities can be separated by their trace-element composition. Download the March 2017 report at <http://tinyurl.com/mwctgfh>. CMS



World Bank Report: Ethiopia's Coloured Gemstone Industry

The World Bank recently commissioned a study of Ethiopia's coloured stone industry to learn more about the state of the industry in terms of commercial and social development. The resulting June 2016 report, 'An analysis of the commercial potential of Ethiopia's coloured gemstone industry', reveals factors that are contributing to and limiting its commercial success in light of lessons learned from other gem-producing nations, including Afghanistan, Australia, Brazil, Madagascar, Nigeria, Sri Lanka and Tanzania. Visit <http://documents.worldbank.org/curated/en/386891474020338559/An-analysis-of-the-commercial-potential-of-Ethiopia-s-coloured-gemstone-industry>. CMS



OTHER RESOURCES

Gemstone Knowledge Hub

Launched in April 2017, this new resource contains science-based information on various aspects of coloured gemstones, with the goal of enhancing sustainability efforts and providing education and training for the coloured-stone supply chain. Topics include coloured stone varieties, mining and geology, processing and manufacturing, environmental/social/gender issues, and economic development impacts. The hub is a collaboration of the University of Delaware's Department of Geography, the University of Queensland's Center for Social Responsibility in Mining and the University of Lausanne's Faculty of Geosciences, and is supported by the Tiffany & Co. Foundation. Visit the hub at www.sustainablegemstones.org. BML



What's New provides announcements of instruments, technology, publications, online resources and more. Inclusion in What's New does not imply recommendation or endorsement by Gem-A. Entries were prepared by Carol M. Stockton (CMS) or Brendan M. Laurs (BML), unless otherwise noted.

Gem Notes

COLOURED STONES

Amethyst from Brazil with Interesting Inclusion Patterns

During the FIPP 2016 International Gemstone Show in Teófilo Otoni, Brazil, that took place in August, a new find of amethyst debuted with interesting zoned patterns created by inclusions. The deposit was discovered in November 2016 in Minas Gerais, Brazil, and from approximately 10 kg of rough material (e.g. Figure 1), about 4,000–5,000 carats were cut and polished as cabochons and tablets in a variety of shapes (e.g. oval, pear and marquise), including a large number of matched pairs (e.g. Figure 2). These stones were marketed as ‘Passion Amethyst’ (due to their red and purple coloration) at the February 2017 gem shows in Tucson, Arizona, USA, where they were exhibited by gem dealer Mona Khan (Vista Gems, Skillman, New Jersey, USA). One of the polished tablets was kindly donated to Gem-A by Khan, and was examined for this report.

The attractive colour patterning is caused by layered assemblages of inclusions (i.e. ‘phantoms’) that crystallized at distinct intervals on



Figure 1: Two crystals of amethyst from Brazil (up to 2.7 cm long) show layers of inclusions along ‘phantom’ growth faces. The c-axis of both crystals is approximately vertical. Courtesy of Michele Macri; photo by B. M. Laurs.

the growing rhombohedral faces of the amethyst. Although the inclusions were not analysed to confirm their identification for this report,

Figure 2: Various patterns created by inclusions are visible in these rough and cut amethyst specimens. The largest polished sample measures 24 × 19 mm. Photo by Jeff Scovil.



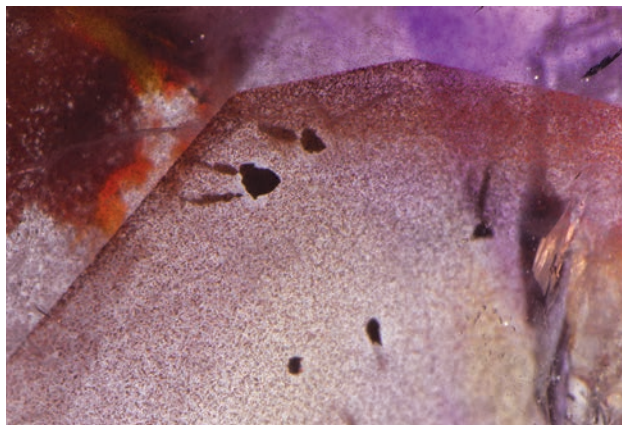


Figure 3: A phantom layer of what appear to be hematite particles is shown here in 'Passion Amethyst' from Brazil. Photomicrograph by N. D. Renfro; image width 5.6 mm.

they appeared typical for quartz, most probably consisting of orangey red to yellow brown iron oxides/hydroxides (i.e. hematite and goethite) and dark greenish grey chlorite. During crystallization of the amethyst, the typical sequence of the phantoms started with particles of hematite (Figure 3) followed by particles of chlorite and finally by local brush-like bundles of hematite/goethite that were oriented perpendicular to the crystal faces. Cutting and polishing brought out various inclusion-related patterns and colours that were superimposed over the pale purple body colour of the host amethyst, creating an unusual appearance.

Brendan M. Laurs FGA and Nathan D. Renfro

Beryllonite from Pakistan

Beryllonite (NaBePO_4) is an uncommon mineral that is more typically seen as a mineral specimen than as a faceted gemstone. Nevertheless, its hardness of $5\frac{1}{2}$ –6 on the Mohs scale makes it suitable for faceting and use in gently worn



Figure 4: Pakistan is the source of this beryllonite, which weighs 14.79 ct and is completely colourless. Photo by Dean Brennan.

jewellery. Both chatoyant cabochons and transparent faceted gems are sold as collector's stones, but they have seldom been documented in the gemmological literature (e.g. Koivula and Kammerling, 1991; Muylar and Sun, 2016).

During the February 2017 Tucson gem shows, Dudley Blauwet (Dudley Blauwet Gems, Louisville, Colorado, USA) showed one of the authors (BML) a faceted 14.79 ct beryllonite from northern Pakistan (Figure 4). He purchased the rough material 15–20 years ago in Chhappu village in Pakistan's Braldu Valley. The crystal was large (338.1 g), but Blauwet hesitated to send it to his cutting factory because he could not determine how much gem material was inside. In March 2016 he finally sent it for cutting, and the factory returned 102 pieces weighing 176.94 carats. The largest gem weighed ~28 ct, while the two largest clean stones were between approximately 9.7 and 8.6 ct, with the majority less than 3 ct including numerous melee-sized stones.

Blauwet loaned the 14.79 ct beryllonite to authors CW and BW for examination. It measured $17.81 \times 14.56 \times 10.28$ mm and was so colourless that it appeared silver-white. The RIs were 1.551–1.560 (birefringence 0.009) and the hydrostatic SG was 2.81. It was inert to UV radiation. These properties are consistent with those reported for beryllonite, and the identification was confirmed by Raman analysis with a GemmoRaman-532SG instrument. Energy-dispersive X-ray fluorescence (EDXRF) chemical analysis with an Amptek X123-SDD instrument revealed only the expected major amount of P and no significant trace elements.

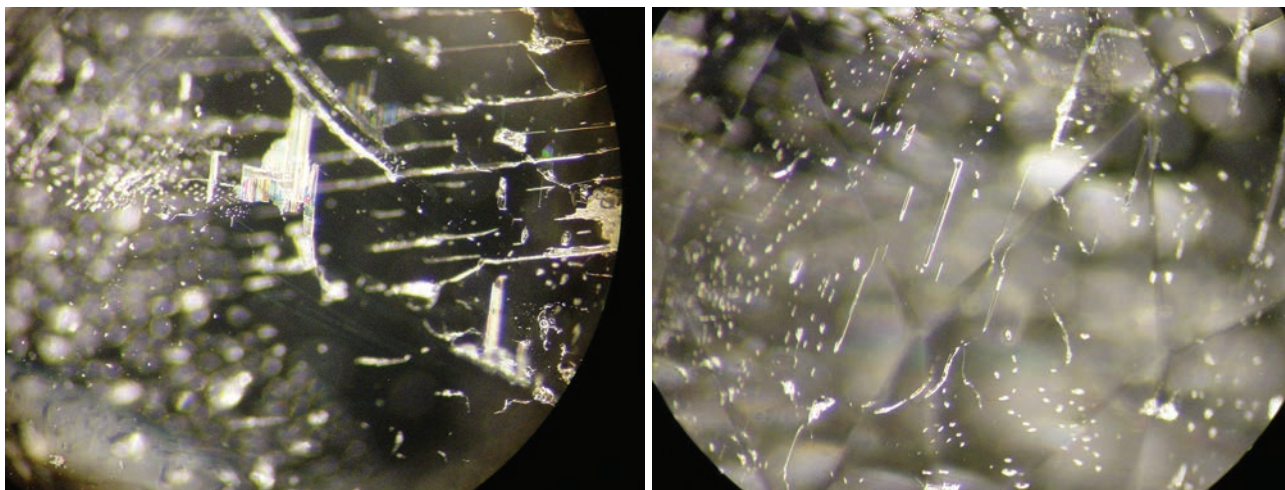


Figure 5: Internal features in the beryllonite consisted of iridescent planar fluid inclusions (left) and variably shaped two-phase inclusions (right). Photomicrographs by C. Williams; magnified 40×.

Numerous small inclusions were evident upon close examination of the stone without magnification. Microscopic observation with darkfield illumination revealed fluid-filled partially healed fissures, including one geometric-shaped iridescent inclusion that appeared to follow a cleavage plane (Figure 5, left). Also present were two-phase (fluid-gas) inclusions containing tiny bubbles (Figure 5, right).

Gem-quality beryllonite is known mainly from Afghanistan and Brazil, although Pakistan is also an occasional source of this rare gem material, as seen in this report.

Cara Williams FGA and Bear Williams FGA
 (info@stonegrouplabs.com)
 Stone Group Laboratories
 Jefferson City, Missouri, USA

Brendan M. Laurs FGA

References

- Koivula J.I. and Kammerling R.C., Eds., 1991. Gem News: Cat's-eye beryllonite. *Gems & Gemology*, **27**(1), 47–48.
- Muyal J. and Sun Z., 2016. *G&G Micro-World: Growth blockages in cat's-eye beryllonite. Gems & Gemology*, **52**(2), 311–312.

Apache Blue Stone (Chrysocolla) from Arizona, USA

The south-western USA is a well-known source of colourful secondary copper minerals such as malachite, azurite, chrysocolla, turquoise, etc. In 2013, a temporary partnership between a copper-mining company and Apache Way LLC (Chiricahua Apache Nde Nation, San Carlos Apache Reservation, Arizona) produced several tonnes of bright blue rough material from a large open pit located approximately 1 km from the now-inactive Sleeping Beauty turquoise mine. The appearance of the material varies from uniformly coloured to showing substantial amounts of matrix. Approximately 225 kg have been stabilized by polymer impregnation, and this material is being sold as Apache Blue Stone. More than 400 gems of various sizes and shapes have been cut and polished on the San

Carlos Apache Reservation, with some contract cutting also being done overseas. In addition, silver- and gold-mounted jewellery and *objets d'art* are being manufactured and sold with Apache Blue Stone in indigenous and American heritage-inspired designs.

During the February 2017 Tucson gem shows, three pieces of rough were donated to Gem-A, and five cut-and-polished pieces were loaned for examination, by Charles Vargas and Warren Boyd (Apache Gems, San Carlos, Arizona). The rough material (Figure 6) was untreated, while the polished stones (Figure 7) had been stabilized by different polymer impregnation processes.

The samples were characterized by authors CW and BW. The rough stones were vibrant blue



Figure 6: These untreated rough pieces of Apache Blue Stone range from 4.4 g (~2 × 2 cm) to 90.3 g (~6 cm in maximum dimension). Gift of Charles Vargas; photo by Dean Brennan.

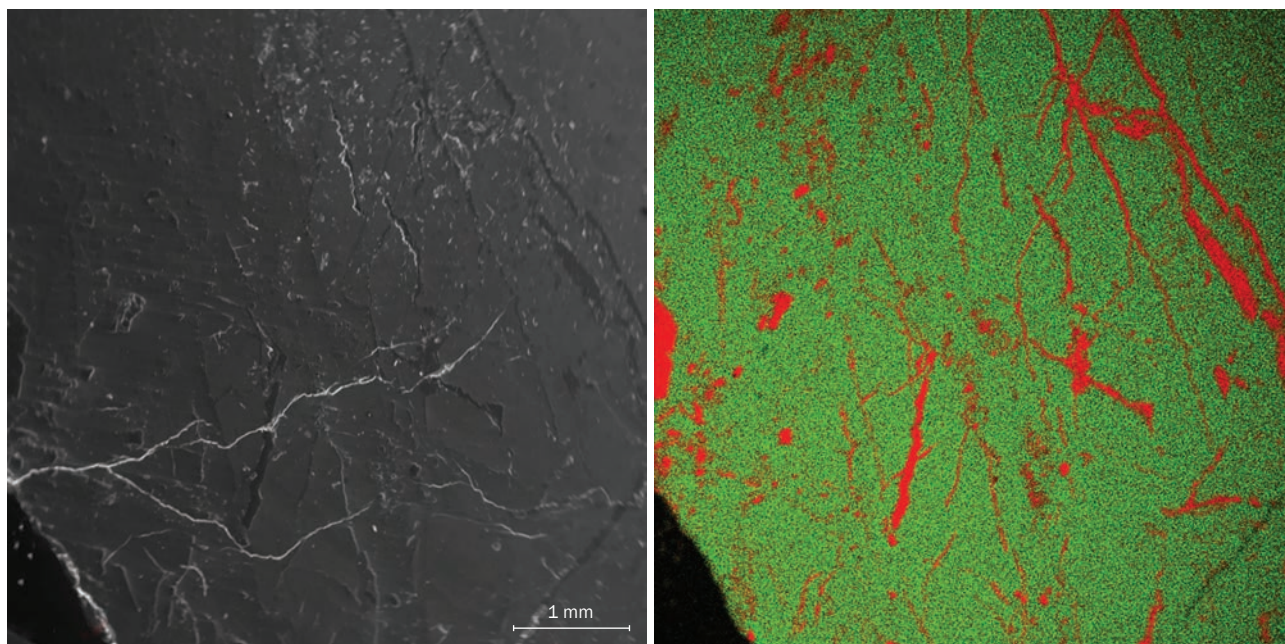
to greenish blue. One rough sample appeared to consist of a brecciated rock with blue colour running in veins and along areas of the surface. The other pieces appeared more homogeneous, with translucent colourless areas of quartz. All of them had a chalky texture. Standard-based scanning electron microscopy–energy-dispersive spectroscopy (SEM-EDS) chemical analysis (Figure 8) of a rough sample by author AUF (using a Jeol JSM-6400 instrument with the Iridium Ultra software package by IXRF Systems Inc.) revealed major amounts of Si and high Cu contents (40.03–40.79 wt.% CuO). There also was minor Ca (~1 wt.% CaO) and traces of Mg, Fe and Mn. This composi-



Figure 7: These polished samples consist of Apache Blue Stone that has been stabilized by polymer impregnation. The pieces on top (23.4 × 5.6 mm) were treated by the currently used stabilization method, while those on the bottom (drop shapes of 22.0 × 14.0 mm and an oval cut of 12.3 × 9.4 mm) were treated by an older polymer impregnation technique that partially darkened their colour. Photo by Dean Brennan.

tion is consistent with chrysocolla, and the identification was confirmed by Raman spectroscopy with a GemmoRaman-532SG instrument.

Figure 8: SEM-EDS imaging of the rough Apache Blue Stone showed features consistent with chrysocolla that is veined with quartz. The backscattered electron image on the left shows variations in overall atomic number (with darker areas corresponding to lower values, and vice versa), and the X-ray map on the right of the same area has been colourized according to contents of Cu (green) and Si (red). Images by A. U. Falster.



Of the five polished samples examined, three were treated using an older, now-discontinued process, and they showed areas of darker and lighter blue to greenish blue. Raman analysis identified the samples as chrysocolla, regardless of colour intensity. In addition, Fourier-transform infrared (FTIR) spectroscopy revealed bands associated with serpentine in some areas of these stones, as well as the expected presence of artificial resin that was used for stabilizing the material. EDXRF spectroscopy showed traces of K in these three samples, which may be due to mineral impurities. The other two polished samples were treated by the currently used stabilization method, and they displayed a lighter shade of blue (similar to the rough material) and contained quartz veining with some brown matrix. FTIR spectroscopy revealed artificial resin associated with the stabilization, but no K was detected with EDXRF analysis. Although RI readings could

not be obtained from most of the samples, one of them yielded an approximate spot RI of 1.53. Hydrostatic SG was not measured due to the porosity of the material (rough) or the presence of polymer impregnation (polished samples).

Although Apache Blue Stone was reportedly mined within sight of the Sleeping Beauty mine, it is not related to turquoise other than exhibiting a similar colour and appearance. Due to overlapping values of RI and SG, and complications caused by the common presence of impregnation treatment, the identification of turquoise vs. chrysocolla is best determined by a well-equipped gemmological laboratory.

*Cara Williams FGA, Bear Williams FGA and
Brendan M. Laurs FGA*

*Alexander U. Falster and William 'Skip' B. Simmons
Maine Mineral & Gem Museum
Bethel, Maine, USA*

Tianhuang, an Unusual Yellow Stone: Dickite or Nacrite?

In a collection of family heirloom jewellery that a client brought in for appraisal, we encountered an unusual yellow stone carving that we initially thought to be talc because of its soft and soapy feel. The yellow translucent stone—finely carved with a stylized lion—weighed 28.90 g and measured 44.90 × 26.58 × 12.19 mm (Figure 9). The

object was typical for a Chinese stone seal, but its base was not yet engraved. It was slightly chipped due to wear and tear, and the softness of the material also was demonstrated by the presence of polishing marks and in the corresponding blurry reading on the refractometer caused by the poor polish. A faint shadow edge ranged from



Figure 9: Left: This yellow stone carving (44.90 × 26.58 × 12.19 mm) was found to be a material known as Tianhuang in China, which may consist of the kaolinite-group minerals dickite and/or nacrite. Right: In this view, the main flat side of the carving displays whitish vein-like patterns. Photos by Tay Thye Sun.



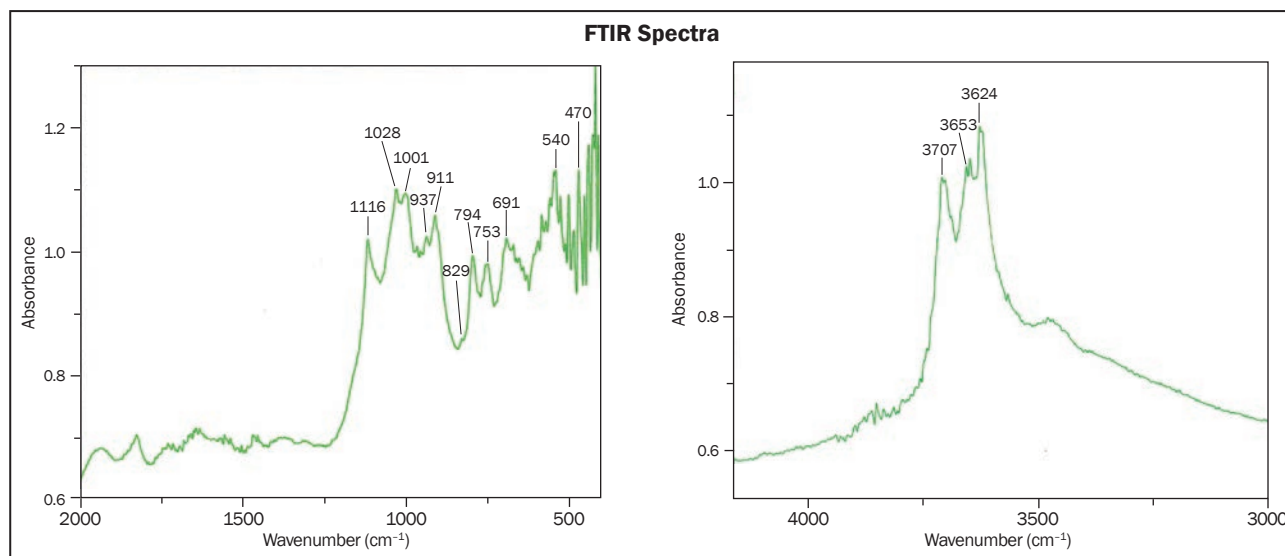


Figure 10: FTIR spectroscopy of the yellow stone carving revealed several absorption bands in the low-wavenumber region that point to a kaolinite-group mineral (left), while the three hydroxyl-related bands at 3707, 3653 and 3624 cm^{-1} in the high-wavenumber region correspond to dickite (right).

approximately 1.55 to 1.58, which is typical for clay minerals. Close examination of some areas of the object showed whitish vein-like markings (e.g. Figure 9, right).

To identify the material, a very minute amount of powder was extracted from the chipped corner. Infrared spectroscopy was performed using a Jasco FT/IR-4100 with a single beam and resolution of 4.0 cm^{-1} . Absorption bands were recorded at 1116, 1028, 1001, 937, 911, 829, 794, 753, 691, 540 and 470 cm^{-1} in the low-wavenumber region (Figure 10, left), and at 3707, 3653 and 3624 cm^{-1} in the high-wavenumber range (Figure 10, right). These features identify the material as a kaolinite-group mineral (cf. Farmer, 1964; Johnston et al., 1990), and the three sharp bands in the high-wavenumber region are characteristic of dickite (van der Marel and Krohmer, 1969). There are four types of non-equivalent OH in the crystal structure of kaolinite minerals, of which 3707 cm^{-1} belongs to the telescopic vibrations of ordered hydroxyl- OH_3 . It is evident that the sample has a high degree of order; the 3653 and 3624 cm^{-1} bands are attributed to the inner-surface hydroxyl of OH_4 (Balan et al., 2005).

The same powder sample was analysed by Raman spectroscopy using a Bruker Senterra spectrometer, equipped with a red laser (785 nm) with a power of 100 mW; the measurement time was 100 seconds. The Raman spectra of dickite and nacrite are quite similar in the range 915–120 cm^{-1} , and the main distinction is the presence of peaks between 1120 and 1050 cm^{-1} that are typical of dickite (Figure 11).

The properties of this stone carving are consistent with those of Tianhuang, which consists of clay related to the kaolinite group of minerals, in which dickite and nacrite are among the rarer polymorphs (Deer et al., 1992). *Tianhuang* means ‘field’ and ‘yellow’, and is known to occur in rice paddy fields along the Shoushan stream in the northern suburbs of Fuzhou, the capital of Fujian Province in south-east China (Liu and Chen, 2012). It has been valued since ancient times—an ounce of Tianhuang was once reportedly worth an ounce of gold—and was treasured by various Chinese emperors for making stone seals. Yellow Tianhuang is more desirable than other colours such as red, white, black and grey.

Our investigation showed that a combination of infrared and Raman spectroscopy can identify a specific clay mineral, and in this case, our analysis of the yellow stone carving revealed that it was composed of dickite.

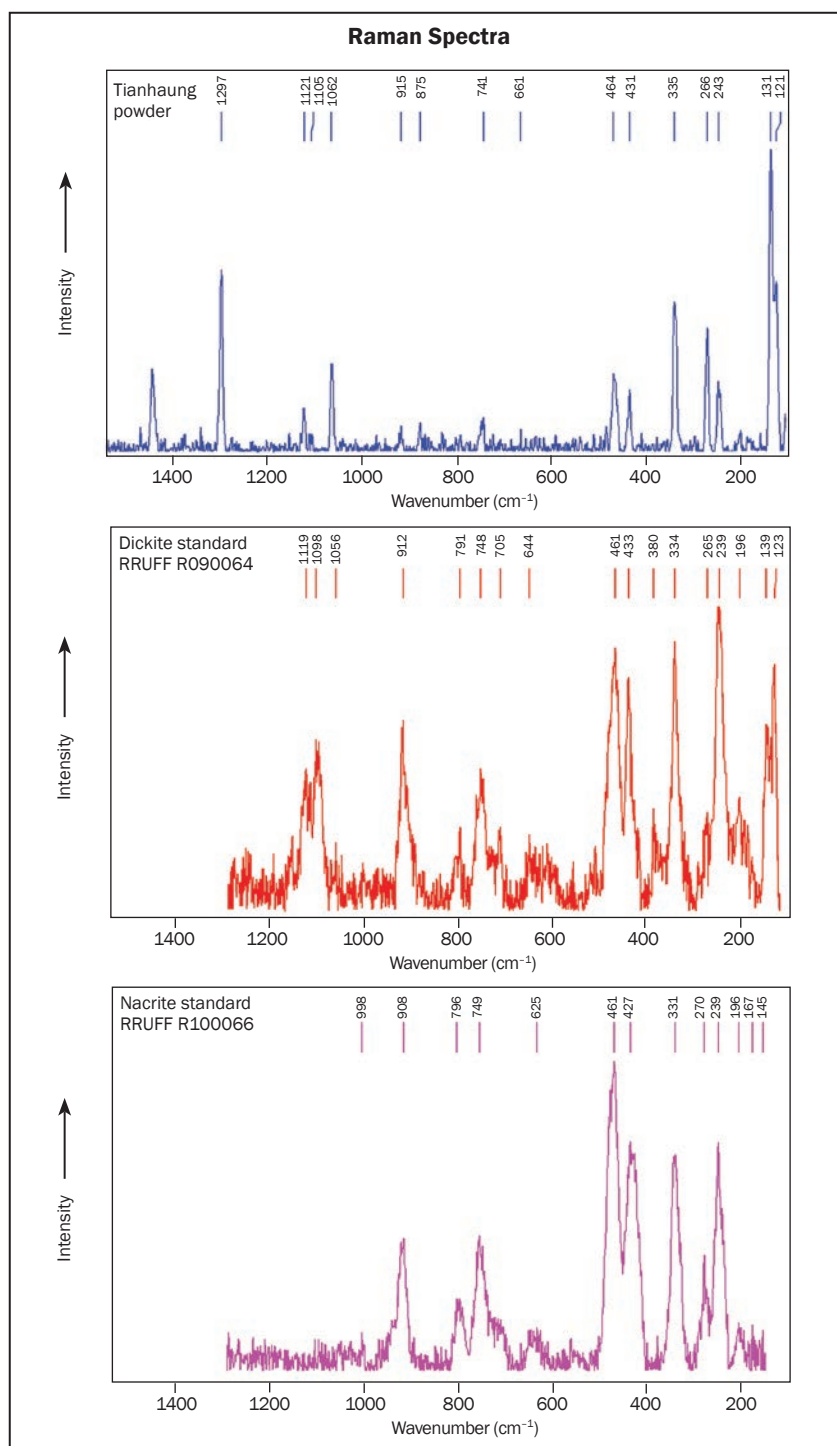
Acknowledgements: Many thanks to Dr Lo Wai Kit and family for allowing the yellow stone to be analysed, and to Dr Eugene Huang for assistance with English translation.

Tay Thye Sun FGA (tay@gem.com.sg)
Far East Gemological Laboratory, Singapore

Prof. Dr Leander Franz
University of Basel, Switzerland

Li Jianjun
National Gold & Diamond Testing Center
Shandong Institute of Metrology, Shandong, China

Figure 11: The Raman spectrum from the yellow carving displays features corresponding to both dickite and nacrite from the RRUFF database (<http://rruff.info>). Peaks between 1120 and 1050 cm^{-1} are typical of dickite.



References

- Balan E., Lazzeri M., Saitta A.M., Allard T., Fuchs Y. and Mauri F., 2005. First-principles study of OH-stretching modes in kaolinite, dickite, and nacrite. *American Mineralogist*, **90**(1), 50–60, <http://dx.doi.org/10.2138/am.2005.1675>.
- Deer W.A., Howie R.A. and Zussman J., 1992. *An Introduction to the Rock-Forming Minerals*, 2nd edn. Longman Scientific and Technical, Essex, 696 pp.
- Farmer V.C., 1964. Infrared absorption of hydroxyl groups in kaolinite. *Science*, **145**(3637), 1189–1190, <http://dx.doi.org/10.1126/science.145.3637.1189>.
- Johnston C.T., Agnew S.F. and Bish D.L., 1990. Polar-

- ized single-crystal Fourier-transform infrared microscopy of Ouray dickite and Keokuk kaolinite. *Clays and Clay Minerals*, **38**(6), 573–583, <http://dx.doi.org/10.1346/ccmn.1990.0380602>.
- Liu Y.-G. and Chen T., 2012. Infrared and Raman spectra study on Tianhuang. *Spectroscopy and Spectral Analysis*, **32**(8), 2143–2146 (in Chinese with English abstract).
- van der Marel H.W. and Krohmer P., 1969. O-H stretching vibrations in kaolinite, and related minerals. *Contributions to Mineralogy and Petrology*, **22**(1), 73–82, <http://dx.doi.org/10.1007/BF00388013>.

Copper-Stained Quartzite from Badakhshan, Afghanistan

Badakhshan Province in north-eastern Afghanistan is a source of various gem materials and is especially well known as the world's oldest locality for lapis lazuli. A new material appeared in the summer of 2016 that reportedly originated from the Tushkan District of Badakhshan, and has been sold as 'Tushkan jade' because of its green colour and translucency. More than 100 kg of rough have been sent to Europe, and additional production is expected. However, the deposit is situated in high mountains, so the mining season is limited.

Rough specimens show green to blue-green areas within white rock (Figure 12), and the ma-



Figure 12: These two rough pieces of copper-stained quartzite are from Badakhshan, Afghanistan. The specimen on the right is ~8 cm across. F. Naubahar collection; photo by J. Hyršl.



Figure 13: The copper-stained quartzite is available as cabochons (left, up to 17.26 ct) and faceted stones (right, up to 18.77 ct). F. Naubahar collection; photos by J. Hyršl.

Figure 14: Areas of bornite (dark purple) and chalcocopyrite (yellow) add interest to these cabochons of copper-stained quartzite. The larger stone weighs 29.29 ct. J. Hyršl collection and photo.



terial can be cut as cabochons or faceted (Figure 13). The greenish areas often contain metallic grains up to 15 mm in dimension that display various colours (Figures 12 and 14). Mineralogical analysis of a rough sample by powder X-ray diffraction revealed quartz as the main component and, because of its granular structure, it is therefore called quartzite. The metallic grains consisted of three different copper sulphides: bornite (dark purple), chalcocite (grey) and chalcocopyrite (yellow). The overall green to blue-green colour of the material is caused by copper as a secondary mineral, very probably malachite, which forms an extremely thin coating between quartz grains.

The gemmological properties of the material were typical for quartzite. The spot RI of the cabochons was approximately 1.54 and the hydrostatic SG was 2.64 (for samples not containing sulphides). All of the samples were translucent and they appeared green under the Chelsea filter. Visible-near infrared (Vis-NIR) spectroscopy showed a broad absorption band centred at 660 nm (Figure 15). The spectrum was rather similar to that of gem silica (copper-bearing chalcedony) from Peru, but in the latter material the band is shifted to centre at 720 nm.

Quartzite is quite durable but malachite is easily soluble in acids, so jewellery containing this copper-stained quartzite should not be cleaned in acid.

Jaroslav Hyršl (hyrsl@hotmail.com)
Prague, Czech Republic

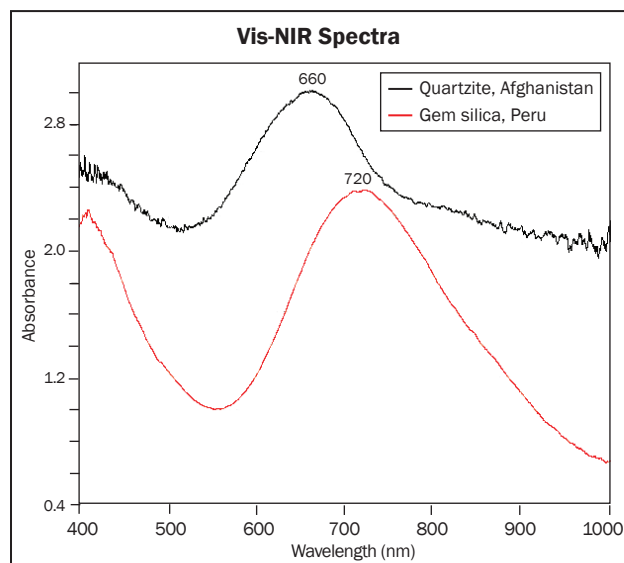


Figure 15: A broad absorption band centred at 660 nm is seen in the Vis-NIR spectrum of the copper-stained quartzite. By comparison, the absorption band for gem silica (copper-bearing chalcedony) from Peru is centred at 720 nm.

Sapphires from Canada—An Update

Corundum from Ontario, Canada, was first discovered in the 1870s by Henry Robillard. The large primary deposit was mined in the early 1900s and resulted in the development of the town of Craigmont. At this time, the corundum (mostly of brown colour) was primarily used as an abrasive, and was shipped all around the world (Adams and Barlow, 1910). A fire in February 1913 destroyed the mining mill, which ultimately turned Craigmont into a ghost town and halted mining (Barlow, 1915).

With the growing demand for unique faceted material, Canadian corundum is experiencing a slow-but-steady revival. However, rough material remains hard to come by, as no commercial mining has taken place since the 1920s, and most of the mine sites are overgrown by bush. Nevertheless, new initiatives are focused on cutting Canadian sapphires, and the stones are being featured in some interesting jewellery. So far, approximately 134 gemstones (about 656 carats total) have been faceted primarily as checkerboard

cuts in round, oval and cushion shapes (Figure 16). They have been cut to accommodate the manufacture of comfortable-sized rings, ranging from 7 to 12 mm for cushion cuts and 9 to 13 mm for round stones. In February 2017, the first ‘Snowflake Cut’ (Lurie, 2000) Canadian sapphire was faceted by Rudi and Ralph Wobito (Wobito Gems, Stouffville, Ontario; again, see Figure 16). Also being produced are some rare large slices that weigh up to 134.5 ct (58.5 × 36.0 × 4.4 mm). These slices provide the preforms from which the best faceted stones are cut. They also have been used to make large, one-of-a-kind, reversible pendants that are polished on one side to show the beautiful growth pattern and left unpolished on the other side to display the natural surface (Figure 17). In addition, some of the sapphires are being carved and incorporated into *objets d’art* such as butterflies and fish (Figure 18).

One of the rarest Canadian sapphire varieties shows a greyish blue colour. A very few of these stones have been found by rock and mineral col-



Figure 16: This selection of Canadian (Ontario) sapphires features: a large rough crystal (top centre); two sapphire-and-diamond halo rings set in 14-carat yellow gold, together with three corundum crystals (right side); an ~14 ct checkerboard-cut greyish blue sapphire set in a 14-carat white gold diamond halo ring, sitting on a piece of rough (left); and a 14-carat yellow gold pendant set with a freeform-cut sapphire and diamonds, which is sitting next to a loose 3.90 ct 'Snowflake Cut' sapphire (centre). The other stones consist of various checkerboard-cut sapphires in oval, round and cushion shapes. The brown stones are from the Craigmont area and the greyish blue gem is from Sharbot Lake. Photo by R. Schroetter.

lectors at Sharbot Lake in Ontario (Barlow, 1915; see geological map no. 1023, p. 57), and also pale blue/white and yellow sapphires are known from the Cabonga Reservoir terrane of Québec (Hudon et al., 2006; see, e.g., Figure 19). Of particular note is a 14+ ct greyish blue checkerboard cut from Sharbot Lake that is set with diamonds in 14-carat white gold (Figure 16).

The production of such faceted stones, jewelry and *objets d'art* will remain quite limited, but

Figure 17: The freeform slice of Canadian brown sapphire in this 10- and 14-carat yellow and white gold pendant measures approximately 50 × 35 mm. The stone has been polished on one side (left) and shows its natural surface on the other side (right). Pendant and photo by R. Schroetter.



Figure 18: The butterfly wings (approximately 69 × 30 mm) in this objet d'art are carved from Canadian brown sapphire; the body is 10-carat yellow gold, and the base consists of a stilbite mineral specimen from India. Objet d'art and photo by R. Schroetter.



these recent initiatives will nonetheless expand the availability of these Canadian sapphires.

Ralph Schroetter GG FGA (IJewelCad@outlook.com)
IJewelCad.com, Ontario, Canada

References

- Adams F.D. and Barlow A.E., 1910. *Geology of the Haliburton and Bancroft Areas, Province of Ontario*. Memoir No. 6, Canada Department of Mines, Ottawa, Ontario, 426 pp.
- Barlow A.E., 1915. *Corundum, Its Occurrence, Distribution, Exploitation, and Uses*. Memoir No. 57, Canada Department of Mines, Ottawa, Ontario, 377 pp.
- Hudon P., Friedman R.M., Gauthier G. and Martignole J., 2006. Age of the Cabonga nepheline syenite, Grenville Province, western Québec. *Canadian Journal of Earth Sciences*, **43**(9), 1237–1249, <http://dx.doi.org/10.1139/e06-022>.
- Lurie M., 2000. Canadian cutters Rudi and Ralph Wobito bring a German edge to their sparkling cuts. *Lapidary Journal*, **54**(3), June, 22–26.



Figure 19: The four cushion-cut yellow and pale blue/white sapphires in the centre are from Québec, and the surrounding stones are from Sharbot Lake in Ontario. The 13 checkerboard-cut sapphires have a total weight of ~78 carats and range from 8.9 mm rounds to 14.5 × 14.0 mm cushions. Photo by R. Schroetter.

New Sapphire Deposit in Northern Ethiopia

In December 2016, a large alluvial sapphire deposit was discovered in the Tigray region of northern Ethiopia. According to gem dealer Hussain Rezayee (Rare Gems & Minerals, Los Angeles, California, USA), who visited Ethiopia in April 2017, the deposit is located in the Axum (or Aksum) area of Rama District, near the town of Chila. The mining area (e.g. Figure 20) appears to be quite large, extending north of Axum

Figure 20: Local diggers mine alluvial sediments for sapphires in northern Ethiopia. Photo courtesy of Hussain Rezayee.



toward the border with Eritrea and west toward the Sudan border for 100+ km. Although foreigners are not allowed to visit the mining area, he was told that there are 10,000–12,000 people working there. According to Rezayee, only about 10% of the stones are of moderate-to-good gem quality. The sapphires range from pure blue to blue-green, grey-blue, and yellow to golden yellow, and some of them are quite large (e.g. Figures 21 and 22). Numerous local stone dealers

Figure 21: These rough sapphires from northern Ethiopia consist of a large milky colour-zoned pebble (left, 61.2 g), a transparent water-worn crystal (centre, 2.6 g) and a dark blue stone (20.0 g). Courtesy of Hussain Rezayee; photo by Orasa Weldon.





Figure 22: The sapphires in Figure 21 are illuminated from below or from the side with strong lighting to show their body colours. The geuda-type stone on the left appears more yellow when viewed here with transmitted light (see Figure 21 for comparison). Photos by B. M. Laurs.



Figure 23: Northern Ethiopia is also the source of this trapiche sapphire. Photo by Farooq Hashmi.

have opened offices near the mining area and also in the capital city, Addis Ababa. Most of the buyers are Sri Lankan, as well as some Thais and also wealthy Ethiopians who buy the gems for investment.

In May 2017, rough stone dealer Sir-Faraz Ahmad (Farooq) Hashmi (Intimate Gems, Glen Cove, New York, USA) spent several days in northern Ethiopia, and reported seeing 3–5 kg of the rough sapphires in the market in Axum. Although many large stones were commonly available (20–70 g),

they tended to be overly dark, and the best material for cutting gemstones weighed 2–10 g. The most attractive colour displayed by the rough material was pure blue, while the lower-quality stones appeared ‘inky’ or had grey banding. In addition, some trapiche sapphires were available (Figure 23). Hashmi found the prices of the rough to be quite high, regardless of the colour and clarity characteristics of the stones.

The colour appearance of sapphires from this deposit is consistent with typical magmatic corundum. Compared to the magmatic sapphires reported from Yabelo in southern Ethiopia (Beaton, 2011), stones from the Axum area are more blue (commonly without a green tint or yellow coloration), available in larger sizes, and they are hosted by a much larger deposit. The presence of magmatic sapphires in the Axum area is consistent with the abundance of Cenozoic alkali basalts that underlie this part of northern Ethiopia (Hagos et al., 2010).

Brendan M. Laurs FGA

References

- Beaton D., 2011. Gem News International: Sapphire and zircon from Ethiopia. *Gems & Gemology*, **47**(3), 247–248.
- Hagos M., Koeberl C., Kabeto K. and Koller F., 2010. Geochemical characteristics of the alkaline basalts and the phonolite-trachyte plugs of the Axum area, northern Ethiopia. *Austrian Journal of Earth Sciences*, **103**(2), 153–170.

Tourmaline from Mwajanga, Tanzania

A new deposit of tourmaline was discovered in mid-2014 near Mwajanga village, in the Komolo area of the Manyara Region of north-eastern Tanzania. The initial production—some of which

was shown at the East Coast Gem, Mineral & Fossil Show in Springfield, Massachusetts, USA, in August 2014—consisted mostly of pale yellow-to-colourless crystals with pale brown, blue and



Figure 24: (a) This dravite from Mwajanga, Tanzania, is 2.3 cm tall and has a white chatoyant zone at the top of the crystal; courtesy of Dr Alexander Schauss, photo by Jeff Scovil. (b) Multicoloured tourmaline crystals such as this one were produced from Mwajanga in March 2015. Photo by Steve Ulatowski.

pink areas (Polityka, 2014). Crystals up to 10 cm long were available, and although they were well formed, they tended to have dull lustre. In addition, only small areas were transparent enough for faceting. Further production from Mwajanga in 2014 yielded deeper yellowish-to-orangey brown (e.g. Figure 24a) and pale green crystals, some of which were quite gemmy and possessed high lustre; they have been referred to as dravite (Moore, 2014). Some of the brown crystals contained sharply defined white chatoyant zones, or displayed evidence of multiple breakage and re-growth events, producing the appearance of bent crystals. Such tourmalines were seen by author BML at the February 2015 Tucson gem shows, with rough stone dealers Steve Ulatowski (New Era Gems, Grass Valley, California, USA) and Farooq Hashmi/Michael Puerta (Intimate Gems, Glen Cove, New York, USA). Also on display were colourless prismatic crystals of natrolite up

to nearly 4 cm long that reportedly were found at the same deposit as the tourmaline. Additional production in March 2015 consisted of multicoloured tourmaline crystals that ranged from black to orangey brown, yellowish green and bright pink (e.g. Figure 24b).

Most of the Mwajanga tourmaline has been sold as crystals to mineral collectors, and until recently these authors were unaware of any faceted material. However, in July 2016 gem dealer Dudley Blauwet had some pale brownish yellow and greenish brown faceted gems that ranged from 0.20 to 0.82 ct. The 42 stones (17.43 carats) were cut from 36 pieces weighing a total of 15.1 g. He obtained the rough material during the February 2016 Tucson gem shows from a stone dealer who purchased the tourmaline in Mwajanga. The rough consisted mostly of gem nodules, as well as some 'flawless' complexly formed crystals.

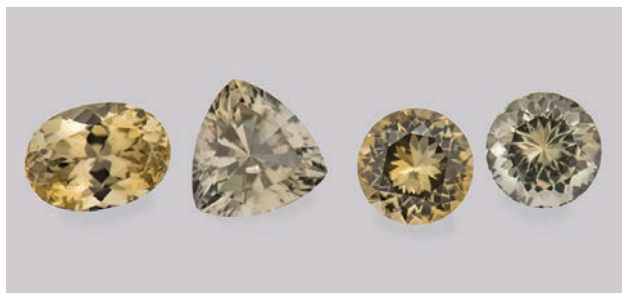


Figure 25: These pale brownish yellow and greenish brown tourmalines (0.56–0.82 ct) were found to consist of dravite with a minor uvite component. Photo by Orasa Weldon.

Blauwet loaned four of the cut stones for examination (Figure 25), and authors AUF and WBS performed standard-based SEM-EDS chemical analysis using a Jeol JSM-6400 instrument with the Iridium Ultra software package by IXRF Systems Inc. The results showed that all four samples had a very similar composition that consisted of dravite with a minor uvite component (0.90–0.96 wt.% CaO). Consistent with the pale coloration, there were few minor and trace ele-

ments; MnO and FeO were present in very low amounts (0.01–0.02 wt.%), V_2O_3 was only slightly above the detection limit (0.01 wt.%) and TiO_2 and Cr_2O_3 were not detectable.

Most recently, in April 2017, Ulatowski reported obtained some matrix specimens of translucent Mwajanga tourmaline that were mostly colourless but with deep blue terminations. The future potential of the deposit is unknown, but clearly it has already produced a variety of colours of tourmaline as attractive crystals and also a limited amount of rough material suitable for faceting.

Brendan M. Laurs FGA, Alexander U. Falster and William 'Skip' B. Simmons

References

- Moore T.P., 2014. What's new in the mineral world?—Report #39. *Mineralogical Record*, Tucson, Arizona, USA, 6 December, [www.minrec.org/pdfs/Toms Online report 39.pdf](http://www.minrec.org/pdfs/Toms%20Online%20report%2039.pdf).
- Polityka J., 2014. What's New: Springfield Show 2014. *Mineralogical Record*, **45**(6), 693–698 (see p. 695).

Tourmaline (Dravite) from Simanjiro District, Tanzania

'Chrome tourmaline' is well known from East Africa (e.g. Sun et al., 2015), and in mid-2016 a significant new discovery occurred at the Commander mine in Simanjiro District, Manyara Region, north-eastern Tanzania. These tourmaline crystals first appeared on the market at the October 2016 Munich Show (Moore, 2017), and additional material was offered at the February 2017 Tucson gem shows. According to rough stone dealer Steve Ulatowski, the mine is located about 14 km from Nadonjukin village and was initially explored in 1997, but was soon abandoned. In late August 2016, a local miner referred to as 'Commander' reopened the deposit. He extended the previous workings by hand digging and blasting to ~12 m depth, where he found a large pocket that produced ~5 kg of mixed-grade crystals. A subsequent pocket was recovered that yielded an additional ~3 kg of tourmaline. The crystals were well formed with lustrous faces and ranged up to 10+ cm long. They typically were bicoloured with yellowish

to orangey brown bases and green terminations (e.g. Figure 26). A few of the tourmalines were recovered on a matrix of blocky white crystals (probably calcite or dolomite), but most of them had been broken off the matrix by the miners.

Most of the tourmaline production has been sold as crystals, with only a limited amount of gem rough available. Ulatowski faceted four stones ranging from ~0.7 to 1.1 ct; two of them were bicoloured and two were pure green (again, see Figure 26). He donated a crystal fragment and loaned one of the green gems (1.09 ct) for examination. The faceted stone was characterized by authors CW and BW. It displayed an overall lively deep green colour and yellowish green/bluish dichroism. The RIs were 1.620–1.638 (birefringence 0.018) and the hydrostatic SG was 3.06. These data are very similar to those reported for 'chrome tourmaline' by Sun et al. (2015). The stone was inert to a standard long- and short-wave UV lamp, but emitted a red glow when exposed to 405 nm excitation from a hand-held laser. It ap-



Figure 26: These faceted stones (1.09 and 0.70 ct) and crystal (4.7 cm tall) consist of dravite that was recently produced from Simanjiro District in Tanzania. Photo by Jeff Scovil.

peared red under a Chelsea colour filter. Microscopic observation revealed two small fractures and also a long, needle-like growth mark (Figure 27). Raman analysis with a GemmoRaman-532SG instrument provided a good match to reference spectra for dravite.

Standard-based SEM-EDS chemical analysis of the crystal fragment was performed by author AUF using a Jeol JSM-6400 instrument with the Iridium Ultra software package by IXRF Systems Inc. In addition, Na was analysed by a direct-coupled plasma spectrometer to check the results. These data confirmed the tourmaline is dravite with a lesser uvite component. Analyses of green and brown portions of the crystal fragment yielded a fairly similar composition, with the following chromophoric elements: 0.71–1.12 wt.% TiO_2 , 0.11–0.27 wt.% V_2O_5 , 0.03–0.11 wt.% Cr_2O_3 , 0.04–0.07 wt.% FeO and 0.04–0.07 wt.% MnO . These elements also were detected in the faceted stone by authors CW and BW using an

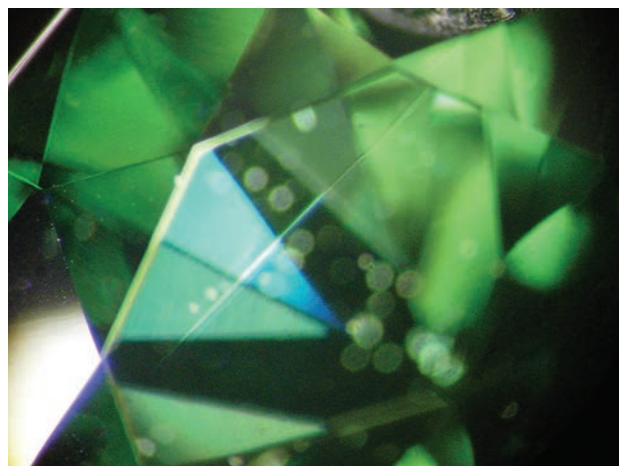


Figure 27: This microscopic view of the 1.09 ct dravite in Figure 26 shows a needle-like growth mark. Photomicrograph by C. Williams; magnified 40 \times .

Amptek X123-SDD EDXRF. A similar composition was reported for Cr- and V-bearing tourmaline from Kenya (Williams and Williams, 2015).

Due to the common presence of inclusions in this tourmaline and the fact that the well-formed crystals are sold as mineral specimens, it is unlikely that many gemstones will be cut from this dravite. In May 2017, gem dealer Dudley Blauwet received 34 faceted stones weighing 21.38 carats from his cutting factory; they were cut from a parcel of this dravite that he purchased at the 2017 Tucson gem shows that consisted of 31 pcs of rough weighing 17.8 g. The gems ranged from 0.10 to 1.62 ct, and from a fine light yellowish ‘mint’ green to brownish green to deep ‘chrome’ green.

A small amount of the Commander mine dravite contained abundant growth tubes oriented parallel to the c-axis that could produce chatoyancy if cut as cabochons.

*Cara Williams FGA, Bear Williams FGA,
Brendan M. Laurs FGA, Alexander U. Falster
and Dr William ‘Skip’ B. Simmons*

References

- Moore T.P., 2017. Munich Show 2016. *Mineralogical Record*, **48**(1), 141–156 (see pp. 144–145).
- Sun L., Yang M. and Wu G., 2015. Gemmological and spectroscopic characteristics of chrome tourmaline appeared on the market recently. *Journal of Gems & Gemmology*, **17**(1), 31–37 (in Chinese with English abstract).
- Williams C. and Williams B., 2015. Gem Notes: Colour-zoned Cr- and V-bearing tourmaline from Kenya. *Journal of Gemmology*, **34**(6), 476–477.

SSEF+

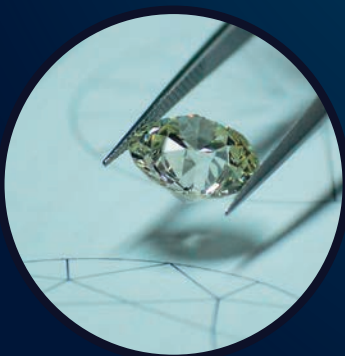
SCHWEIZERISCHES GEMMOLOGISCHES INSTITUT
SWISS GEMMOLOGICAL INSTITUTE
INSTITUT SUISSE DE GEMMOLOGIE



ORIGIN DETERMINATION · TREATMENT DETECTION

DIAMOND GRADING · PEARL TESTING

EDUCATION · RESEARCH



THE SCIENCE OF GEMSTONE TESTING

DIAMONDS

Recent Alluvial Diamond Mining in South Africa

In August 2016, this author joined a five-day pre-conference field trip associated with the 35th International Geological Congress (held in Cape Town, South Africa) that visited many historical and currently active alluvial diamond deposits in South Africa. The excursion was led by Dr Mike C. J. De Wit (Tsodilo Resources Ltd. and University of Pretoria, South Africa) and was attended by 26 participants from at least six countries. This report focuses on the three largest active mining areas that we visited: Tirisano and London Run in the North West Province, and Saxendrift on the Middle Orange River.

The Tirisano mine is located in the Lichtenburg–Ventersdorp Field (26° 5.218' S; 26° 47.121' E) and has been worked most recently (since 2012) by Badenhorst Diamante. The deposit has produced a total of ~100,000 carats, with a current average value of US\$400–\$500/ct and an overall grade of 1–2 carats per hundred tonnes (CPHT). At the time of our visit, the operation employed 50 people and included seven trucks and two excavators. Two open pits were being mined in a series of benches (e.g. Figure 28). The gravels were trucked to a washing plant (Figure 29), where they were screened to remove +100 mm clasts and then passed into a scrubber or trommel for sizing to 2–32 mm. This gravel fraction was then fed into rotary washing pans, and the heavy material that concentrated along the outer edge of the pans was routed into a secure

area for X-ray and hand sorting. Most of the Tirisano diamonds are near-colourless (typically H colour), and daily production is usually around 5 carats, but may range up to 300 carats; approximately 60% are of gem quality. The largest diamond was found in June 2016 and weighed ~100 ct; the second largest weighed 68 ct, and some additional significant stones weighed 13–30 ct. The diamonds are sold at a monthly tender in Johannesburg.

The London Run deposit (27° 20.380' S; 25° 25.662' E), mined by Namakwa Diamonds Ltd., is located near the town of Bloemhof, and forms part of the Southern Field of alluvial diamond deposits in South Africa. The gravels are 200–400 m wide and generally 5 m thick (Figure 30), but the upper 3–4 m are commonly cemented by calcrete



Figure 28: An excavator and dump trucks are used to mine this open pit at the Tirisano deposit. Photo by B. M. Laurs.

Figure 29: This view of the processing plant at the Tirisano mine shows vibrating screens (centre-background), a scrubber (right) and rotary washing pans (left). Photo by B. M. Laurs.





Figure 30: Field trip participants survey one of the mining trenches at the London Run deposit. The light-coloured sediments in the pit walls are diamond bearing, and they are overlain by a dark-coloured soil horizon and previously mined material. Photo by B. M. Laurs.

and must be blasted in places. The best diamond production comes from the bottom portion, so in most cases only the lower 2–3 m of the gravel unit is mined. The deposit typically produces diamonds averaging 0.8–0.9 ct with a value of slightly below US\$1,000/ct (e.g. Figure 31). Grades are fairly constant at 0.8–1+ CPHT. The largest stone produced in the past year weighed 62 ct. Other notable stones include a 27 ct diamond and a flat-shaped 55 ct type II stone that was recovered in early 2015. Although very rarely, the area produces a significant number of fancy-coloured dia-

Figure 31: This parcel of London Run diamonds weighs a total of 24.32 carats and consists of '3 grainers' (stones weighing $\frac{3}{4}$ ct). Courtesy of John Ward, Namakwa Diamonds Ltd.



monds (i.e. yellow, pink, purple, orange, blue). Our group visited one of the several small operations that mine the deposit in partnership with Namakwa Diamonds Ltd. It had 12 employees and produced some 300–400 carats per month. The processing plant used two vibrating screens (to size the material to 2–32 mm) and two rotary washing pans, with a throughput of 4,000 tonnes in a 24-hour period. The plant produced 4 tonnes of concentrate in each 12-hour shift. The concentrate was taken to a nearby privately operated facility for further processing (dense media separation and X-ray sorting). The diamonds are sold at tender in Kimberley, South Africa.

The Middle Orange River deposits are located between the towns of Douglas and Prieska (e.g. 29° 19.308' S; 23° 15.257' E), and have yielded many large diamonds over 100 ct and several over 200 ct. The fluvial-alluvial gravels are developed on terraces along the banks of the present Orange River, in a sequence comprising basal gravels 2–4 m thick that are overlain by <5 m of variably calcreted sands and silts. At the time of our visit, Rockwell Diamonds was processing tailings piles that had been stockpiled from the upper gravels at the Saxendrift mine by the previous company, Trans Hex Group. They also were preparing for a new mining operation at a nearby deposit called Wouterspan. Rockwell uses trommels to remove oversized material, and then mobile screening equipment is employed for de-sanding, and magnets remove clasts of banded iron formation (which forms most of the concentrate as it has a higher density than diamond) before the remainder is processed through washing pans. The resulting concentrate is passed through X-ray sorting machines. During the past five years, more than 10 diamonds weighing in excess of 100 ct have been recovered by Rockwell from newly mined gravels and tailings. The overall grade varies from 0.3 to 2 carats per hundred cubic meters, with better grades from the lower gravel layers. Despite the low grade, the deposit has a high diamond value of \$1,800–\$2,000/ct. About 70–80% of the value of the deposit lies in 10–20+ ct stones, so relatively large-sized material (5–36 mm) is processed. The diamonds are sent to Johannesburg, where most of the production is sold in sights that are held every two weeks; large diamonds (10+ ct, referred to as 'specials') are sold separately.

Brendan M. Laurs FGA

INCLUSIONS IN GEMS

Quartz from Brazil with Colourful Epigenetic Inclusions

Epigenetic fracture fillings of hematite and goethite in quartz are quite common, but occasionally they create attractive displays of colour and pattern that are noteworthy, particularly when viewed with different types of lighting (see, e.g., Koivula, 2003, p. 16). Recently, a significant amount of such quartz was produced in Brazil and made its way to the February 2017 Tucson gem shows.

According to Leonardo Silva Souto (Cosmos Gems, Teófilo Otoni, Brazil), the included quartz was mined from a granitic pegmatite in the Governador Valadares area, where similar material was initially found about 15 years ago. The recent production was notable for the size of some of the pieces (e.g. Figure 32) and the vibrant inclusion displays. According to Silva Souto, cutting the quartz to display the colourful inclusions

Figure 32: This large display specimen (14.9 cm tall) consists of recently produced quartz with colourful fractures that most likely are filled by hematite and goethite. Courtesy of Leonardo Silva Souto; photo by Jeff Scovil.



Figure 33: This quartz specimen (weighing 102 ct and measuring 46 × 29 mm) is shown under normal lighting (top) and in a polariscope (bottom). The cross-polarized light reveals radial crystallization textures in the hematite inclusions. Specimen and photos courtesy of Luciana Barbosa.

has been challenging since the coloured areas are present in only small areas of large crystals, and they usually are accompanied by an abundance of typical colourless inclusions (i.e. fluids and feathers) that reduce the transparency of the surrounding quartz. Most of the quartz has been cut as polished tablets to show off the inclusions, and dealer Luciana Barbosa (Gemological Center, Weaverville, North Carolina, USA) had approximately 1,000 carats that ranged from about 5 to 30 ct each, as well as two pieces in the 100 ct range (e.g. Figure 33).

The vast majority of the inclusions in the material seen in Tucson were orange to orangy red, typ-



Figure 34: The red and yellow inclusion assemblage in the quartz on the left (~19 ct) probably consists of hematite and goethite, respectively. Dendritic patterns are seen in the hematite inclusions within the quartz on the right (4.68 ct). Specimens and photos courtesy of Luciana Barbosa.

ical of epigenetic hematite, although some pieces contained yellow areas that are probably goethite (e.g. Figure 34, left). Radial inclusion formations were quite common, and dendritic patterns were displayed by a few pieces (Figure 34, right).

This quartz demonstrates that even common materials (quartz and iron oxide/hydroxide) can

come together to create specimens that are quite attractive.

Brendan M. Laurs FGA

Reference

Koivula J.I., 2003. Photomicrography for gemologists. *Gems & Gemology*, **39**(1), 4–23, <http://dx.doi.org/10.5741/gems.39.1.4>.

Quartz from Brazil with Pyrite Inclusions

Well-formed crystals of pyrite are known to occur as inclusions in quartz, particularly from Brazil (e.g. Koivula and Laurs, 2007). At the February 2017 Tucson gem shows, a new production of pyrite-included quartz was displayed by gem dealer Leonardo Silva Souto. The deposit was discovered at an old mine site in early 2016, while being prospected for aquamarine in Brazil's Tocantins State. Although no aquamarine was found, the work did yield a fairly large quantity of quartz that contained

an abundance of pyrite inclusions. Approximately 400 kg of quartz were produced, with most of the inclusions concentrated on only a single layer in the quartz. Although one large piece was polished (Figure 35), most of the quartz was sliced along the pyrite-rich layers so that smaller gems could be cut to showcase the inclusions (e.g. Figure 36). The polished stones consisted of cabochons and freeform tablets that ranged from 11 × 9 to 65 × 50 mm. In addition to pyrite, the gems commonly



Figure 35: Leonardo Silva Souto displays a large (~10 kg) polished piece of quartz, which contains a layer of pyrite inclusions that follow the rhombohedral faces of the host quartz. Isolated pyrite inclusions are also present further inside the quartz, along with some iron-stained fractures. Photos by B. M. Laurs.

contained fractures that were locally iron stained, which provide splashes of colour within the arrays of pyrite crystals.

Brendan M. Laurs FGA

Reference

Koivula J.I. and Laurs B.M., 2007. Gem News International: Citrine with pyrite inclusions. *Gems & Gemology*, **43**(2), 166–167.

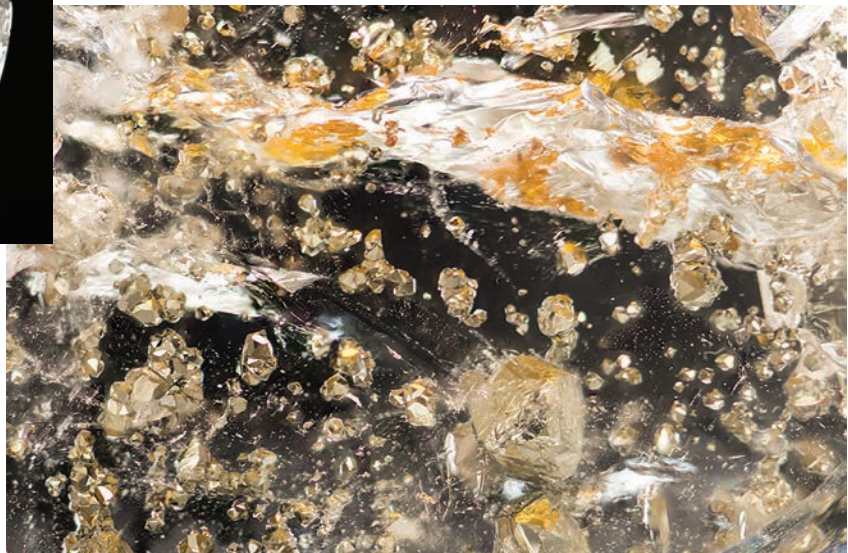
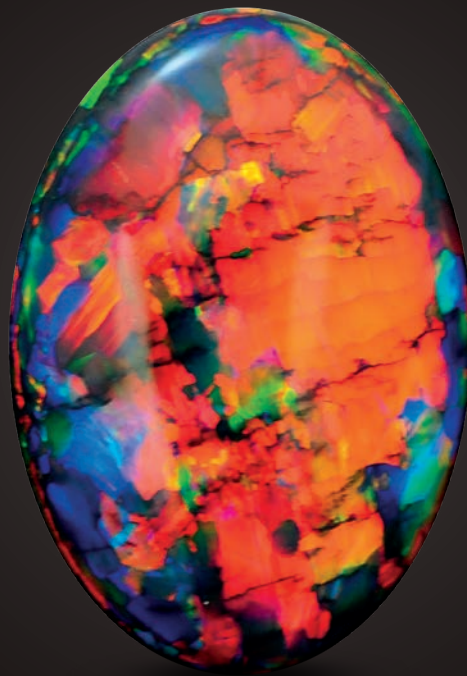


Figure 36: Numerous pyrite crystals and some fractures that are locally iron stained decorate this quartz specimen (above, 26 × 17 mm; gift of Leonardo Silva Souto). A closer view (right, image width 1.5 mm) shows that the pyrite inclusions consist of combinations of the cube and octahedron. Photos by Jeff Scovil, with image stacking for the photomicrograph by Lucas Fassari.

The Fire Within

“For in them you shall see the living fire of the ruby, the glorious purple of the amethyst, the sea-green of the emerald, all glittering together in an incredible mixture of light.”

- Roman Elder Pliny, 1st Century AD



BLACK OPAL 15.7 CARATS

Suppliers of Australia's finest opals to the world's gem trade.

CODY  OPAL

LEVEL 1 - 119 SWANSTON STREET MELBOURNE AUSTRALIA

T. +61 3 9654 5533 E. INFO@CODYOPAL.COM

WWW.CODYOPAL.COM

ICA
INTERNATIONAL
COLORED GEMSTONE
ASSOCIATION
MEMBER

Quartz from Brazil with Rhodochrosite Inclusions

Gem-quality rhodochrosite from granitic pegmatites in Minas Gerais, Brazil, was recently described in *The Journal* (Zwaan, 2015). During the February 2017 Tucson gem shows, the present author encountered rhodochrosite as inclusions in quartz from one of the localities mentioned in that report—Virgem da Lapa. The 230 ct stone was displayed by gem dealer Luciana Barbosa, and consisted of a faceted light smoky quartz containing a cluster of pink rhodochrosite crystals, which were surrounded by fluid inclusions and planar feathers (Figure 37). Barbosa indicated she cut a total of three stones containing such inclusions, with one being slightly larger than 230 ct and the other weighing ~25 ct. The rough material was produced in mid-2015 and was associated with loose crystals of rhodochrosite in addition to the included quartz specimens.

Although rhodochrosite inclusions in quartz have been previously reported from tungsten deposits (Hyršl, 2006), this is the first time to this author's knowledge that they have been encountered from a granitic pegmatite. Considering the rarity of rhodochrosite in these pegmatites, it is unlikely that there will be significant additional production of such specimens in the future.

Brendan M. Laurs FGA

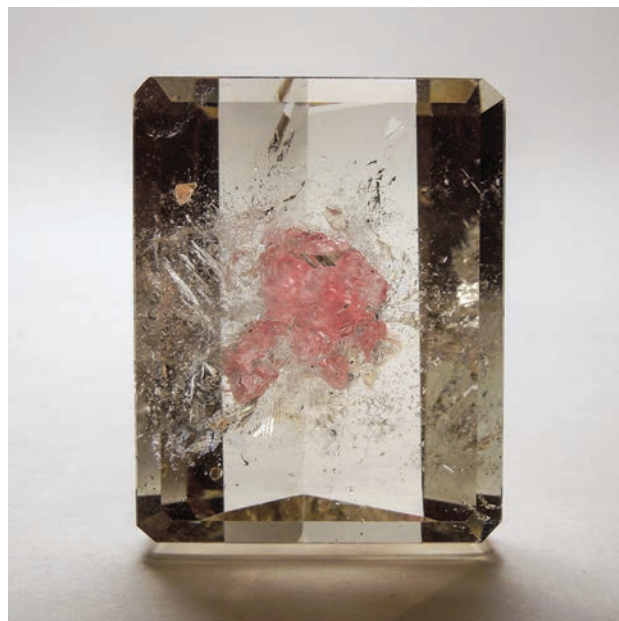


Figure 37: Weighing 230 ct (40 × 32 mm), this smoky quartz contains a cluster of rhodochrosite crystals. Photo by Luciana Barbosa.

References

- Hyršl J., 2006. Genetic classification of mineral inclusions in quartz. *Gems & Gemology*, **42**(3), 97–98.
- Zwaan J.C., 2015. Gem Notes: Rhodochrosite from Brazil. *Journal of Gemmology*, **34**(6), 473–475.

Some Inclusions in Quartz from Pakistan

For decades, Pakistan has been an important source of a variety of mineral specimens and gem materials, particularly from granitic pegmatites and Alpine-type hydrothermal veins. During the February 2017 Tucson gem shows, Syed Iftikhar Hussain (Syed Trading Co., Peshawar, Pakistan) showed one of the authors (BML) some quartz specimens containing inclusions from both of these genetic environments, and he kindly donated one of them to Gem-A.

The 53.36 ct smoky quartz in Figure 38 was mined from pegmatites in the Skardu area of northern Pakistan, and contained numerous randomly oriented pale brown flakes. Raman analysis identified them as biotite. The interface between the quartz and the biotite inclusions lo-

cally showed reflective mirror-like areas that displayed thin-film interference colours (Figure 39).

Conspicuous bluish green needles were present in a 5.70 ct quartz (Figure 40) from Zagi Mountain, which is located in Khyber Pakhtunkhwa (formerly North-West Frontier Province), approximately 40 km north-west of Peshawar. At this famous mineral deposit, Alpine-type veins are hosted by alkaline granite gneiss of the Warsak igneous complex (Obodda and Leavens, 2004). Raman analysis confirmed the needles in this quartz (Figure 41) to be an amphibole, and it provided a good match to reference spectra for actinolite. Interestingly, similar amphibole inclusions in mineral specimens of quartz from Zagi Mountain have been referred to as riebeckite



Figure 38: Numerous inclusions of biotite decorate the interior of this 53.36 ct smoky quartz from Skardu, Pakistan. Photo by Robison McMurtry, © GIA.



Figure 39: This biotite inclusion in quartz showed a highly reflective mirror-like interface and a circular area of thin-film interference colours. Photomicrograph by N. D. Renfro, © GIA; image width 4.7 mm.



Figure 40: This 5.70 ct oval modified brilliant from Zagi Mountain, Pakistan, consists of quartz with abundant actinolite needles. Gift of Syed Iftikhar Hussain; photo by Robison McMurtry, © GIA.

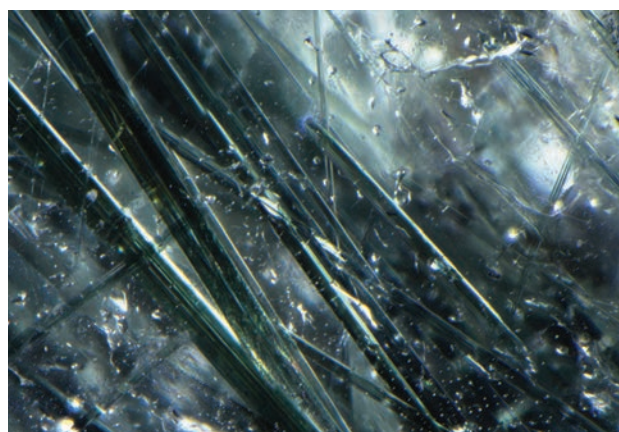


Figure 41: Actinolite forms locally dense networks of needles in this quartz. Photomicrograph by N. D. Renfro, © GIA; image width 2.7 mm.

(<http://tinyurl.com/lbx5btz>), but the Raman spectrum of these particular inclusions did not match the reference spectra for riebeckite.

Brendan M. Laurs FGA and Nathan D. Renfro

Reference

Obodda H.P. and Leavens P.B., 2004. Zagi Mountain—Northwest Frontier Province, Pakistan. *Mineralogical Record*, **35**(3), 205–220.

SYNTHETICS AND SIMULANTS

A Research Facility in The Netherlands for the HPHT Growth of Synthetic Diamonds and HPHT Treatment

In 2008, AOTC Group B.V. (Advanced Optical Technologies Corporation) established a research-and-development site in Westknollendam (Zaanstad), The Netherlands. While AOTC does not commercially produce synthetic diamonds at this particular facility, they do per-

form research on how to improve the growth process using single-axis presses with a modified Bridgman-type (toroid) high-pressure apparatus. During a visit in May 2016, the authors were shown old and new systems that were in operation.



Figure 42: At the AOTC research facility in The Netherlands, two older presses, each weighing 17 tonnes, are still in use. Co-author Branko Deljanin poses for scale. Photo by J. C. Zwaan.

In addition to two older 17-tonne presses (Figure 42), the facility includes two new 5.5-tonne presses (e.g. Figure 43). These employ improved hydraulic, heating and control systems that are much more efficient, and a cooling system that

exactly matches the ambient temperature at the air-conditioned facility. The repeatability of experiments has greatly improved as a result of these developments. In addition, the new presses have lower running costs, less maintenance, and can be manufactured on demand. The old presses are no longer readily available for purchase.

The new Bridgman-type apparatus is capable of producing pressures up to 10 GPa (100 kbar) and temperatures as high as 2,300°C (Choudhary and Bellare, 2000) in a reasonably large working volume, which is important for the commercial growth of high-pressure, high-temperature (HPHT) synthetic diamonds. By comparison, the two main types of devices that have been traditionally used are ‘belt’ and multi-anvil presses (also known as BARS or cubic presses), and both of them can reliably generate pressures up to 6 GPa.

The Bridgman-type apparatus (Figure 44) consists of a frame, a hydraulic cylinder, a high-pressure component within three plates on each outer side (not depicted in Figure 44), backing

Figure 43: New Bridgman-type presses such as this one (front and back) provide significant advances in the efficiency of growing synthetic diamonds. Photos by J. C. Zwaan.



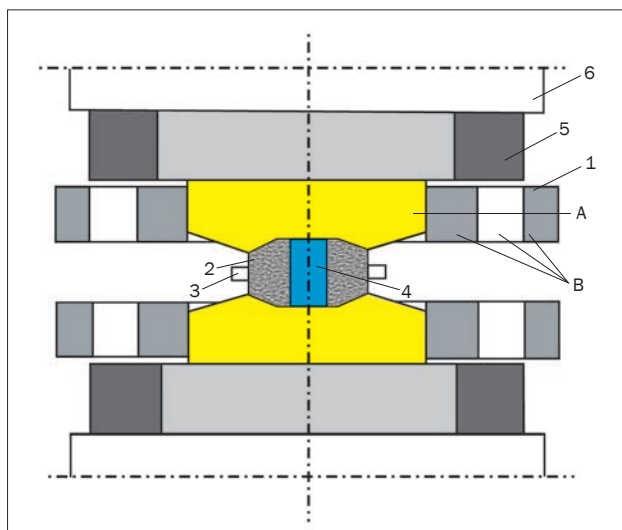


Figure 44: The Bridgman-type, toroidal HPHT apparatus is shown in this diagram: 1 – anvil (A – central part made of sintered carbides and B – supporting steel rings); 2 – ceramic container; 3 – pyrophyllite gasket; 4 – growth cell; 5 – backing plate; 6 – supporting plate. Diagram courtesy of AOTC.

and support plates, and cooling rings. The central high-pressure apparatus consists of shrunk-fit steel-alloy rings and tungsten-carbide anvils supporting a ceramic container and a cell for growing synthetic diamond crystals on a seed by a temperature-gradient method. The critical components of the high-pressure apparatus are the compressible gasket/container and the growth cell. The gasket, made from pyrophyllite, permits compressive movements of the conical piston and helps distribute the loading between the chamber and the piston. When the pyrophyllite gasket is compressed between opposed anvils, the outward flow of pyrophyllite from the central region is stopped by the inward flow of gasket material from the toroidal region, creating ultra-high pressure in the reaction cell (Choudhary and Bellare, 2000).

One synthesis cycle typically is completed in six days when growing yellow synthetic diamonds, but a cycle might be more than eight days to grow blue synthetics and more than two weeks to produce colourless material (D’Haenens-Johansson et al., 2014). During the growth process, a mixture of carbon and catalyst metal (in this case, iron) is heated high enough for the carbon to dissolve in the molten catalyst; the temperature of 1,500°C is generated with 2,000 watts of power. A pressure of ~5.5 GPa (55 kbar) is applied so that the system is thermodynamically stable for diamond formation. Under these conditions, a temperature gradient of

25°C (between 1,475°C and 1,500°C) causes diffusion of carbon atoms through molten iron, resulting in the crystallization of synthetic diamond. The growth cell has a diameter of 40 mm, allowing production of single-crystal synthetic diamonds weighing up to 8 ct. Typically, however, three smaller crystals of <1 ct are produced in each run. A single crystal of 3 ct (Figure 45) can be faceted into a polished synthetic diamond of ~1 ct. To extract the synthetic diamond(s) after growth, the researchers use ‘royal acid’ (a mixture of nitric and hydrochloric acid, optimally in a molar ratio of 1:3) to dissolve the metals at 245°C for a period of more than three hours.

Due to their improved properties and relative portability, the new toroid presses manufactured in The Netherlands by AOTC also are used worldwide for the HPHT treatment of type IIa natural diamonds and CVD-grown synthetics. Temperatures of more than 2,200°C and pressures above 5.5 GPa provide conditions at which the colour of light brown type IIa natural diamonds and off-colour CVD-grown synthetics can be improved to colourless (D–F range) and consequently increased in value (Pope et al., 2016).

Gemmologists very rarely have an opportunity to visit research facilities where equipment is designed to perform HPHT growth and treatment of diamond, and to observe results of actual experiments. AOTC is one of the few producers of synthetic diamonds that have been very open in the past 10 years to share samples and information on growth technology. They were even willing to show us their research facility in The Netherlands.

Figure 45: Typically, three crystals of synthetic diamonds (each less than 1 ct) are produced during each growth cycle, but single crystals up to 3 ct (as shown here) and occasionally up to 8 ct have been produced. Photo by J. C. Zwaan.



Acknowledgements: We thank Alexei Zarakhani, CEO of AOTC, Canada, for supplying Figure 44 and for useful comments. Alexander Lisenkov is thanked for organizing our visit to the AOTC research facility in The Netherlands.

*Dr. J. C. (Hanco) Zwaan FGA
(hanco.zwaan@naturalis.nl)
Netherlands Gemmological Laboratory
Naturalis Biodiversity Center
Leiden, The Netherlands*

*Branko Deljanin FGA DGA
CGL-GRS Swiss Canadian Gemlab Inc.
Vancouver, British Columbia, Canada*

References

Choudhary D. and Bellare J., 2000. Manufacture of gem quality diamonds: A review. *Ceramics International*, **26**(1), 73–85, [http://dx.doi.org/10.1016/S0272-8842\(99\)00022-x](http://dx.doi.org/10.1016/S0272-8842(99)00022-X).

D’Haenens-Johansson U.F.S., Moe K.S., Johnson P., Wong S.Y., Lu R. and Wang W., 2014. Near-colorless HPHT synthetic diamonds from AOTC Group. *Gems & Gemology*, **50**(1), 30–45, <http://dx.doi.org/10.5741/GEMS.50.1.30>.

Pope S., Deljanin B. and Chapman J., 2016. Improving the color of diamonds through HPHT processing. *InColor*, No. 32, 17–20.

Borosilicate Glass Resembling Gem Crystals

At the February 2017 Tucson gem shows, authors LK and BML encountered some interesting objects that were handcrafted from borosilicate glass to recreate the aesthetic appearance of natural gem crystals. They were created by glass artist Jeremy Sinkus of Artisan Made Gemstones, Massachusetts, USA. On display in his booth and in his case at the Tucson Gem and Mineral Show were items resembling variously coloured tourmaline (including crystals, slices, cutting rough and faceted pieces), as well as replicas of aquamarine,

crystal clusters (simulating rock crystal and fluorite, tourmaline, etc.) and fossils (ammonites). Also present were various soda-lime glass items such as drinking glasses, vases and lamps with crystal-themed motifs (e.g. Figure 46).

Sinkus is a former mineral collector who first displayed his gem crystal simulants at the August 2016 East Coast Gem, Mineral & Fossil Show in Springfield, Massachusetts. He then brought several hundred pieces to Tucson, including some of his newest creations, resembling kunzite, pur-

Figure 46: A variety of borosilicate glass objects were on display at the Tucson Gem and Mineral Show, including many pieces that imitated tourmaline as variously coloured crystals, slices and faceted pieces (left). Also shown (right) are replicas of aquamarine crystals and an ammonite, as well as artistic soda-lime-type drinking glasses that resembled colour-zoned tourmaline crystals. The largest ‘crystal’ in the left photo measures ~7 cm tall, and the ‘ammonite’ in the right photo is ~4 cm long. Photos by B. M. Laurs.





Figure 47: This sample of borosilicate glass was sliced into two pieces and examined for this report. The length of the larger piece is 30 mm. Photo by Lore Kiefert.

ple apatite and pale pink or blue danburite. The overall shape/form of the pieces, as well as surface details such as striations and growth marks, are imparted during the glassmaking process, and then the crystal models are finished by hand-lapping flat faces for their terminations. The different colours of the glass are controlled by the addition of various substances, along with the temperature and time they are held in the kiln. Due to the high heat needed to work borosilicate glass (typically around 1,650°C), the size of the pieces is limited by the amount of glass that can be heated by torches to attain the working temperature; Sinkus' largest multi-coloured tourmaline 'crystal' measures 6.3 × 15.2 cm.

The Gübelin Gem Lab acquired a dark greenish blue 'crystal' that weighed 15 ct and sliced it into two pieces for analysis (Figure 47). It possessed a trigonal-shaped cross-section and had fine parallel striations along its length, as commonly seen on tourmaline crystals. In cross-section, it had a pink core and a dark greenish blue rim. The RI value was 1.480 and the average hydrostatic SG was 2.27. It was inert to long- and short-wave UV radiation. Microscopic observation showed swirly and uneven features within both colours of the glass, and along the boundary between them, which gave an artificial impression (Figure 48a,b). Also seen were multiple tube-like inclusions that were arranged parallel to the length of the piece (Figure 48c); with higher magnification, these could be identified as elongated bubbles.

A cross-section of one of the slices was analysed by laser ablation inductively coupled plasma mass spectrometry (LA-ICP-MS), and Table I gives the chemical concentrations of the most relevant elements in the core and rim of the specimen.

Table I: Representative LA-ICP-MS trace-element analyses (in ppmw) of the borosilicate glass imitation of tourmaline in Figure 47.*

Element	Rim 1	Rim 2	Core 1	Core 2
Li	21	10	21	15
B	31713	31287	30506	30379
Na	29893	28561	26674	27128
Mg	96	210	119	124
Al	19518	18331	17621	16983
K	1106	1212	1162	888
Ti	95	75	23	33
V	5.2	10	2.5	3.1
Cr	500	433	31	14
Mn	19	15	9.4	13
Fe	314	488	135	95
Co	272	259	3.38	1.90
Rb	2.3	3.2	33	31
Sr	11	8.4	5.0	7.3
Y	5.4	5.6	7.1	5.3
Zr	1552	541	595	517
Cs	2.0	3.6	1.8	2.6
Ba	13	12	21	19
La	2.3	1.5	0.9	1.2
Ce	14	13	10	8.6
Nd	174	162	4.9	3.5
Er	27	29	26055	25492
Tm	<0.79	<1.0	3.3	2.6
Hf	36	13	15	13
W	1.7	<2.1	16	13
Pb	0.55	<0.82	1.1	0.80
Bi	2.0	<1.0	2.4	1.0
Th	2.5	1.2	1.4	<0.58

* Data are from laser spots of 100 µm in diameter, with a laser energy of 3 J/cm² and a 20 Hz pulse rate. Helium was the carrier gas and argon was the plasma and cooling gas. All values are normalized against NIST 610 glass using Al as an internal standard.

The glass was found to be composed mainly of Si, together with B, Na and Al. Compared to the pink core, the greenish blue rim comprised significantly greater values of Cr, Co, Fe, Ti and Nd. The pink core was enriched in Er, and also contained slightly higher Rb, Tm and W. Fairly constant values in both zones were measured for trace elements such as Ce, Hf and Ba; these were most probably related to the basic glass material.

The sharp border between the rim and core sections is clearly evident in the LA-ICP-MS line scan shown in Figure 49. The abrupt change in

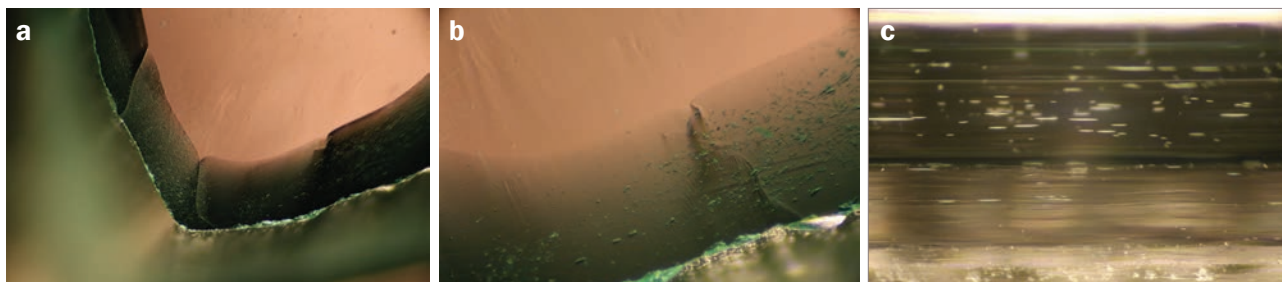
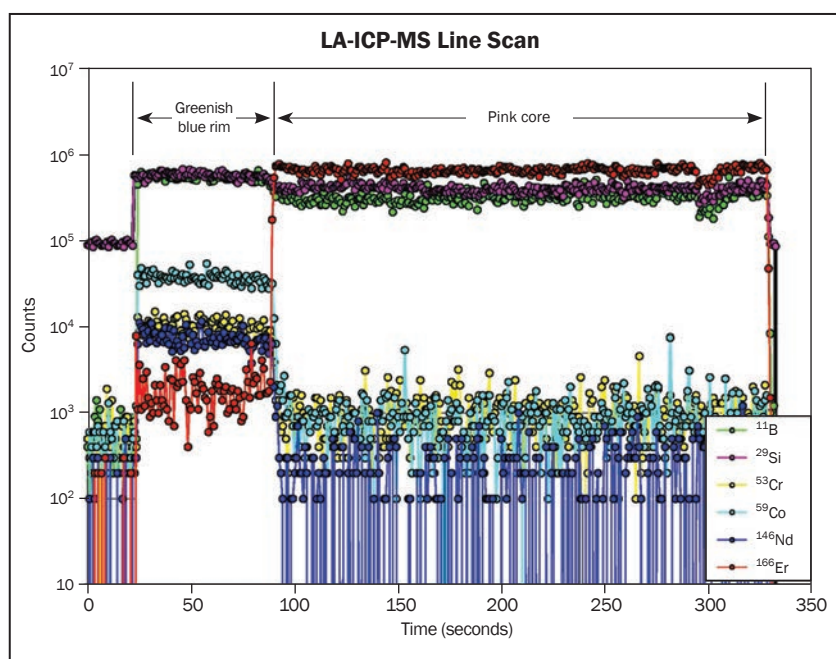


Figure 48: Colour swirls are seen in both the pink and greenish blue areas of the glass, and the colour boundary shows uneven curved surfaces that would not be seen in natural tourmaline (a,b). Tube-like inclusions with tapered pointy ends are arranged parallel to the length of the sample (c). Photomicrographs by B. Huber; magnified 50× (a), 65× (b) and 40× (c).

Figure 49: This LA-ICP-MS line scan across a slice of the glass tourmaline replica starts on the greenish blue rim and ends in the pink core. During the analysis, the laser traversed the sample at a speed of 11 microns per second (total length 3.4 mm) with a pulse rate of 30 Hz. (The first 20 seconds represent the background before turning on the laser.) This method is useful for visualizing chemical differences between the colour zones for several elements according to the counts obtained, which can then be converted to chemical concentrations, as partially reported in Table I.



composition between the two colour zones could point to a two-step manufacturing process in which the pink core was made first, and then in a later step after cooling and hardening the greenish blue rim was applied as a second layer.

Beryl Huber (beryl.huber@gubelingemlab.com),
Klemens Link and Dr Lore Kiefert FGA
Gübelin Gem Lab, Lucerne, Switzerland

Brendan M. Laurs FGA

Synthetic Ruby Resembling Burmese Ruby

Synthetic corundum displaying a natural-like sheen has been known in the trade for years (e.g. Choudhary, 2009), although it is not encountered very often. In addition, there have been reports of a few treated (e.g. fracture-filled) synthetics that are particularly reminiscent in appearance of natural stones (e.g. Choudhary, 2008). Recently this author received for identification another such example—a 6.20 ct bright purplish red syn-

thetic ruby with a strong sheen effect and eye-visible orange-stained fractures (Figure 50).

Identification of the specimen as ruby was straightforward by its standard gemmological properties, and at first glimpse it appeared natural because of the strong sheen, surface-reaching orange-stained fractures (consistent with iron staining) and the cutting style. The pavilion of the sample was not properly faceted, and had a large



Figure 50: Left: This 6.20 ct bright purplish red oval cut with pronounced orange fractures was identified as a synthetic ruby. Note also the subtle milkiness throughout the sample. Right: The pavilion of the synthetic ruby exhibits a large cavity instead of a culet, which is a common cutting style in 'old' stones originating from Burma (Myanmar). Also visible is a strong sheen effect in some areas. With this combination of features, this synthetic could easily be mistaken for a natural ruby. Photos by G. Choudhary.

cavity instead of a culet (Figure 50, right)—a cutting style that is commonly seen in 'old' stones originating from Burma (Myanmar). The presence of the sheen made this presumption stronger.

When observed with a microscope, the sheen effect appeared to be caused by fine particles (pinpoints) and short needles (Figure 51), mainly restricted near the surface, forming subtle zones. These pinpoints and needles had a diffused appearance, so their orientations could not be discerned. Such an inclusion pattern has been seen previously in synthetic star corundum and in natural corundum with asterism induced by the diffusion of titanium oxide (e.g. Mayerson, 2001). Surface-reaching fractures displayed thick,

granular orange material not commonly associated with natural iron-stained films. These two features were sufficient to raise doubt about a natural origin for this sample. Careful observation with transmitted light revealed curved growth lines as well as curved zones of minute particles (Figure 52), as commonly seen in Verneuil synthetics. Interestingly, some planes consisting of minute droplets reminiscent of 'fingerprint' inclusions also were present (Figure 53), as were some elongated or 'bomb-shaped' gas bubbles.

For the record, the specimen glowed bright red under long-wave UV radiation, while short-wave UV yielded a chalky blue fluorescence mainly restricted to the surface, with an internal red glow.

Figure 51: Minute particles and short needles cause the sheen effect in the synthetic ruby. Also note the subtle zoning (see arrows). Photomicrograph by G. Choudhary; image width 5.5 mm.

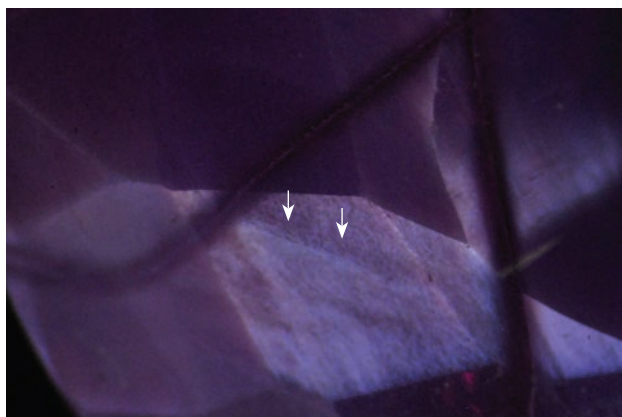
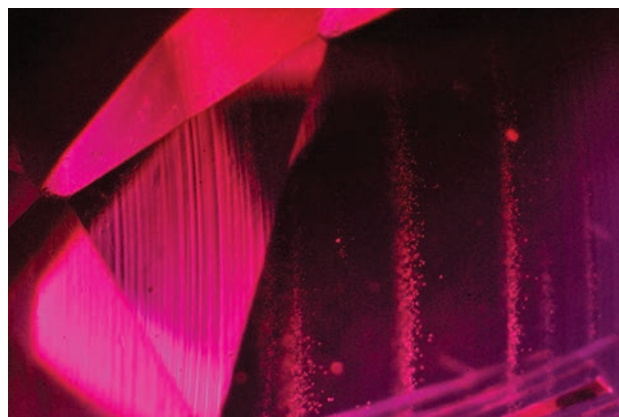


Figure 52: Curved growth lines and curved zones of minute particles confirmed the 6.20 ct sample as Verneuil synthetic ruby. Photomicrograph by G. Choudhary; image width 5.1 mm.



The overall features suggest that this synthetic ruby had undergone multiple treatment processes: first to induce sheen-causing titanium oxide inclusions, followed by quench crackling and impregnation with an orange substance. Further, this specimen also reminds us that synthetics can still be very tricky to identify—not only for novice gemmologists, but also for experienced gem dealers—making a buying decision much more challenging, especially in situations where only limited gem-testing tools are available.

*Gagan Choudhary FGA (gagan@gjepcindia.com)
Gem Testing Laboratory, Jaipur, India*

References

- Choudhary G., 2008. Gem News International: Two interesting synthetic rubies. *Gems & Gemology*, **44**(3), 279–281.
- Choudhary G., 2009. Synthetic sapphires with ‘natural-like’ sheen. *Gems & Jewellery*, **18**(3), 6–9.

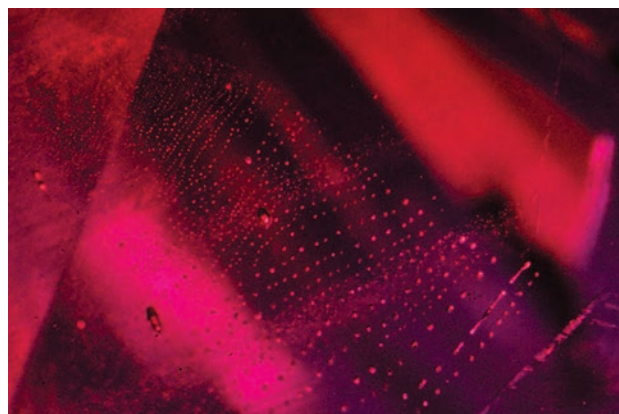


Figure 53: A plane of droplets reminiscent of a ‘fingerprint’ inclusion was present in the synthetic ruby. Photomicrograph by G. Choudhary; image width 5.1 mm.

- Mayerson W., 2001. Gem Trade Lab Notes: Sapphires with diffusion-induced stars. *Gems & Gemology*, **37**(4), 324–325.

‘Sea Sediment Jasper’, a Dyed Composite Material

In January 2016, author FS acquired a pendant of so-called ‘Sea Sediment Jasper’ (Figure 54) while visiting New Zealand. Equivalent material has been offered on the Internet under this and other trade names such as ‘Emperor Jasper’ for years. Observed with the unaided eye, this sample consists of a composite of coloured fragments in a reflective metallic matrix. The disc in the present pendant was offered and described as follows: “Pyrite and coloured Sea Sediment Jasper make up these totally unique stones....We know that it is a jasper material from Africa but no one in the market knows what exactly to call it yet....”

The hydrostatic SG of the sample was determined as 2.45, and the spot RI reading of the most readable surfaces yielded a value of around 1.53–1.56. Microscopic observation showed that the sample was held together by a matrix of colourless material, into which fragments of pyrite (identified by Raman spectroscopy) were embedded (Figure 55). Each of the main colourful pieces showed a heterogeneous colour distribution and resembled marble or some other sedimentary rock that evidently had been dyed. The colour was concentrated in fractures and around the edges of the fragments, and was dispersed



Figure 54: This pendant, marketed as ‘Sea Sediment Jasper’, consists of a flat, slightly curved round piece that is polished on one side, with a diameter of 4 cm and a thickness of 7 mm. Courtesy of the German Gemmological Association.

throughout each piece to varying degrees depending on the texture of the material, indicating the presence of an artificial dye.



Figure 55: Microscopic observation of the surface of the sample in Figure 54 shows differently coloured areas with heterogeneous colour distribution, including some fragments that appear to be partially without colouring. The reflective metallic matrix consists of a colourless substance embedded with fragments of pyrite. Photomicrograph by F. Schmitz; magnified 30 \times .

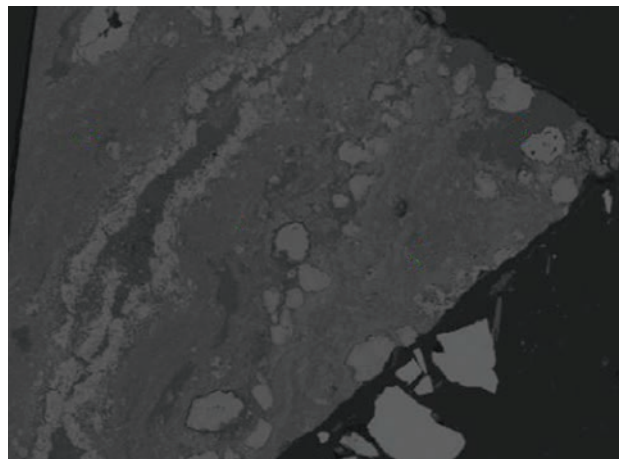


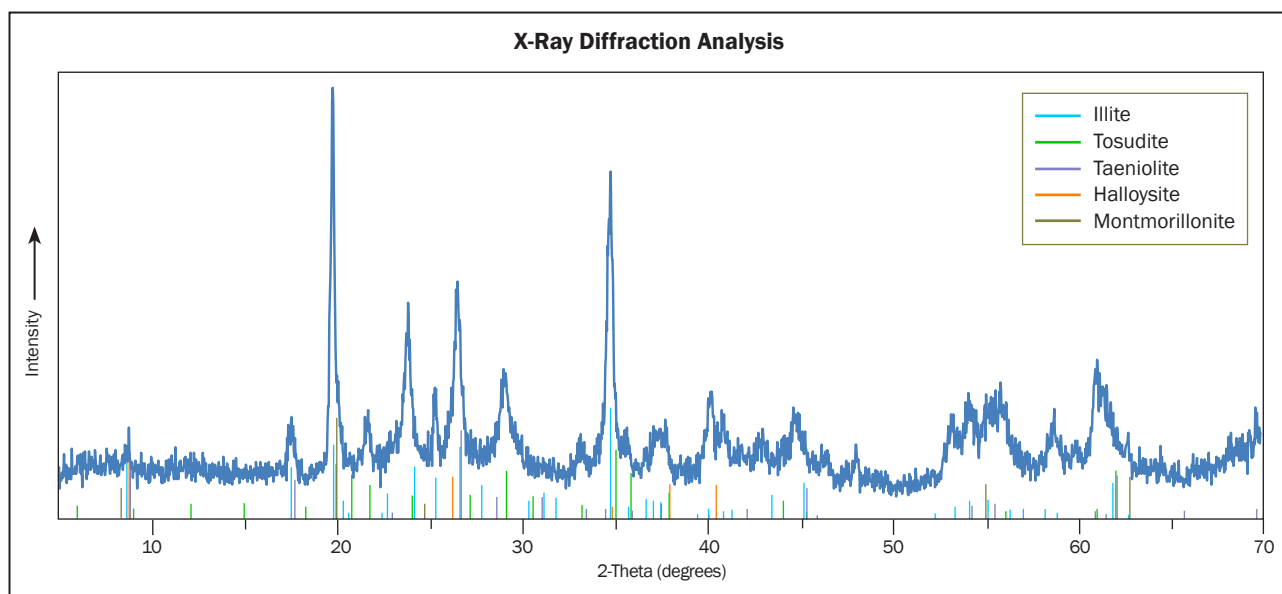
Figure 57: This backscattered-electron image obtained with an electron microprobe reveals the compositional differences of various fragments in the 'Sea Sediment Jasper', as shown by different grey tones. The brightest areas in the lower right consist of pyrite, and the darkest area on the left is the polymer binding agent. Magnified 45 \times .

To characterize the coloured components, X-ray diffraction was conducted on a small powdered sample with a Seifert XRD 3000 TT instrument using RayfleX ScanX software. The results showed a mixture of several clay minerals: illite, tosudite, taeniolite, halloysite and montmorillonite (Figure 56). Therefore, the coloured fragments consist of clay rocks with a high percentage of layered silicates (Brinkmann et al., 1967), and this was confirmed with infrared spectroscopy (Oinuma and Hayashi, 1965; Farmer, 1974). Such material might best be called mudstone (with no carbonate content, as

it did not react to hydrochloric acid). Backscattered-electron imaging of the coloured fragments with a Jeol JXA-8200 electron microprobe showed greyscale variations corresponding to differences in composition, and further revealed details of the texture of the material (Figure 57). In addition, microprobe analysis showed greater amounts of Ti in the more colourful parts of the sample, suggest a Ti-containing colourant.

Raman spectroscopy revealed an artificial polymer as the colourless binding agent holding together the fragments. The pyrite pieces evidently

Figure 56: X-ray diffraction analysis of the main coloured components of the 'Sea Sediment Jasper' revealed several clay minerals.



were added to the polymer to create a metallic lustre in the matrix.

The name 'Sea Sediment Jasper' is deceptive, as this is a dyed composite material that does not contain any microcrystalline quartz but only clay minerals. By comparison, a reference sample of natural 'porcellanite' in our collection consists of clays and other minerals such as feldspar and quartz.

*Fabian Schmitz (f.schmitz@dgemg.com)
and Tom Stephan
German Gemmological Association
Idar-Oberstein, Germany*

*Dr Stephan Bubre
Institute of Petrology
University of Mainz, Germany*

References

- Brinkmann R., Correns C.W., Schmidt-Thomé P. and Frechen J., 1967. *Lehrbuch der allgemeinen Geologie*, Vols. 1–3. Ferdinand Enke Verlag, Stuttgart, Germany, 1,741 pp.
- Farmer V.C., Ed., 1974. *The Infrared Spectra of Minerals*. Mineralogical Society, London, 539 pp.
- Oinuma K. and Hayashi H., 1965. Infrared study of mixed-layer clay minerals. *American Mineralogist*, **50**(9), 1213–1227.

An Unusual Blue Synthetic Star Spinel

In late 2016, the Gem and Jewelry Institute of Thailand's (GIT) laboratory encountered an unusual 28.21 ct blue synthetic spinel that displayed a six-rayed star (Figure 58). Although various synthetic spinels have been reported previously in the literature (e.g. Nassau, 1980), this sample merited a more in-depth study due to the uncommon presence of its asterism.

We measured a spot RI value of ~1.72 and a hydrostatic SG of approximately 3.59. The sample displayed obvious cross-hatched anomalous double refraction (ADR) in the polariscope, and also exhibited strong pinkish red fluorescence to

long-wave UV radiation and strong chalky blue luminescence to short-wave UV. Such ADR and fluorescence behaviours are commonly displayed by blue flame-fusion synthetic spinel (Schwarz, 1981; Webster, 1994), whereas natural blue spinel displays a singly refractive polariscope reaction and is inert to UV radiation.

Observation with a gemmological microscope revealed various internal features indicative of a synthetic origin, such as a group of tiny gas bubbles (Figure 59, left) and dispersed stream-like minute inclusions (Figure 59, right) that were observed by using reflected light together with an oblique fibre-optic illuminator. These clouds of reflective inclusions were probably responsible for its asterism. Similar features have been documented (Nassau, 1981) near the surface of shallowly diffused star sapphires that create asterism by the exsolution of minute rutile needles, which are seen as stream-like clouds. The sample showed no evidence of oriented surface scratches that might have been applied to induce asterism.

The photoluminescence (PL) spectrum (obtained with a Renishaw inVia Raman spectrometer with 532 nm laser excitation) gave a broad emission band at ~689 nm that was similar to that of a reference sample of Co-bearing blue flame-fusion synthetic spinel. In contrast, the PL spectrum of our natural Co-blue spinel reference sample displayed a sharp Cr-related peak at 685 nm (Figure 60). The Vis-NIR spectrum (obtained with a PerkinElmer Lambda 950 spectrometer) of the cabochon displayed clear Co-related absorp-

Figure 58: This 28.21 ct blue synthetic star spinel (18.6 × 17.5 × 9.3 mm) was sent to GIT's laboratory for an identification report. Photo by C. Onlaor.



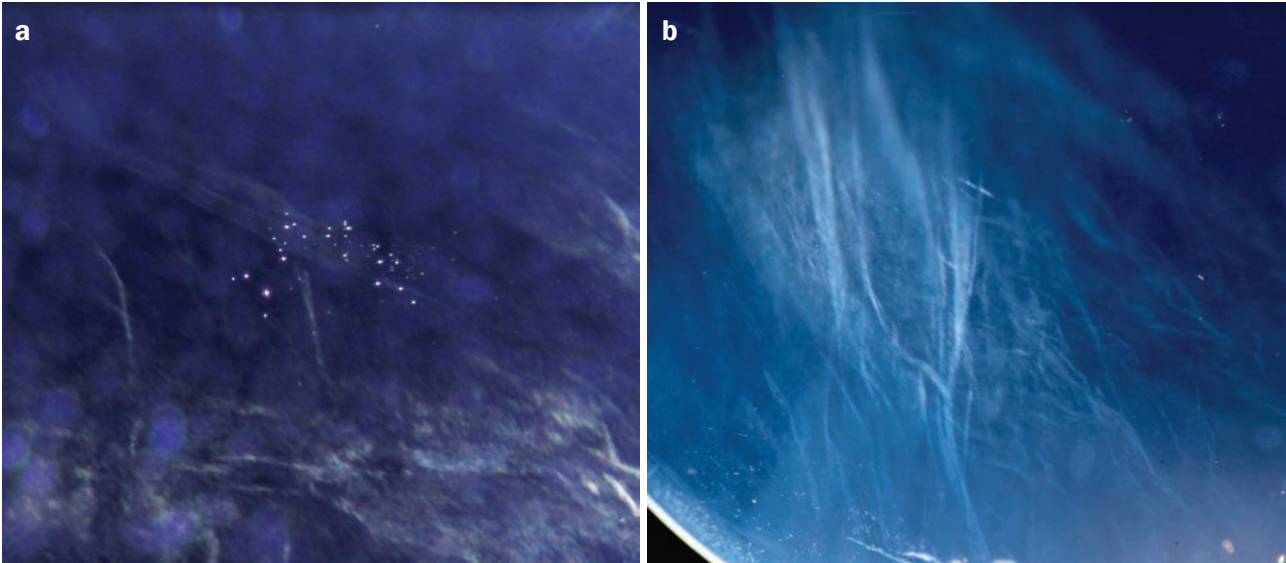


Figure 59: Internal features in the synthetic star spinel consist of a group of very tiny gas bubbles (left, image width 3.3 mm) and unusual stream-like minute inclusions when closely observed using reflected light combined with oblique fibre-optic illumination (right, image width 6.2 mm). These inclusions indicate a synthetic origin. Photomicrographs by S. Promwongnan.

tions at ~545, 580 and 625 nm (Muhlmeister et al., 1993), similar to those of our synthetic reference sample, while our natural blue spinel showed these Co features as well as an Fe-related peak at around 460 nm (Figure 61).

Semi-quantitative chemical analysis of the cabochon by EDXRF spectroscopy using an Eagle III system showed major amounts of Al and Mg with minor-to-trace levels of Si, Fe and Ga. As compared to the composition of our reference

samples of natural and synthetic blue spinels, the relatively low contents of Mg, Zn and Ga confirm its synthetic origin (Table II).

The gemmological properties (ADR and UV fluorescence), inclusion aspects, PL and absorption spectra, and chemical composition of the cabochon clearly indicate its synthetic origin. While asterism is not commonly seen in synthetic spinel, it may have resulted from post-growth heat treatment by inducing the partial exsolution

Figure 60: PL spectra are shown for the synthetic star spinel cabochon, together with our blue flame-fusion synthetic spinel and natural Co-blue spinel reference samples.

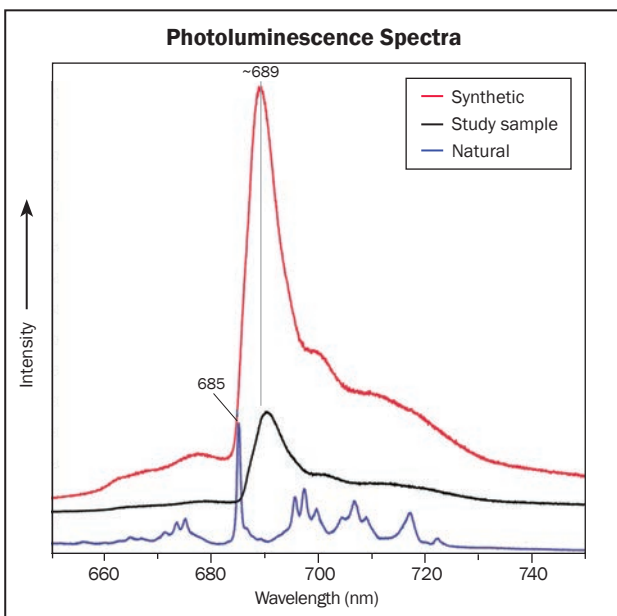
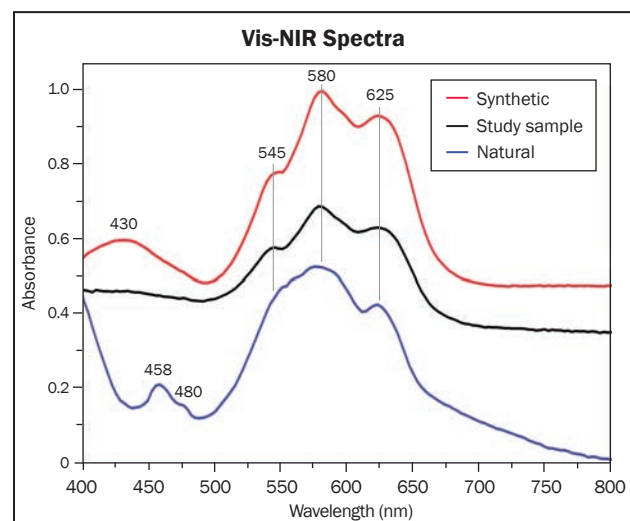


Figure 61: Vis-NIR spectra of the synthetic star spinel cabochon and our reference samples of blue flame-fusion synthetic spinel and natural Co-blue spinel display absorption bands at ~545, 580 and 625 nm due to cobalt, which produces their blue coloration. The natural sample also shows Fe-related features at around 460 nm.



of aluminium oxide, which could produce the reflective irregular stream-like minute particles (Webster, 1994; Steinbach, 2016; Hodgkinson, 2017). Such a process is known to create an adularescent-like or star effect in colourless synthetic spinel to imitate moonstone. Thus, a similar post-growth treatment may have been applied to this sample.

*Supparat Promwongnan, Papawarin Ounorn,
Marisa Maneekrajangsaeng and
Thanong Leelawatanasuk (lthanong@git.or.th)
GIT, Bangkok*

References

- Hodgkinson A., 2017. Practical Gemmology: Moonstone mystery. *Journal of Gemmology*, **35**(5), 378–379, <https://doi.org/10.15506/jog.2017.35.5.378>.
- Muhlmeister S., Koivula J.I., Kammerling R.C., Smith C.P., Fritsch E. and Shigley J.E., 1993. Flux-grown synthetic red and blue spinels from Russia. *Gems & Gemology*, **29**(2), 81–98, <https://doi.org/10.5741/gems.29.2.81>.
- Nassau K., 1980. *Gems Made by Man*. Chilton Book Co., Radnor, Pennsylvania, USA (see p. 246).
- Nassau K., 1981. Heat treating ruby and sapphire: Technical aspects. *Gems & Gemology*, **17**(3), 121–131, <https://doi.org/10.5741/gems.17.3.121>.
- Schwarz D., 1981. Chernismus und Fluoreszenzverhalten natürlicher und synthetischer Spinelle. *Uhren fuwelen Schmuck*, No. 20, 57–60.
- Steinbach M.P., 2016. *Asterism: Gems with a Star*. MPS Publishing and Media, Idar-Oberstein, Germany (see p. 243).
- Webster R., 1994. *Gems: Their Sources, Descriptions and Identification*, 5th edn., revised by P.G. Read. Butterworth-Heinemann, Oxford (see p. 149).

*Table II: Chemical composition obtained by EDXRF of the blue synthetic star spinel, a reference synthetic spinel and a natural Co-blue spinel.**

Oxide (wt.%)	Synthetic star cabochon	Synthetic reference	Natural reference
MgO	9.03	11.67	23.86
Al ₂ O ₃	89.49	87.89	73.07
SiO ₂	1.43	0.28	0.37
Fe ₂ O ₃	0.02	0.01	2.49
CoO	bdl	0.13	0.04
ZnO	bdl	0.01	0.12
Ga ₂ O ₃	0.01	bdl	0.03

* Abbreviation: bdl = below detection limit.

MISCELLANEOUS

The Gemstone Collection of the Natural History Museum in London

For more than 260 years, minerals, gemstones, gem materials and worked objects have been purposefully gathered to form one of the world's most outstanding mineralogical collections, housed at the Natural History Museum (NHM) in London. This report provides a brief overview of the gem collection at the NHM, as a prelude to a series of future Gem Notes and articles in *The Journal* about noteworthy specimens in the collection.

The collection contains around 185,000 specimens, of which some 5,000 are gemstones or worked objects. A number of the gems are on display in the historic systematic Mineral Gallery, unchanged since 1881, and additional highlights are visible to the public in 'The Vault' and as sparkling arrays of colour in the Earth's Treasury permanent exhibitions (e.g. Figure 62).

The collections of the NHM have their foundations with Sir Hans Sloane (1660–1753). As a

physician to royalty, he had the resources to both travel and collect widely. During his time, the sciences were in their infancy and collections were about exotic curiosities—flora, fauna, coins, books and minerals. At the time of Sloane's death his collection numbered 71,000 items, more than half of which were books. Sloane's will allowed Parliament to buy his collection for the undervalued sum of £20,000, and it was opened to the public in 1759 as the British Museum. It has since gone on to be separated into the British Library, the NHM and the British Museum. Sloane did not have a great interest in minerals, but we can trace certain gemstones and worked objects such as cameos, bowls and archers' rings back to his collection, dating them prior to 1753. Particularly notable is a 31.5 ct rose-cut blue sapphire set in a Mogul button.

As knowledge of mineralogy and crystallography progressed, the diversity of the NHM's



Figure 62: This image shows a small portion of one of the glittering arrays of gemstones on display in the Earth's Treasury gallery at the Natural History Museum. Courtesy of NHM London, © The Trustees of the Natural History Museum, London.

gem and mineral collections steadily increased. The strength of the gem collection is in its historic depth, and highlights include a wealth of early gem materials preserved from Ceylon/Sri Lanka and Burma/Myanmar, alluvial diamonds from the earliest discoveries in Brazil, opals from the then-new colony of Australia and some of the first diamonds from South Africa.

As a scientific institute, research by the mineralogical staff has led to many significant discoveries, including some of gemmological interest. The first specimens of sinhalite were discovered in the collection, erroneously documented as peridot, and significant donations facilitated by research have included the first specimens of taaffeite and the first two crystals of painite (once considered the world's rarest gem). Other important specimens or collections include:

- A range of gemstones obtained between 1906 and 1933 from Edward Hopkins, including a 598 ct morganite from Madagascar, obtained in 1913, which to our knowledge is the largest flawless faceted morganite in the world.
- A collection of gemstones set in rings from Lady Church, wife of chemist Sir Arthur H. Church, who was fascinated by their chemical and physical properties as well as their colours.
- Several Australian gemstones from Prof. Archibald Liversidge, acquired in 1927.
- An array of coloured diamonds and a 27 ct Mexican fire opal from T. B. Thornhill in 1934.
- A significant collection of both rare and fine gemstones from the Mogok region of Myanmar, including a 130 ct peridot, from Dr A. C. D. Pain.
- A choice collection of 268 fine gemstones, including at least 40 from Myanmar, from C. R. Mathews, obtained in 1993.

Perhaps the most significant development, adding some 1,500 gemstones, occurred when the gem and mineral collections of the Geological Museum were merged with the NHM in the 1980s. Highlights include a pale blue Brazilian topaz of 2,982 ct (the largest cut gemstone in the NHM collection), a 424 ct Brazilian kunzite, a 20 ct sillimanite from Myanmar (Figure 63), a 146 ct peridot from St John's Island in the Red Sea, a 57 ct padparadscha sapphire from Sri Lanka (Figure 64) and a diamond-studded gold snuff box given in 1867 to Sir Roderick Impey Murchison by Tsar Alexander II in recognition of his geological exploration of Russia (Figure 65).

The gemstone holdings of the NHM are amongst the most historically important preserved in any museum, and combined with one of the world's

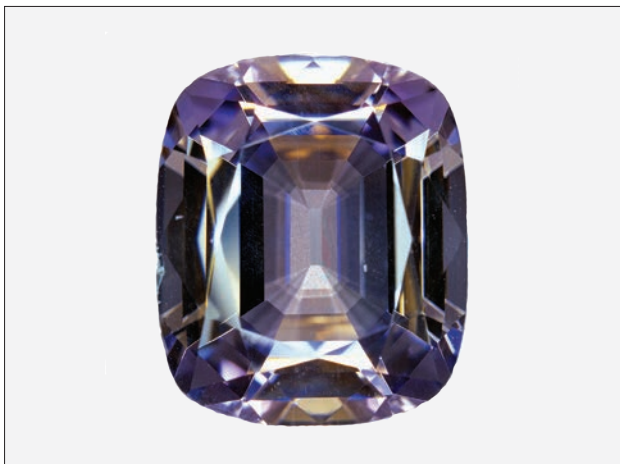


Figure 63: Among the numerous highlights of the gemstone collection at the Natural History Museum is this 20 ct sillimanite from Myanmar (BM.1985,MI29639). Courtesy of NHM London, © The Trustees of the Natural History Museum, London.

most extensive mineral collections, provide an impressive scientific, historical and cultural resource. In our most recent phase of strategic collection building, we are looking to expand representative examples of new finds and modern simulants, synthetics and treatments to continue to develop and

Figure 64: The Natural History Museum's 57 ct padparadscha sapphire from Sri Lanka (BM.1985,MI33163) is shown here with a 9.35 ct pink sapphire (BM.54811). Photo by Robert Weldon; courtesy of the Trustees of the Natural History Museum, London.



Figure 65: In 1867, this diamond-studded gold snuff box (~10 cm tall, BM.1935,1219) was given to Sir Roderick Impey Murchison by Tsar Alexander II, Emperor of Russia. It features an enamel portrait of the tsar. Courtesy of NHM London, © The Trustees of the Natural History Museum, London.

provide a complete scientific resource to serve the gemmological and mineralogical community for education, inspiration and research.

The public is welcome to browse the beta version of our collections catalogue at <http://data.nhm.ac.uk> by clicking 'Mineralogy', then 'Configure fields & filters', and then filtering the 'Specimen' field as 'Collection Kind' = 'Gems'.

*Robin Hansen FGA (r.hansen@nhm.ac.uk)
and Mike Rumsey*

*Earth Science Department
Natural History Museum, London*

*Alan Hart FGA DGA
Gem-A, London*

World Ruby Forum 2017



Bangkok, Thailand

In association with CIBJO Congress

4th November 2017

At Ballroom 1, Shangri - La Hotel, Bangkok

More Information please visit www.worldrubyforum.com



Distinction of Natural and Synthetic Ametrine by Microscopic Examination— A Practical Approach

Karl Schmetzer

Rough and faceted ametrine samples from the Anahí mine, Bolivia, were studied and compared with synthetic samples grown hydrothermally using seeds cut with various orientations and elongated in different directions. Examination with an immersion microscope yielded sufficient diagnostic features to allow differentiation between natural versus synthetic origin. Specifically, it was found that a combination of features could be used to distinguish natural from synthetic ametrine; these include the interference patterns caused by twinning, the orientation of violet/yellow colour boundaries, the orientation of growth striations and the appearance of the fluid inclusions.

The Journal of Gemmology, 35(6), 2017, pp. 506–529, <http://dx.doi.org/10.15506/JoG.2017.35.6.506>
© 2017 The Gemmological Association of Great Britain

Introduction

Ametrine is a quartz variety that contains both amethyst (violet to purplish violet or purple; hereafter, referred to simply as 'violet') and citrine (yellow to brownish yellow or yellow-orange; hereafter 'yellow') sectors within the same stone (e.g. Figure 1). Such colour-zoned violet/yellow natural quartz is available primarily from the Anahí mine in Bolivia (Koivula, 1980; Collyer et al., 1994; Vasconcelos et al., 1994; Laurs, 2001; Weldon, 2009). The synthetic counterpart is grown hydrothermally from iron-bearing solutions. Commercial production employs seed material consisting mainly of basal quartz plates (Balitsky et al., 1999, 2000, 2001). Iron is incorporated in different forms into the synthetics, resulting in yellow and colourless growth zones in the as-grown crystals. Irradiation then develops the desired bicoloured ametrine appearance, with yellow basal **c** growth sectors and violet rhombohedral **r** and **z** sectors (Balitsky

and Balitskaya, 1986, 2005, 2009). Additionally, it is possible in some cases to produce heat-treated ametrine using natural amethyst from specific localities. The treatment may lighten intense violet **r** growth zones and turn light violet **z** growth zones to light yellow (Neumann and Schmetzer, 1984).

Although infrared spectroscopy can be an effective tool for distinguishing natural and synthetic amethyst and ametrine (see, e.g., Kitawaki, 2002; Balitsky et al., 2004; Karampelas et al., 2005, 2011; and various references therein), microscopic examination will reveal information about twinning, colour zoning and occasionally also about inclusions—features that differ in natural versus synthetic ametrine (Crowningshield et al., 1986; Lu and Shigley, 1998; Balitsky et al., 1999; Notari et al., 2001; Hainschwang, 2009). Because it is a widespread practice in the trade to mix synthetic quartz into parcels of natural amethyst, citrine and ametrine, a simple method for separating these natural quartz varieties from their synthetic counterparts



Figure 1: Set in a gold ring, this ametrine from Bolivia weighs approximately 7 ct. Photo courtesy of Udo Reimann.

is commercially warranted. Furthermore, for such relatively low-priced goods, a cheap method for mass screening is highly desirable.

Within the past few years, a simple technique was suggested for discriminating between natural and synthetic ametrine, using standard gemmological tools such as the refractometer and polariscope (Payette, 2013). The method relied on the presence or absence of twinning in combination with the orientation of the violet/yellow boundary in faceted samples. Useful results were yielded by this method, provided the table facet had been cut at an appropriate orientation relative to the crystal structure. However, difficulties could occur with samples displaying other orientations, complex colour zoning and/or twin structures. Thus, the present study was under-

taken to evaluate if efforts at separation might be advanced by additional characteristic growth-related properties that could be easily seen in an immersion microscope, similar to the approach previously described in detail for natural and synthetic amethyst and heat-treated amethyst, the latter of which is transformed to citrine by the annealing process (Schmetzer, 1986, 1989; Kiefert and Schmetzer, 1991a,b,c). In so doing, it also became apparent that an investigation of the different seeding techniques used for producing the synthetic crystals would be key to understanding such diagnostic growth-related properties.

Natural Ametrine

The Anahí mine, which lies in the tropical rainforest of south-eastern Bolivia, is the only known commercial source of bicoloured amethyst-citrine quartz (i.e. natural ametrine; see again Figure 1). The mine has been operated since the early 1990s by *Minerales y Metales del Oriente*. Comprehensive descriptions of the mining operation were published by Collyer et al. (1994) and Vasconcelos et al. (1994), and Weldon (2013) provided a detailed update. Biste and Burgoa (2002) discussed the formation of ametrine at the Anahí mine.

Although open-pit mining is performed on a small scale, the main recovery of amethyst, ametrine and citrine at Anahí occurs underground via a system of shafts and tunnels. The unearthed material then undergoes initial sorting and washing before being transported to the company's processing facility (Figure 2) in the city of Santa Cruz.



Figure 2: These crystal clusters occupy the storage room of the company *Minerales y Metales del Oriente* in Santa Cruz, Bolivia. Only small portions of the crystals are of facetable quality. Photo taken in 1997; courtesy of Udo Reimann.

Figure 3: Quartz crystals from the Anahí mine are sawn and/or cobbled at the processing plant of the company *Minerales y Metales del Oriente*. Photo taken in 1997, courtesy of Udo Reimann. This process leaves irregularly shaped pieces of quartz (here, 5.7–9.3 g) that commonly exhibit a distinct colour boundary (inset photo by K. Schmetzer).



Most of the crystals are heavily included, with only a small percentage being gem grade. Extensive sawing and cobbing (hammering) is thus required to extract the clear gem-quality areas (Figure 3). Such operations are frequently begun on-site at the mine to reduce weight before transporting the goods to Santa Cruz. The clean material, estimated at several thousand kilograms per year, may be pre-shaped or cut in Bolivia. A significant percentage of the facetable gem material, however, is sold and cut elsewhere, mostly in Asia.

The combination of amethyst and citrine colours in natural ametrine from the Anahí mine has been attributed to colour zoning that differentiates rhombohedral **r** (violet) and **z** (yellow) growth sectors (Vasconcelos et al., 1994; Notari et al., 2001; Payette, 2013). However, in larger natural crystals, a sharp colour boundary is difficult to observe (Figure 4). Although the colouring mechanism is not completely understood, there are definite differences in Fe content between various growth sectors, with higher amounts in the yellow portions (Vasconcelos et al., 1994, 2002).

Synthetic Ametrine

A method for growing synthetic ametrine crystals was developed by Prof. V. Balitsky and his co-workers in the late 1980s at the research facilities of the USSR Academy of Sciences in Chernogolovka and Alexandrov, Russia. Detailed descriptions of the hydrothermal method employed and the

properties of the resulting synthetics were given in multiple publications (Balitsky and Balitskaya, 1986, 2005, 2009; Balitsky et al., 1999, 2000, 2001, 2004). The synthetic material has been commercially available since the mid-1990s (Johnson and Koivula, 1998).

A number of seeding techniques can be applied for ametrine synthesis, but commercial crystal growth is typically performed using rectangular colourless synthetic quartz seed plates cut perpendicular to the *c*-axis. Production with such seeds leads to a varied incorporation of colour-causing

Figure 4: Ametrine crystals from the Anahí mine can be rather large, as shown by this specimen, which measures approximately 7.5 cm in diameter and weighs 312 g. The violet/yellow colour boundary is not easily seen. Photo by K. Schmetzer.



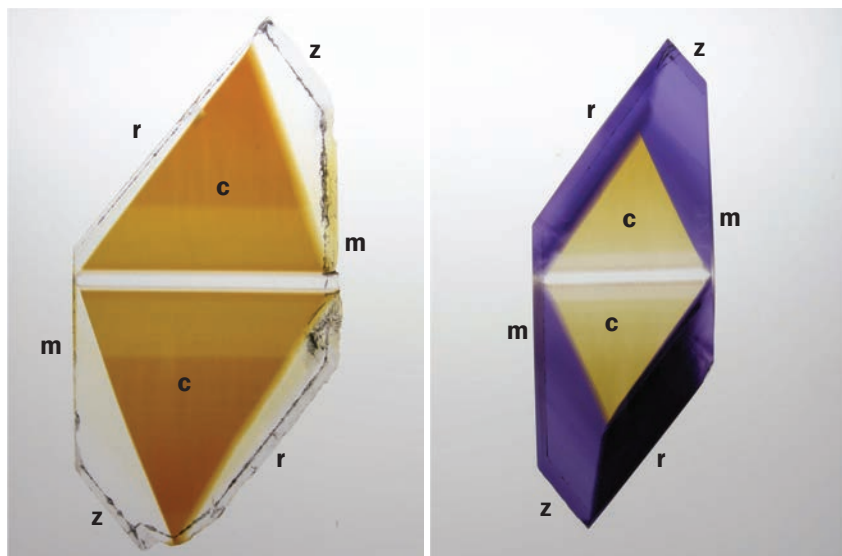


Figure 5: These slices of synthetic quartz show the colour zoning in as-grown crystals (left, 76 × 37 × 10 mm) and after irradiation (right, 63 × 22 × 10 mm). During irradiation, violet (amethyst) colour centres develop in the colourless **r** and **z** growth sectors, but the yellow citrine colour of basal **c** growth sectors remains almost unchanged. Photos by K. Schmetzer.

trace elements, mostly forms of iron, in different growth sectors. Growth rates of the crystal faces depend on temperature gradients in the autoclave. After crystal growth, all sectors of the as-grown crystals are either colourless or yellow to yellowish orange of variable intensity. The violet-to-purplish violet (amethyst) colour of certain sectors is then generated through irradiation, while the existing yellow (citrine) colour centres in general remain unaffected (Figure 5).

At slower growth rates, precursors of the amethyst colour centres (violet after irradiation) are incorporated in **r** and **z** growth sectors, and yellow colour centres are incorporated only in basal **c** sectors. However, with increasing growth rates, yellow colour centres are also developed in **r** and **z** sectors, along with a decreasing concentration of violet colour centres. The colours obtained are detailed by Balitsky and Balitskaya (1986), and a schematic drawing of colour intensity versus growth rates for **r** and **z** sectors is shown in Balitsky et al. (1999, 2000, 2001). As the growth rate increases (on a scale from 1 to 4, with 1 being the slowest and 4 the fastest), the resulting colour centres produce the colours after irradiation that are indicated in Table I.

Table I: Coloration of various sectors in synthetic ametrine according to growth rate.

Growth rate	r sector	z sector	c sector
1	Pale violet	Very pale violet	Yellow
2	Purplish violet	Violet	Yellow-orange
3	Brownish violet	Deep violet	Yellow-orange
4	Yellow	Brownish violet	Yellow-orange

To achieve the best yield for cutting attractive synthetic ametrine, growth rate 2 is selected for its ability to create intense violet **r** and **z** growth sectors along with deep yellow-orange **c** sectors. With growth rate 1, the colours of the **r** and **z** sectors are lighter. At growth rates 3 and 4, yellow colour centres develop in the **r** and **z** sectors, with a simultaneous decrease in violet colour intensity, thus leading to less desirable results.

The author was unable to obtain a complete picture regarding either which companies (e.g. in Russia, China and/or Japan) have ever produced or are presently growing synthetic ametrine (with or without also cutting), and/or which companies were or are only purchasing crystals and cutting this material for distribution through the Internet or at trade fairs. Nonetheless, it became clear that a portion of the purported ‘Chinese’ synthetic ametrine offered previously in the trade was grown in Russia and faceted in China.

Materials and Methods

The present study is based on a range of natural and synthetic ametrine material from multiple sources:

- faceted natural and synthetic ametrine obtained directly from the trade
- complete crystals and cobbled portions of natural ametrine from various collections
- slices of natural ametrine obtained by a German dealer directly at the mine in Bolivia and at the mine’s office in Santa Cruz

- complete crystals and slices of synthetic ametrine (grown with a variety of seeding techniques) from various collections. Some of these crystals and slices were donated by Prof. V. Balitsky to colleagues or friends, while other slices were cut from larger crystals grown commercially.

In summary, and in terms of quantities, the following materials were examined:

- natural ametrine: three complete crystals, nine cobbled gem-quality rough samples, 11 slices cut perpendicular to the *c*-axis and 68 faceted gemstones
- synthetic ametrine: nine complete crystals, 25 slices cut in various orientations and 25 faceted samples

The morphology, colour zoning and growth zoning of the crystals and oriented slices of natural and synthetic ametrine were examined visually with the naked eye or a loupe, as well as with a microscope in transmitted light.

In addition, the cobbled rough and the slices of natural ametrine, the smaller slices of synthetic ametrine, and all the faceted natural and synthetic samples were examined in a horizontal immersion microscope using benzyl benzoate as the immersion liquid. The techniques employed, particularly the use of a special sample holder with two rotation axes, were described in detail by Schmetzer (1986) and by Kiefert and Schmetzer (1991a,b,c). Note that some of the larger samples could not be examined in this way because their sizes precluded the use of an immersion cell.

Moreover, as a preface to the discussions that follow, it should be emphasized that, *in the opinion of the author, the use of an immersion cell and the application of crossed polarizers are necessary to recognize the diagnostic patterns described in this work.* Additional, more specialized equipment can be of assistance but is not mandatory. For example, use of a sample holder with both horizontally and vertically oriented rotation axes is helpful, but all examinations also can be performed with a ‘normal’ sample holder having only a single vertically oriented rotation axis. Likewise, employing various tools to determine angles between different growth structures can aid in *understanding* the features observed, but such measurement tools are not essential to *distinguish* natural and synthetic ametrine.

Results

Natural Ametrine—Cobbled Rough and Slices

Visual Appearance: As mentioned above, the violet/yellow (amethyst/citrine) colour boundaries can be difficult to observe in larger natural crystals, and this held true for a 312 g sample studied here (see again Figure 4). Its morphology was typical for such crystals, which normally show faces of the positive rhombohedron *r* {10 $\bar{1}$ 1} and the negative rhombohedron *z* {01 $\bar{1}$ 1}, occasionally with small prism faces *m* {10 $\bar{1}$ 0}. After such crystals have been sawn and/or cobbled to remove heavily included areas, the remaining facet-quality rough readily displays straight colour boundaries (Figures 3 inset and 6).

Figure 6: Slices of natural ametrine viewed parallel or almost parallel to the *c*-axis show variable colour distribution between violet *r* and yellow *z* growth sectors. In some of the samples, the *r* sectors include a range of hues from violet to purple. The samples weigh from 6.31 to 21.39 ct (sample 7, 20.3 × 19.5 × 5.4 mm). Photo by K. Schmetzer.



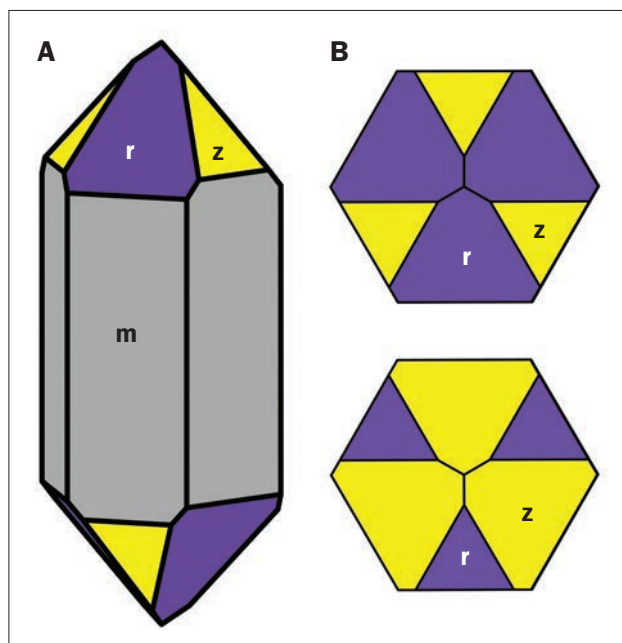


Figure 7: (A) This idealized natural quartz crystal with prismatic habit (clinographic projection) consists of **m** prism faces in combination with **r** and **z** rhombohedra. (B) Two examples of the colour distribution between violet **r** and yellow **z** growth sectors of different sizes are shown for such crystals when viewed parallel to the *c*-axis. The top one corresponds to the size of the rhombohedral faces in drawing A. Drawings by K. Schmetzer.

In idealized crystals such as depicted in Figure 7A, sectorial colour zoning with three-fold symmetry would be apparent, with variable sizes for the two rhombohedral **r** and **z** growth sectors (Figure 7B). However, most natural crystals are somewhat distorted and frequently reveal more complex patterns of growth and colour zoning when viewed as slices cut approximately perpendicular to the *c*-axis. Such slices studied here exemplified this situation, showing irregularities in both the size and the shape of the violet **r** and the yellow **z** growth sectors (Figure 6). Moreover, even within a single slice, the **r** growth sectors may exhibit a range of hues, with some appearing more violet and others more purplish violet or purple. Lighter and darker coloured stripes within **r** growth sectors, often with triangular shapes, could also be observed with the unaided eye in some samples.

Microscopic Examination: The immersion microscope was used to look for twinning features, to establish the orientation of the violet/yellow colour boundaries and the direction of growth striations relative to these boundaries, and to observe any characteristic inclusions.

Between crossed polarizers, especially after orienting the samples to a view exactly perpendicular to the *c*-axis, so-called Brewster fringes were visible in the violet **r** growth sectors of all samples (Figure 8). This interference pattern results from Brazil-law twinning in these sectors of the ametrine crystals. It is generally accepted that such areas consist of polysynthetically twinned lamellae of alternating right-handed and left-handed quartz. The fringes appear black because light travelling along the optic axis passes through almost equal distances (light paths) of right-handed and left-handed quartz. Hence, for purposes of the following discussion, and particularly when describing rotations and angles, the *c*-axis of a sample is assumed to be oriented parallel to the microscope tube if the Brewster fringes appear sharp and black between crossed polarizers.

In slices where darker violet stripes within the **r** growth sectors were visible even to the unaided eye in normal lighting, the Brewster fringes proved to be coincident with this colour zoning. The convoluted patterns observed demonstrated the complexity of the violet and yellow colour zoning present in these highly distorted samples (see again Figure 6).

The violet/yellow colour boundaries between the **r** and **z** sectors ran more-or-less parallel to the *c*-axis and parallel to the **m** prism faces, with a maximum deviation of up to 10°. As the samples were rotated about various axes, growth striations could be seen repeatedly in the violet parts in certain orientations, but none were found within the yellow areas. The striations in the violet growth zones were parallel to the rhombohedral **r** faces and inclined to the violet/yellow colour boundary (Figure 9). However, it should be noted that in the directions of view revealing the striations, the violet/yellow boundary was not an exact plane but fluctuated somewhat within the crystals, especially from the centre to the rim.

With the violet/yellow colour boundary oriented east–west in the microscope and using a north–south rotation axis (i.e. parallel to the main vertical axis of the sample holder and perpendicular to the colour boundary), it was possible to more specifically establish the orientations in which the growth striations in the violet sectors could be seen, as follows. Starting with a view oriented parallel to the *c*-axis (Figure 10, top), in which the Brewster fringes were visible, the **r** growth striations became evident after rotating the sample through an angle of about 40°. This

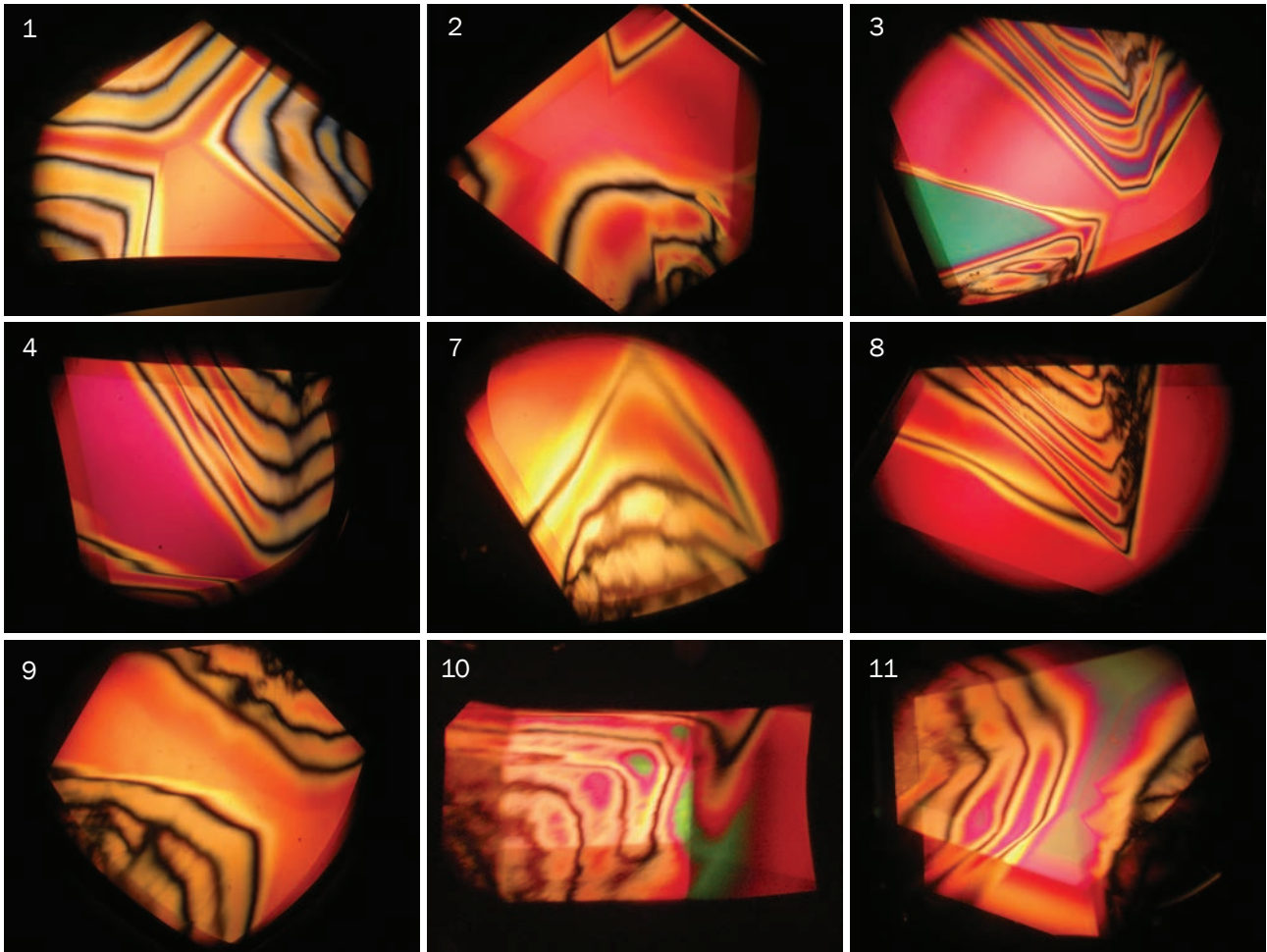
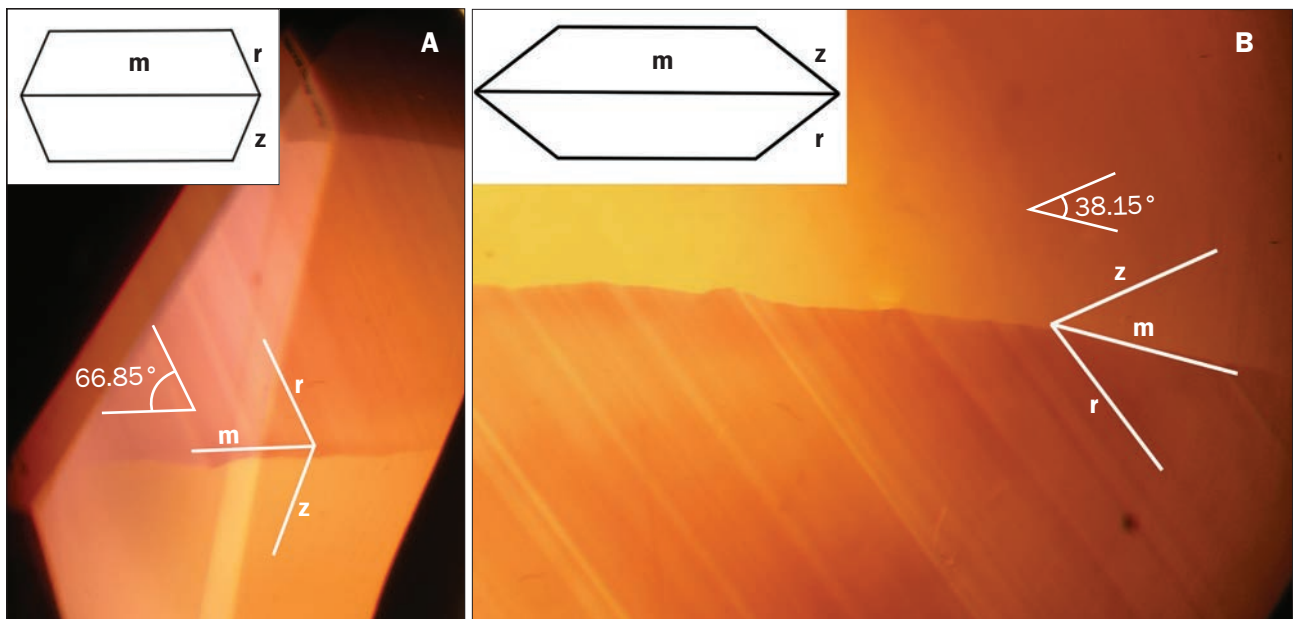


Figure 8: Between crossed polarizers, the samples depicted in Figure 6 show interference patterns (Brewster fringes) that indicate Brazil-law polysynthetic twinning of the violet *r* growth sectors. Photomicrographs by K. Schmetzer, in immersion.

Figure 9: In natural ametrine, the colour boundary between the violet *r* and yellow *z* growth zones more-or-less follows a prismatic *m* crystal face but is not exactly planar. In addition, growth striations are present in the violet *r* sectors, and they are parallel to an external *r* face and inclined to the violet/yellow boundary. The angle between the growth striations and the colour boundary measures approximately (A) 67° or (B) 38°. Photomicrographs by K. Schmetzer, in immersion; field of view (A) 7.5 × 10.0 mm and (B) 9.5 × 7.1 mm.



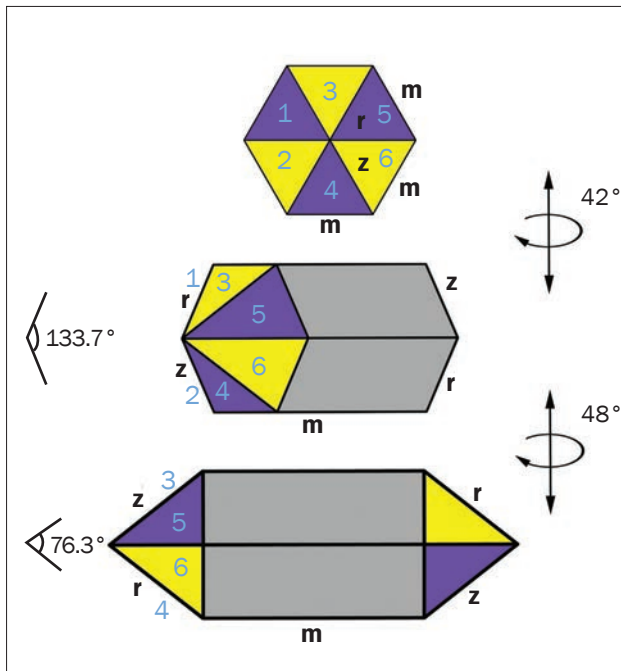


Figure 10: Three views of an idealized natural ametrine crystal are shown in this diagram: parallel to the *c*-axis (top), after rotation through an angle of 42° (centre), and after further rotation through an additional angle of 48° (bottom). The orientation shown at the top exhibits differently coloured *r* and *z* growth sectors, and crossed polarizers will reveal Brewster fringes caused by polysynthetic twinning on the Brazil law, as seen in Figure 8. After rotation through an angle of 42° (centre), the *r* and *z* faces labelled 1 and 2 are parallel to the direction of view, as seen in Figure 9A. After further rotation through an additional angle of 48° (bottom), the *r* and *z* faces labelled 4 and 3 are parallel to the direction of view, as seen in Figure 9B. Drawings by K. Schmetzer.

situation is drawn schematically in Figure 10-centre. The *m* prism faces were then oriented east-west, and adjacent *r* and *z* planes of the crystal (labelled 1 and 2) were parallel to the direction of view (Figure 9A). These rhombohedral faces formed an angle of 133.7° with each other, and the exact rotation angle was calculated as 42.2° . Half of the 133.7° angle (i.e. 66.85°) was measured between these growth striations and the dominant violet/yellow colour boundary.

After further rotation through an additional angle of 47.8° (for a total rotation of 90°), a view exactly perpendicular to the *c*-axis was obtained. At that point, other *r* and *z* faces (labelled 4 and 3, respectively) were oriented parallel to the direction of view, and striations were again potentially visible in the microscope (e.g. Figure 9B). This situation is represented in Figure 10 (bottom). The angle between the *r* and *z* planes in

this orientation measured 76.3° . Half of the 76.3° angle (i.e. 38.15°) was measured between these growth striations and the dominant violet/yellow colour boundary.

The inclusions in the slices consisted only of fluid inclusions, as described below for the faceted samples.

Natural Ametrine—Faceted Samples

Visual Appearance: Commercial ametrine gemstones seen in the trade are normally faceted in a direction and shape which shows a single colour boundary across the table facet, as were most of the samples studied here (Figure 11). Only in a small percentage of samples were two colour boundaries observed. The colour boundaries were frequently more obvious when viewed from the pavilion side. Zoned faceted quartz from the same mine in Bolivia with very light yellow to near-colourless and more intense yellow portions are described in Box A.

Microscopic Examination: The optical properties of the faceted samples were consistent with those described above for the oriented slices. When the optic axis was oriented exactly parallel to the light path of the microscope, complex interference patterns were observed with Brewster fringes corresponding to the violet sectors of the stones (Figure 12). Upon then turning the stones with the colour boundary oriented perpendicular to the rotation axis of the sample holder, growth striations appeared at certain intervals (Figure 13). More specifically, and as already detailed for the natural ametrine slices, rotating a faceted sample about an axis perpendicular to the colour zoning led to orientations revealing two particular features: interference patterns with Brewster fringes in a view parallel to the *c*-axis (Figure 12) and, after a rotation of 42.2° , growth striations parallel to rhombohedral *r* faces (Figure 13A; see again Figure 10-centre).

However, in contrast to the situation typically apparent for the slices, continuing to rotate a faceted stone without removal from the sample holder did not, in general, unveil any additional growth striations. Their absence can be explained by the fact that these faceted ametrines consisted only of two of the six rhombohedral *r* and *z* growth sectors (labelled 1 and 2 in Figure 10). Consequently, because the other sectors (labelled 3 to 6 in Figure 10) were not present in most

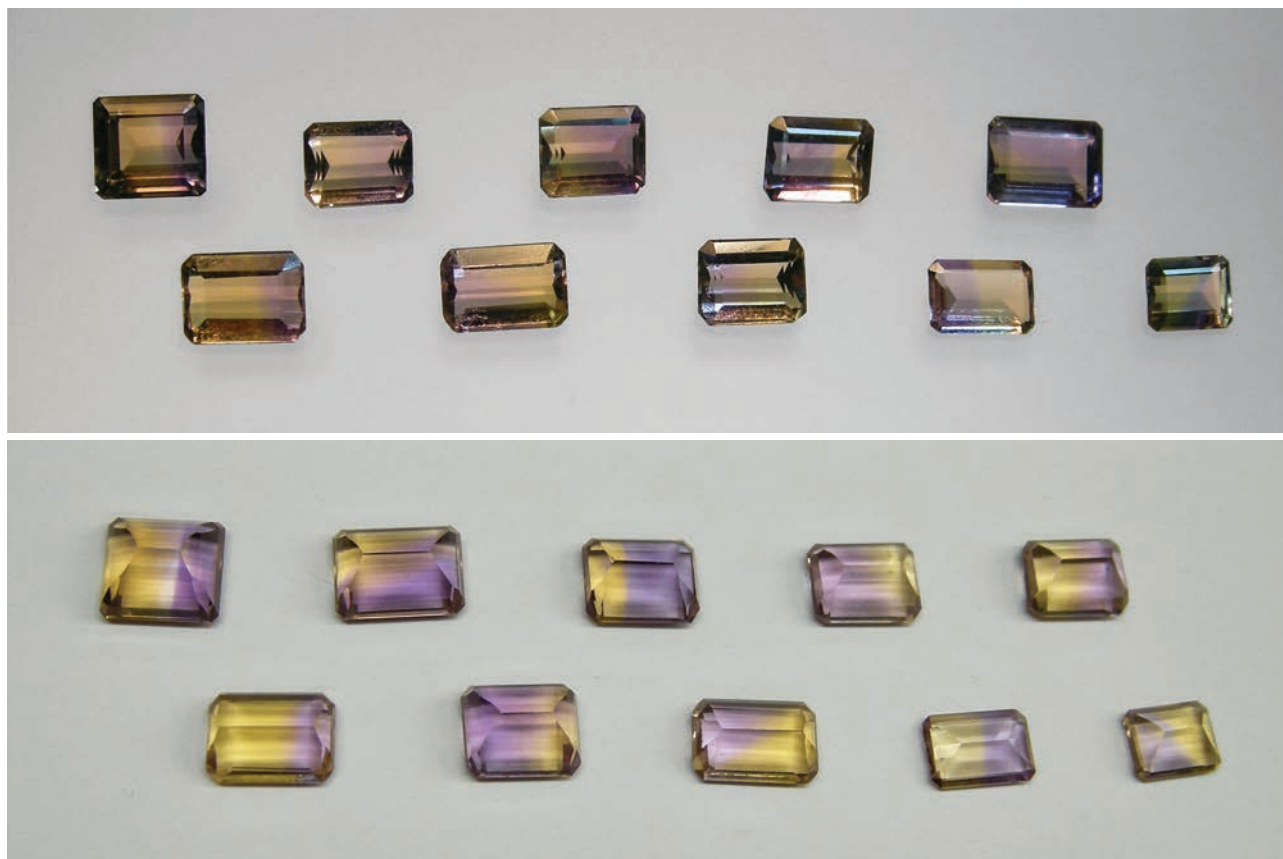


Figure 11: Faceted natural ametrine gemstones from Bolivia typically display only two colour zones, as seen here viewed toward the table facets (top) and toward the pavilions of the same samples (bottom). The stones weigh from 2.45 to 7.45 ct (upper left, 11.7 × 10.8 mm). Photos by K. Schmetzer.

faceted samples, the growth striations in such sectors could not be seen. Nonetheless, in less common faceted samples such as those with two violet/yellow growth boundaries, the possibility remained for locating further growth striations in a view perpendicular to the c-axis, as described for the slices (Figure 13B, see again Figure 10, bottom). Likewise, it should be emphasized that the foregoing applies to a rotational sequence starting from an orientation in which Brewster fringes are observed, but with other starting orientations and/or other rotation axes a different scenario of observations could unfold.

Most of the faceted ametrines obtained from the trade were generally free of inclusions. However, negative crystals in the form of two-phase inclusions were seen occasionally (Figure 14A). Somewhat more common were partially healed fractures, sometimes consisting of elongated fluid inclusions (Figure 14B). The shapes and orientations of the liquid and two-phase inclusions trapped in the partially healed fractures reflected the internal structure of the polysynthetically

twinned crystals and their lamellar microstructure. In particular, a specific parquet-like zigzag pattern of fluid trapped in elongated voids revealed the complex polysynthetic twinning of the violet areas on the Brazil law (Figure 14C). An analogous scenario was previously described for inclusions in natural amethyst (Schmetzer, 1987), and a similar pattern has been seen after etching polished amethyst surfaces (Lu and Sunagawa, 1990; Lu et al., 1990).

Synthetic Ametrine—Crystals and Slices

Variations in Seed Plates, Crystal Morphology and Colour Zoning: Synthetic ametrine is grown by the hydrothermal technique using seeds cut with various orientations and elongations, as described below. Consequently, multiple types of samples must be investigated in any effort to determine whether it is possible to distinguish natural from synthetic ametrine based on, for instance, the orientation of the violet/yellow boundary. In Figure 15A and B, an idealized synthetic crystal with five dominant faces is drawn as

Box A: 'Luna y Sol' Quartz

During the course of the present study involving bicoloured quartz of the traditional violet/yellow variety, the opportunity also arose to examine two faceted samples exhibiting a more unusual bicoloured appearance. These consisted of quartz with very light yellow to near-colourless and more intense yellow portions, referred to in the trade as 'Luna y Sol' (moon and sun) or 'Lunasol' (Figure A-1). They had been obtained by a German dealer at the headquarters of the Anahí mine in Santa Cruz, Bolivia. Such faceted samples have been depicted in earlier publications, and it also has been mentioned that slices of ametrine from Anahí may consist of violet (amethyst), yellow (citrine) and nearly colourless zones (Vasconcelos et al., 1994).

The two samples examined by the author showed a planar boundary between the light yellow zone and the more intense yellow portion. The boundary was oriented parallel to the c-axis, thus corresponding to the violet/yellow boundary in natural ametrine. The stones were optically untwinned single crystals in which neither zone showed a specific interference pattern or any Brewster fringes under crossed polarizers. No growth striations were observed in either part.

Similar bicoloured near-colourless and yellow quartz was mentioned by Henn and Schultz-Güttler (2012). These authors noted that the material can be produced by heat



Figure A-1: Faceted colour-zoned quartz consisting of a lighter yellow, almost colourless, zone and a more intense yellow zone is referred to as 'Luna y Sol' or 'Lunasol' in the trade. These examples weigh 3.17 ct (left, 10.0 × 8.0 mm) and 2.14 ct (right). Photo by K. Schmetzer.

treatment of colour-zoned amethyst from Bolivia or Brazil. However, after a transformation of amethyst to citrine by heat treatment, the typical polysynthetic twin pattern of amethyst is not removed (Schmetzer, 1989). Thus, the lack of twinning in the two samples described in the present study indicates that they are unheated and may consist of two citrine growth zones (i.e. nearly colourless/yellow zones of different colour intensities, cut from an ametrine crystal). It might be possible to learn additional details about the relation of these zones within the complete ametrine crystals if slices made from rough containing such near-colourless zones, along with violet and intense yellow areas, should become available in the future.

a clinographic projection and in a view parallel to the c-axis, respectively. The faces shown are the basal pinacoid **c** {0001}, the prism faces **m** {10 $\bar{1}$ 0} and **x** {11 $\bar{2}$ 0}, the positive rhombohedron **r** {10 $\bar{1}$ 1} and the negative rhombohedron **z** {01 $\bar{1}$ 1}.

For purposes of the following discussion, the present study will use the generally accepted nomenclature established by Prof. V. Balitsky and his co-workers (see references mentioned in the introduction). Small discrepancies in terminology and/or in details describing the synthetics between various publications, which are potentially attributable to inconsistent translations from Russian into English, will not be addressed at any length, provided the intended meanings are obvious.

Seed plates used in producing synthetic ametrine are frequently cut perpendicular to the c-axis (Z-cut). The simplest way to obtain a Z-cut seed plate is to slice a natural quartz crystal with six **m** prism faces perpendicular to its c-axis (Figure 15C). However, Z-cut seeds also may be elongated either parallel to an **x** prism face (parallel to the Y direction; Figure 15D) or parallel to an **m** prism face (parallel to the X direction; Figure 15E).

Commercial ametrine is often grown on Z-cut seed plates elongated parallel to the X direction (parallel to one of the **m** prism faces; Figure 15E). A complete crystal produced with such seed orientation and elongation is depicted in Figure 16.

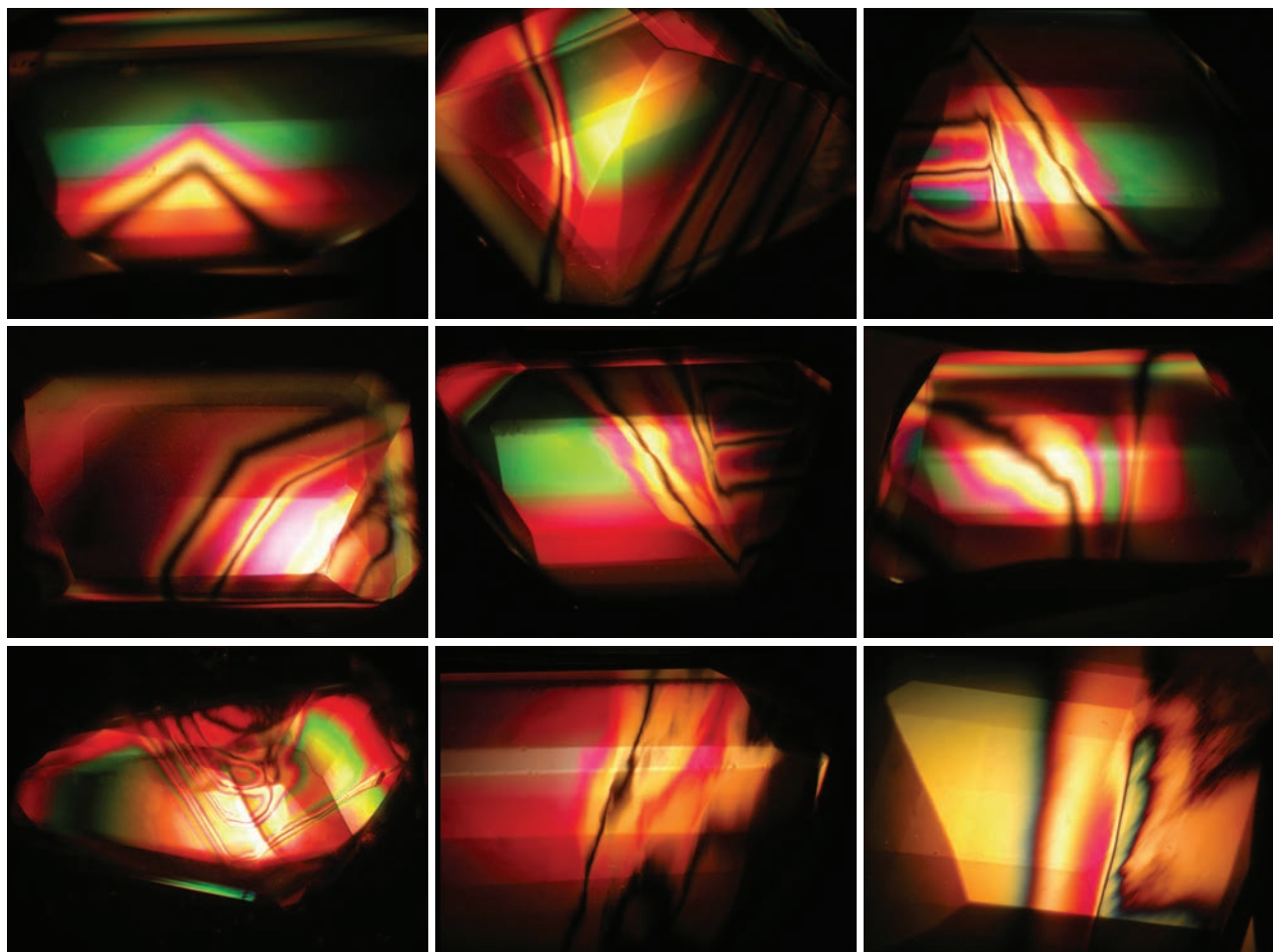


Figure 12: Between crossed polarizers, faceted natural ametrine shows interference patterns (Brewster fringes) when viewed parallel to the *c*-axis, indicating polysynthetic twinning of the violet *r* growth sectors. The samples shown here were chosen from the faceted ametrines depicted in Figure 11. Photomicrographs by K. Schmetzer, in immersion; field of view ranges from 8 × 6 mm to 12 × 9 mm.

Figure 13: The growth boundary between violet *r* and yellow *z* growth zones in natural ametrine is not exactly planar, as shown in these two faceted examples. In addition, growth striations parallel to an external *r* face and inclined to the violet/yellow boundary are observed in the violet *r* sector (forming angles with the violet/yellow boundary of ~67° in A and ~38° in B). Photomicrographs by K. Schmetzer, in immersion; field of view (A) 6.3 × 4.7 mm and (B) 9.5 × 7.1 mm.

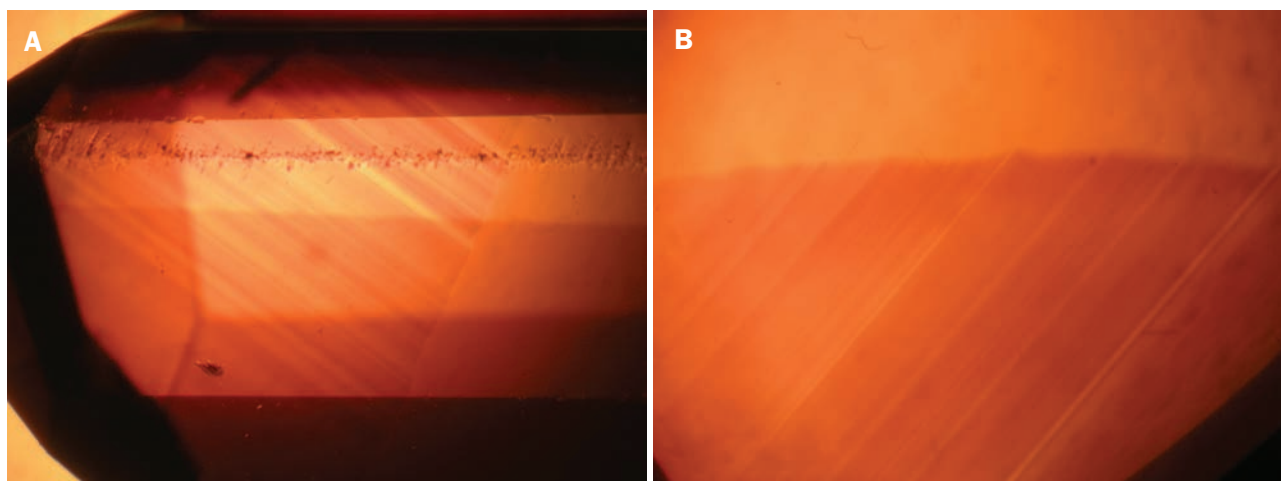




Figure 14: Various forms of fluid inclusions are occasionally seen in faceted natural ametrine, such as (A) negative crystals with two-phase fillings and (B) partially healed fractures with elongated cavities. (C) A parquet-like zigzag pattern of elongated fluid inclusions follows the complex polysynthetic twinning of the violet *r* growth sectors on the Brazil law. Photomicrographs by K. Schmetzer, in immersion; field of view (A) 4.5 × 3.4 mm, (B) 3.1 × 2.3 mm and (C) 2.2 × 1.7 mm.

Figure 15: (A) This clinographic projection of an idealized synthetic quartz crystal with prismatic habit consists of *m* and *x* prism faces in combination with *r* and *z* rhombohedra and basal *c* faces. (B) A view of the same crystal parallel to the *c*-axis shows the colour distribution between violet *r* and *z* growth sectors and yellow basal growth zones. For crystal growth, seeds are frequently cut perpendicular to the *c*-axis, also described as Z-cut seeds. These seeds can display (C) a hexagonal outline consisting of six prismatic *m* faces, or they can be elongated (D) parallel to the *Y* direction or (E) parallel to the *X* direction. Drawings by K. Schmetzer.

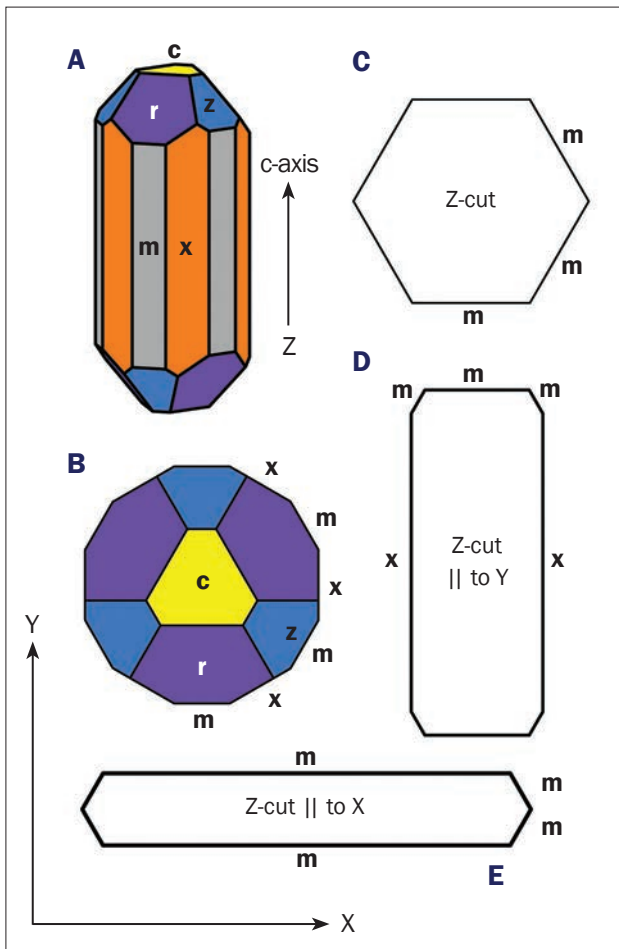
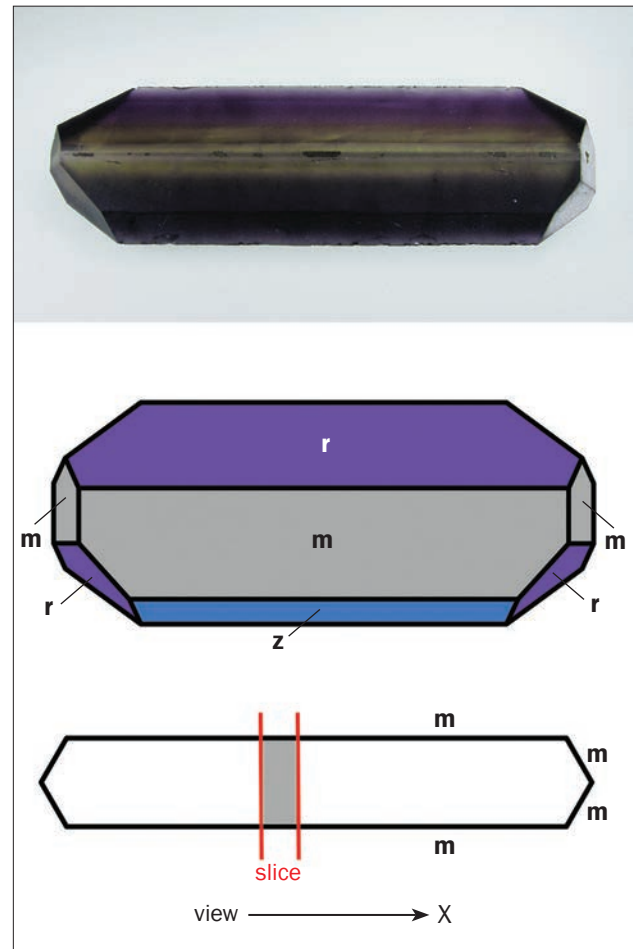


Figure 16: Commercial growth of synthetic ametrine is frequently performed with Z-cut seed plates elongated parallel to the *X* direction. (Top) This complete crystal, weighing 306 g (161 × 46 mm), was grown by this method. (Centre) A clinographic projection of the same crystal shows a habit of *m* prism faces combined with *r* and *z* rhombohedra. (Bottom) This view parallel to the *c*-axis depicts the orientation of the Z-cut seed plate elongated parallel to the *X* direction and the orientation of the slices shown in Figure 17A,B. Photo and drawings by K. Schmetzer.



The crystal has two elongated **m** faces as well as two elongated **r** and **z** faces, together with four smaller **m** and four smaller **r** faces. Colour zoning in crystals so grown was seen best in slices cut perpendicular to the two elongated **m** faces, viewed perpendicular to the cut (Figure 17A,B). In crystals grown with seed plates having the same elongation but cut at an incline of about 30° to the c-axis, the morphology of the crystals obtained was almost identical (Figure 17C).

In both cases, the crystals had yellow to yellow-orange basal **c** growth sectors along with violet **r** and **z** growth zones. For the examples seen in Figure 17A and C, the **r** and **z** growth sectors were purely violet, and the colour of the **r** sectors was somewhat more intense. For the example portrayed in Figure 17B, more iron had been incorporated into the crystal, so the **r** zones began to exhibit a degree of brownish colour admixed with the intense violet.

With these samples, and regardless of whether the seed had been cut parallel to the basal **c** face or angled by about 30°, the inclination of **r** and **z** rhombohedral faces to the c-axis was always constant at 38.2°. The boundary between basal yellow growth sectors and intense violet **r** zones was parallel or nearly parallel to the external **r** faces, with only a small deviation. In contrast, the boundary between basal yellow growth sectors and lighter violet **z** zones was not parallel to the external **z** faces (Figure 17A–C). The angle between this boundary and the c-axis varied mostly between 20° and 30°, and only in one sample was an angle of 35° measured.

However, in crystals grown with seed plates elongated parallel to the X direction but cut parallel to a rhombohedral **z** face, the morphology changed substantially. Alternating violet and brown striations parallel to the seed and the external **z** faces were observed, with small brown **r** growth sectors (Figure 17D); note that the brown areas in this crystal would be yellow or yellow-orange if less iron had been incorporated during crystal growth (see Table I and text on page 511). A related sample with an unusual orientation of the seed plate and the resulting colour zoning thereof is described in Box B.

Synthetic ametrine has also been grown on Z-cut seeds elongated parallel to the Y direction (parallel to one of the **x** prism faces; Figure 18). External crystal faces of such samples studied here were parallel to the **m** and **x** prism faces and

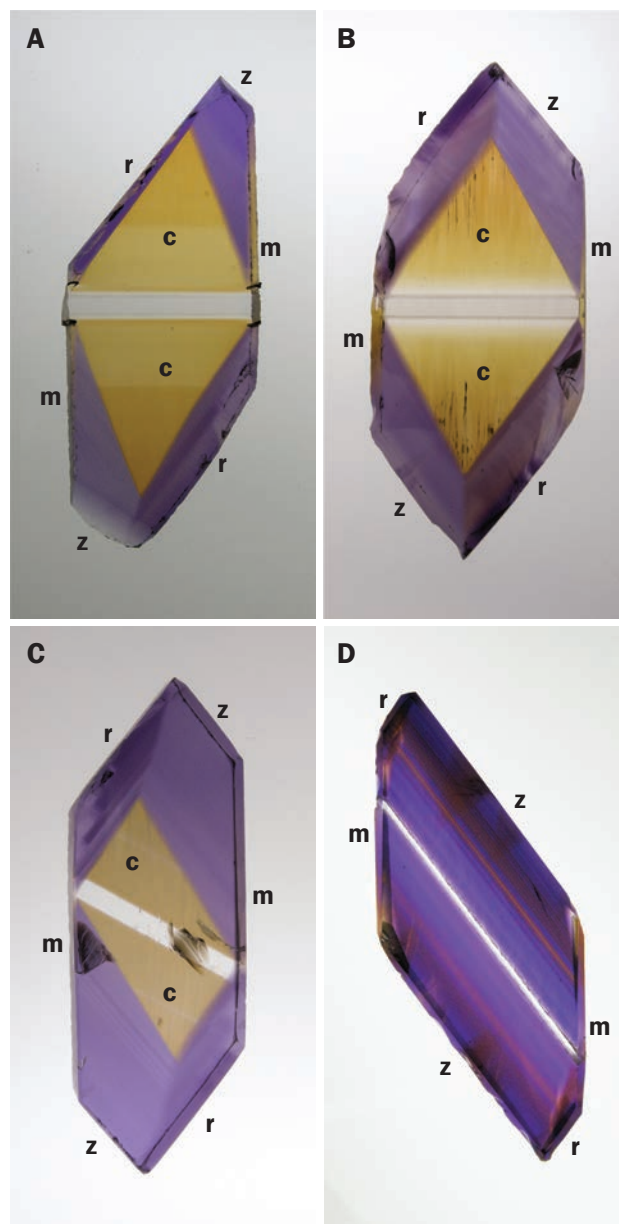


Figure 17: These slices of synthetic ametrine were grown on seed plates elongated parallel to the X direction and were sawn perpendicular to the long **m** prism faces. The seed plates were cut at various orientations: (A,B) perpendicular to the Z direction (i.e. parallel to the basal **c** face), (C) inclined about 30° to the basal face and (D) parallel to the rhombohedral **z** face. The habit of the samples shows prismatic **m** faces in combination with **r** and **z** rhombohedra; the colour distribution within the different growth zones also can be seen. The samples measure (A) 61 × 24 × 5 mm, (B) 71 × 30 × 9 mm, (C) 61 × 22 × 7 mm and (D) 75 × 31 × 14 mm. Photos by K. Schmetzer.

the **r** and **z** rhombohedral faces. Slices cut from such synthetic ametrine crystals showed yellow basal **c** growth sectors, intense yellow-orange ('amber'-coloured) **x** growth sectors, and violet **r** and **z** growth zones. In samples with this seed

Box B: Synthetic Ametrine with Violet and Yellow z Growth Zones

A unique synthetic ametrine sample was obtained in 2015 from the trade in Moscow, Russia. The crystal had been grown using a seed plate cut parallel to a rhombohedral **z** face. The seed could be seen in the slice, together with rhombohedral **r** and **z**, prismatic **m** and small basal **c** faces (Figure B-1). Violet and yellow areas were observed within the main **z** growth zones, with striations parallel to the **z** seed plate visible in both the violet and yellow areas. These growth striations appeared sharp in the immersion microscope.

If such a synthetic ametrine crystal were to be faceted, the cut specimen would contain growth striations parallel to the **z** seed in the violet region, but possibly also in the yellow portion. In addition, the violet/yellow boundary would be parallel to the seed. However, since the seed plate is inclined 38° to the **c**-axis, such faceted material would be easily identified by the microscopic techniques described in this article.

No direct information about the production of this material is available, and the growth conditions for achieving this type of colour zoning in synthetic ametrine are unknown. It is probable that the temperature (and/or the temperature gradient) within the autoclave changed during crystal growth, and this was responsible for incorporation of the different violet and yellow colour centres in the **z** growth sector.

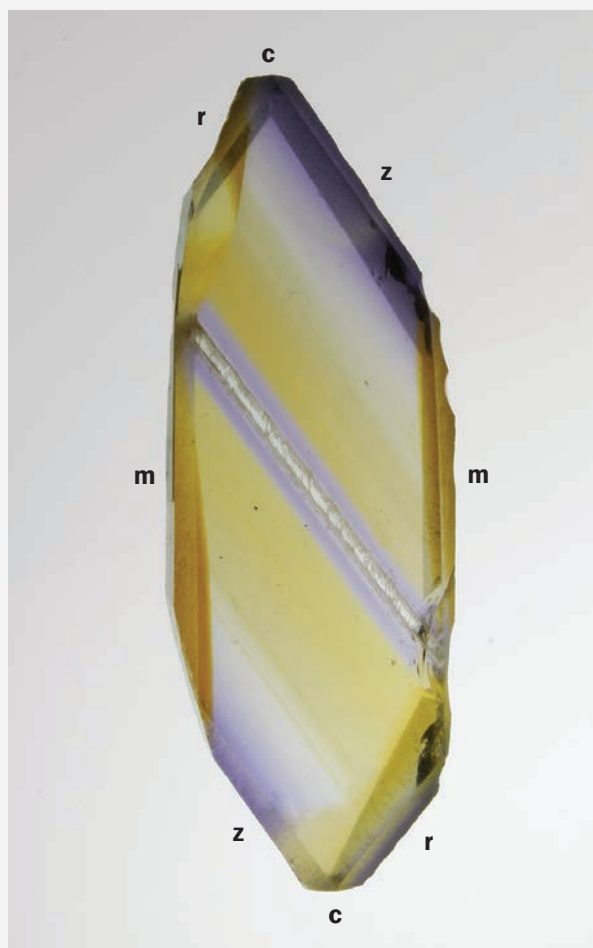


Figure B-1: This synthetic ametrine was grown on a seed plate cut parallel to the rhombohedral **z** face. Parallel to the seed, colour zoning is visible within various violet and yellow areas. The slice measures $61 \times 21 \times 10$ mm. Photo by K. Schmetzer.

configuration, the growth zones adjacent to the seed were either yellow (basal **c** zones) or amber-coloured (prismatic **x** growth zones). This seed-related colour scheme was readily observed in slices cut perpendicular to the **Y** direction (Figure 18C), but was also visible in a crystal with large cobbled basal **c** faces parallel to the seed (Figure 19). The various growth zones in this latter crystal were all either yellow or amber-coloured, and no violet zones had developed adjacent to **r** and **z** faces. From this morphology, it can therefore be concluded that the growth time in the autoclave for the synthetic quartz pictured in Figure 19 with large basal faces was comparatively shorter than that employed for samples such as in Figure 18C with small or no basal faces.

The boundaries between yellow basal growth zones and violet **r** sectors were parallel or almost parallel to the external **r** faces and, consequently, inclined approximately 38° to the **c**-axis. Most of the boundaries between **c** sectors and **z** zones were somewhat less inclined to the **c**-axis, forming angles of $20\text{--}30^\circ$ (Figure 18C,D). The boundaries between intense yellow-orange (amber-coloured) **x** growth zones and violet rhombohedral **r** and **z** sectors were only slightly inclined to the **c**-axis (see below).

In a variation of the situation described above, in some instances steel pins were incorporated during the process of growing synthetic ametrine on **Z**-cut seeds elongated parallel to the **Y** direction (parallel to one of the **x** prism faces). The

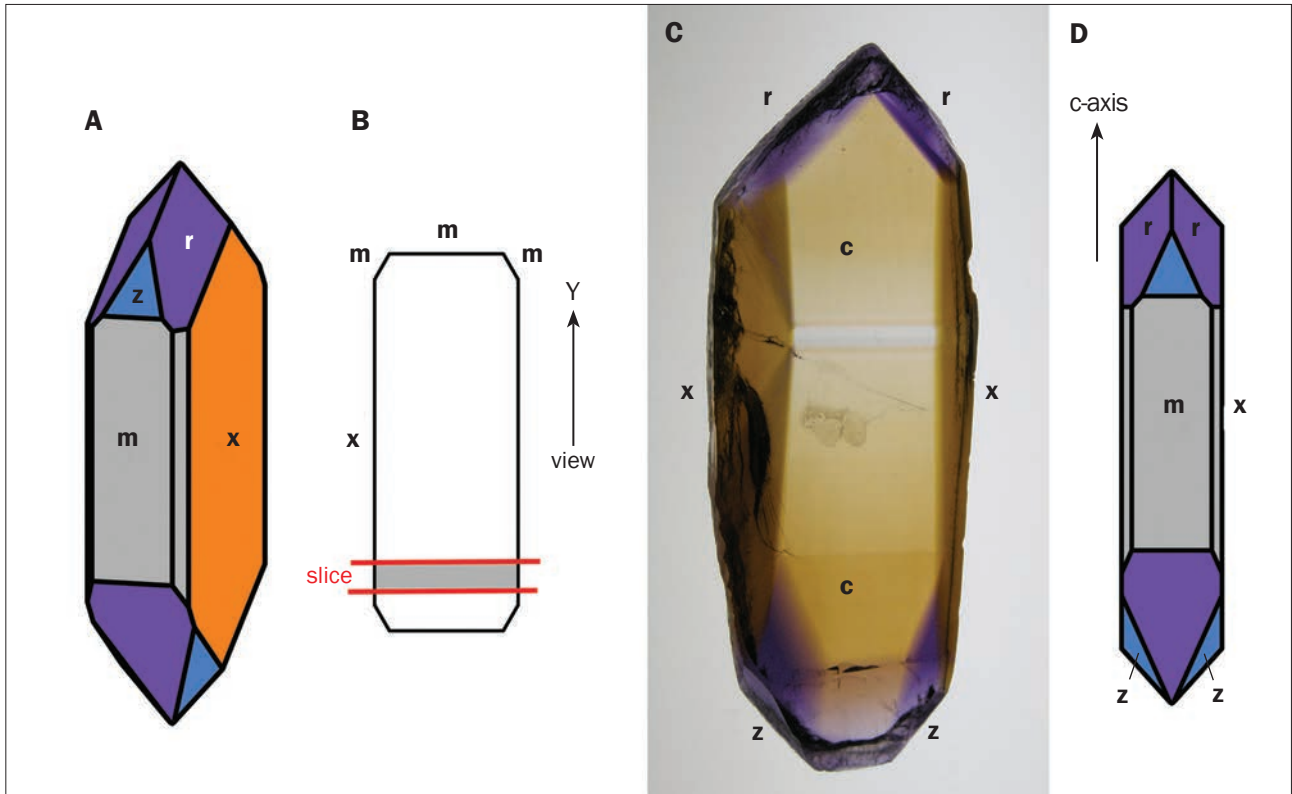
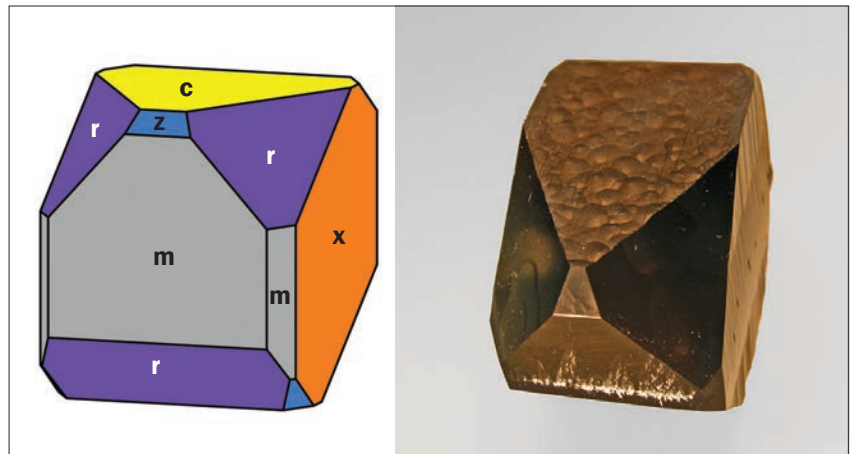


Figure 18: (A) This clinographic projection shows the crystal habit resulting from growth of synthetic ametrine on Z-cut seed plates elongated parallel to the Y direction. The crystals consist of **m** and **x** prism faces combined with **r** and **z** rhombohedra. (B) A view parallel to the c-axis depicts the orientation of the Z-cut seed plate elongated parallel to the Y direction and the orientation of the slice shown in C. (C) This slice of synthetic ametrine cut perpendicular to the Y direction (i.e. perpendicular to the long **x** prism faces) measures 83 × 30 × 6 mm. (D) A clinographic projection, corresponding to the orientation of the slice in C, shows the crystal in a view parallel to the **x** faces. Photo and drawings by K. Schmetzer.

pins served to interrupt crystal growth and resulted in samples comprising several identically oriented crystals, with dominant **m**, **r** and **z** faces (Figure 20). The **r** and **z** growth sectors influenced by the steel pins were highly distorted, with alternating violet, purplish violet, yellow and brown growth lamellae (Figures 20 and 21). Some of these crystals contained essentially pla-

nar boundaries between the **r** and **z** sectors and the yellow central areas, but in others the boundaries between **r** and **c** growth sectors were bent or curved. More precisely, the boundaries between the **z** and **c** growth sectors were inclined 20°–25° to the c-axis, and the boundaries between the **r** and **c** growth sectors were primarily inclined 30°–35° to the c-axis, except that the bent/curved

Figure 19: (Left) This clinographic projection of a synthetic ametrine crystal grown with a Z-cut seed elongated parallel to the Y direction shows a habit consisting of **m** and **x** prism faces combined with **r** and **z** rhombohedra and a large basal face **c**. (Right) This corresponding synthetic ametrine crystal exhibits a large basal face with a cobbled surface, a texture frequently seen in hydrothermal synthetic quartz. The crystal weighs 103 g (49 × 29 mm, and 33 mm along the c-axis). Photo and drawing by K. Schmetzer.



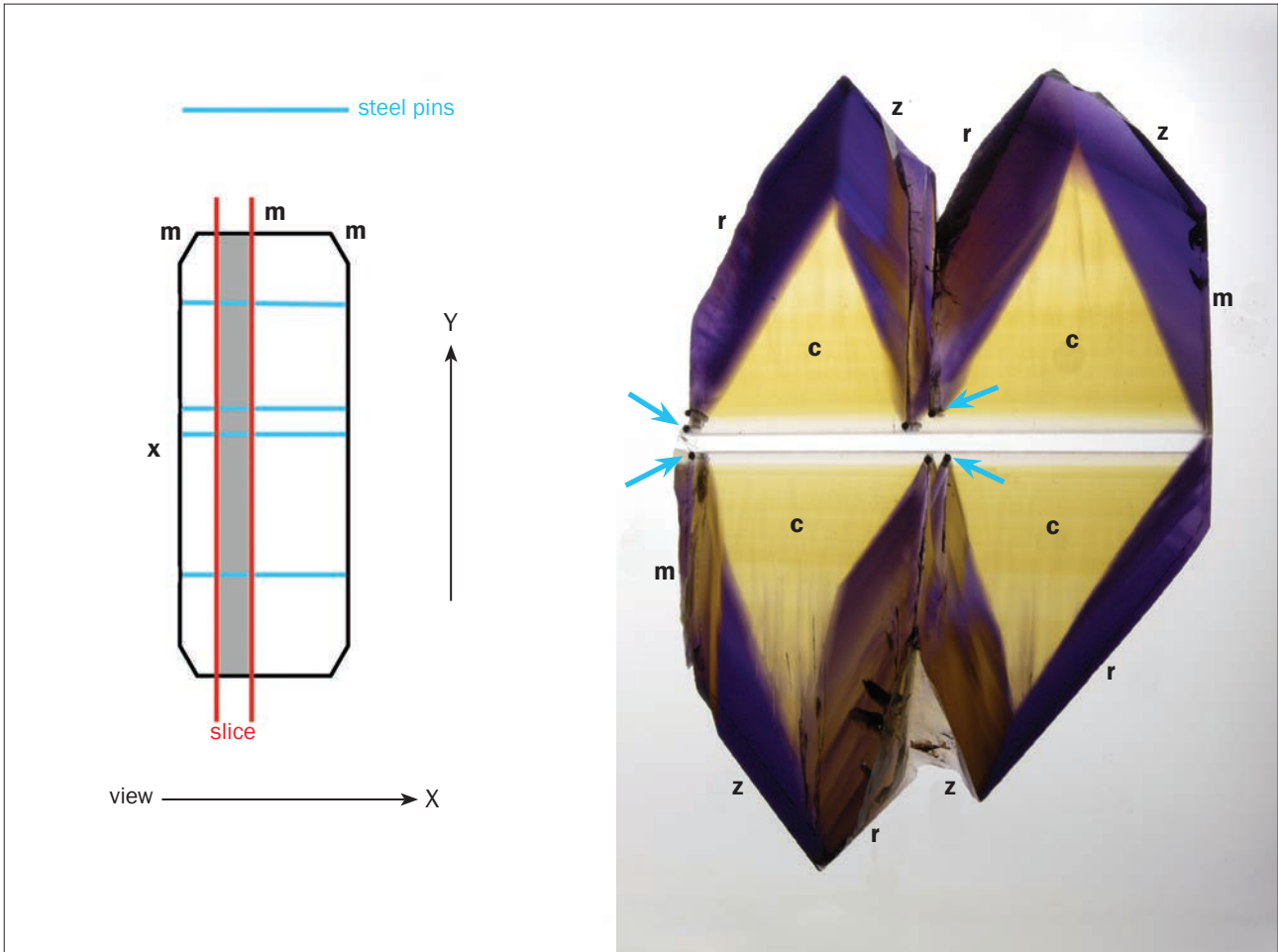


Figure 20: Growth of synthetic ametrine is also performed with Z-cut seed plates elongated parallel to the Y direction but with steel pins interrupting crystal growth. (Above, left) This drawing of a view parallel to the c-axis shows the orientation of the seed plate and the steel pins, as well as the position of the slice shown on the right. (Above, right) This slice of such a synthetic ametrine crystal was cut parallel to the Y direction (i.e. parallel to the long x prism faces); it measures 93 × 59 × 10 mm. The slice consists of two ametrine subindividuals with parallel orientation; steel pins are indicated with blue arrows. The colour distribution within basal c and rhombohedral r and z growth sectors can be seen; some boundaries between basal yellow growth sectors and adjacent violet-to-brown r growth zones are bent. Photo and drawing by K. Schmetzer.



Figure 21: An enlarged partial view of the synthetic ametrine slice in Figure 20 is shown here. Due to the influence of steel pins interrupting crystal growth, the r and z growth sectors are highly distorted, with alternating violet, purplish violet, yellow and brown growth zones, most seen as lamellae. The steel pins are indicated with blue arrows. Photo by K. Schmetzer; field of view 40 × 30 mm.

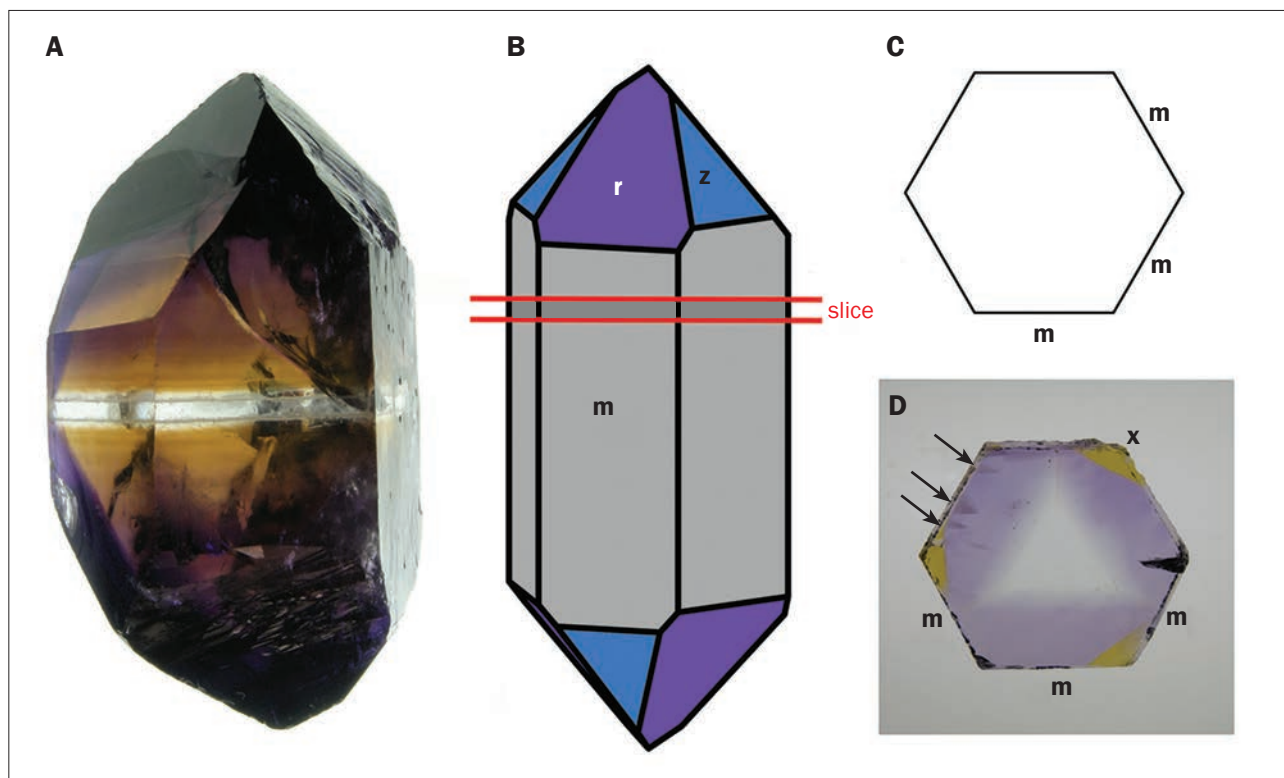


Figure 22: Synthetic ametrine crystals resembling natural quartz in morphology are grown from Z-cut hexagonally shaped seed plates. The colour distribution within such crystals, however, differs from that of natural ametrine. (A) This complete crystal shows prismatic **m** and rhombohedral **r** and **z** faces; diameter 26 mm, length 52 mm and weight 49 g. (B) The clinographic projection shows the crystal habit, consisting of **m** prism faces combined with **r** and **z** rhombohedra. (C) The seed plate is bounded by **m** faces. (D) This slice perpendicular to the *c*-axis shows a light yellow, almost colourless **c** growth sector, three violet rhombohedral sectors and three small amber-coloured **x** growth zones. The arrows point to twinning features. The slice has a diameter of 26 mm and a thickness of 5 mm. Photos and drawings by K. Schmetzer.

areas (close to the tips of the yellow triangles) showed an inclination of about 20°.

When Z-cut seed plates with hexagonal outlines were chosen for crystal growth, synthetic ametrine with a morphology resembling that of natural quartz crystals could be obtained (Figure 22). The dominant external faces were the prism **m** and three larger rhombohedral faces. In addition, some smaller rhombohedral faces could be seen. The central basal **c** growth sectors were yellow (Figure 22A) or very light yellow, almost colourless (Figure 22D). The boundaries between violet rhombohedral growth sectors and yellow basal growth areas were parallel or nearly parallel to the larger external rhombohedral faces. Small intense yellow (amber-coloured) sectors could be seen in one slice cut perpendicular to the *c*-axis and were presumably related to prismatic **x** growth zones (Figure 22D).

The growth boundaries between intense yellow-orange **x** growth sectors and violet rhombohedral sectors in synthetic ametrine with Z-cut hexagonally shaped seed planes (Figure 22D) were only

slightly inclined and almost parallel to the *c*-axis, as was the case above with Z-cut seed plates elongated in the *Y* direction (Figure 18). This growth feature is detailed in Figure 23 and should be taken into consideration if faceted samples of unknown origin are examined with the microscope.

Twinning, Growth Striations and Inclusions: Twinning in synthetic ametrine has been mentioned only briefly in the literature—as Brazil-law twinning in violet **r** sectors and Dauphiné twinning in violet **z** sectors (Balitsky et al., 1999, 2000), and therefore details reported for synthetic amethyst can help explain the properties of synthetic ametrine.

In synthetic amethyst, two different types of twinning have been described for rhombohedral **r** and **z** growth sectors, but no twins have been observed in basal **c** growth zones. More specifically, **z** growth sectors display twinning on the Dauphiné law, while **r** growth zones exhibit twinning on both the Dauphiné and Brazil laws.

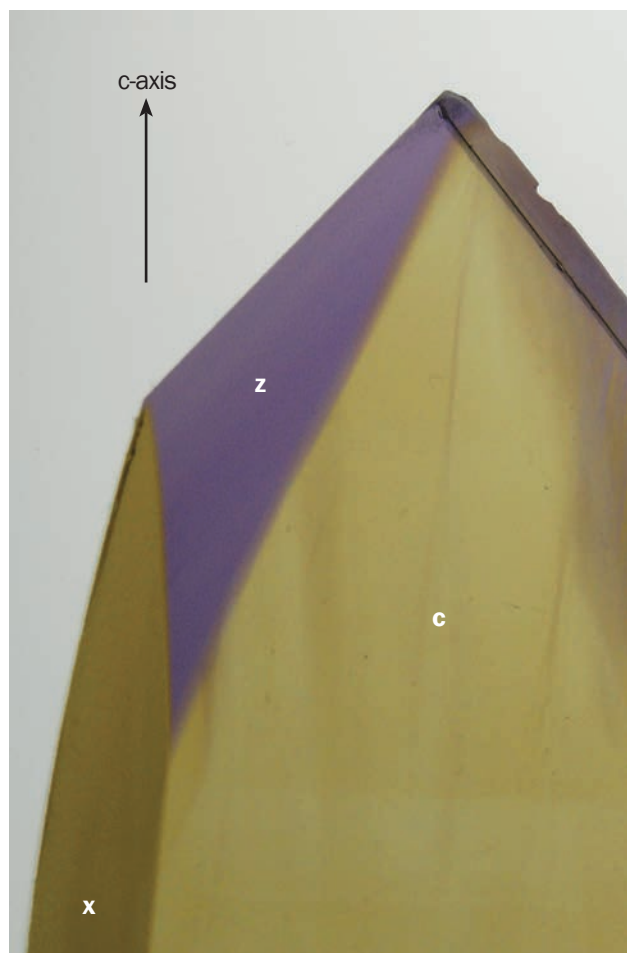


Figure 23: Growth boundaries in synthetic ametrine with amber-coloured **x** growth sectors and violet rhombohedral growth zones frequently run almost parallel to the *c*-axis of the crystals. This slice is oriented parallel to the *c*-axis and is 4.4 mm thick. Photo by K. Schmetzer; field of view 14.7 × 19.6 mm.

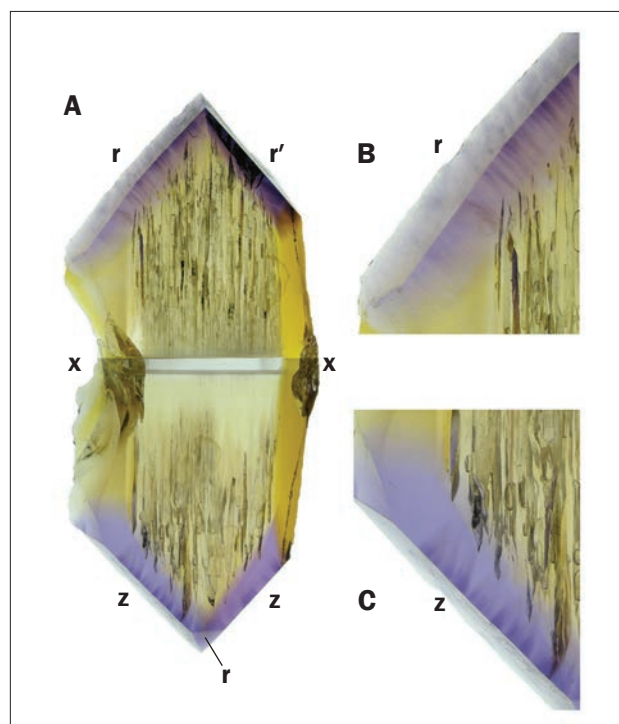
Dauphiné twinning is developed as irregularly shaped, somewhat conical or tapered domains with irregular composition planes, and Brazil twinning is manifested as lamellae with rhombohedral composition planes. Dauphiné twins in **z** growth sectors are equivalent to **r** growth sectors, and vice versa. Furthermore, because Dauphiné twins in **z** growth zones are equivalent to **r** growth zones, these Dauphiné twin domains sometimes contain lamellae of Brazil twins (Lu et al., 1990; Sunagawa et al., 1990; Balitsky et al., 2004; Balitsky and Balitskaya, 2009).

Twinning was observed in four of the 25 slices of synthetic ametrine available for the present study (e.g. Figures 17D, 22D and 24). Such twinning was easily recognized in the form of variously shaped small growth sectors showing darker colour within the lighter area of the sur-

rounding host. In **r** growth sectors, single Brazil-twin lamellae were seen (Figure 24B), with composition planes running parallel to another rhombohedral **r** face (indicated as **r'** in Figure 24A). In **z** growth sectors, somewhat tapered, conically shaped darker colour zones were found (Figure 24C) that correspond to Dauphiné twins.

On the surface of the **r** face representing the **r** growth zone with lamellar twins, a series of dense striations was seen. In contrast, the **z** face showed irregular depressions corresponding to the conical domains of the Dauphiné twins. In the immersion microscope, these tapered domains within the Dauphiné twins themselves showed interference patterns of lamellar twinning on the Brazil law (Figure 25). The depressions formed by the **r** Dauphiné twins in the **z** growth zones result from the fact that **r** faces are relatively slower growing.

Figure 24: Twinning in synthetic ametrine is occasionally observed in the form of comparatively darker violet lamellae or tapered domains within lighter coloured **r** and **z** growth sectors. (A) This slice from a crystal grown with a Z-cut seed plate elongated parallel to the *Y* direction was cut perpendicular to the elongated **x** prism face; 96 × 38 × 8 mm. (B) An enlarged partial view of the sample shows planar dark violet lamellae within the rhombohedral **r** growth zone. The lamellae run parallel to a second rhombohedral face, indicated as **r'** in A. (C) This enlarged partial view of the sample shows dark violet tapered domains within the rhombohedral **z** growth zone. Photos by K. Schmetzer.



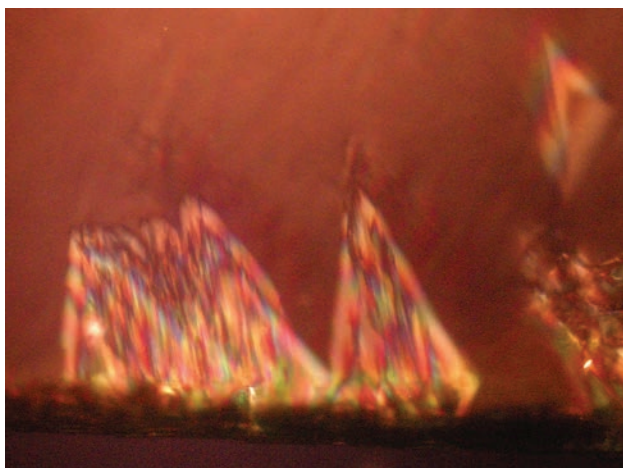


Figure 25: Viewed with crossed polarizers, interference patterns are seen within tapered domains in violet rhombohedral growth zones of synthetic ametrine. These conical domains represent Dauphiné twins that are internally twinned on the Brazil law. Photomicrograph by K. Schmetzer, in immersion; field of view 6.7 × 5.0 mm.

Growth striations in the yellow sectors of synthetic ametrine were in general extremely weak and always parallel to the basal **c** face. Occasionally the **c** growth zone appeared to be subdivided into lighter and darker yellow portions. Growth striations in the violet **r** and **z** sectors were consistently parallel to the external crystal faces. In certain instances, such growth striations in **r** zones were more pronounced than those in **z** sectors (Figure 26A,B), but it was also possible to find **z**

sectors showing intense growth striations (Figure 26C). As compared to the violet/yellow boundary, the inclinations of the growth striations in **r** and **z** zones may be summarized as follows:

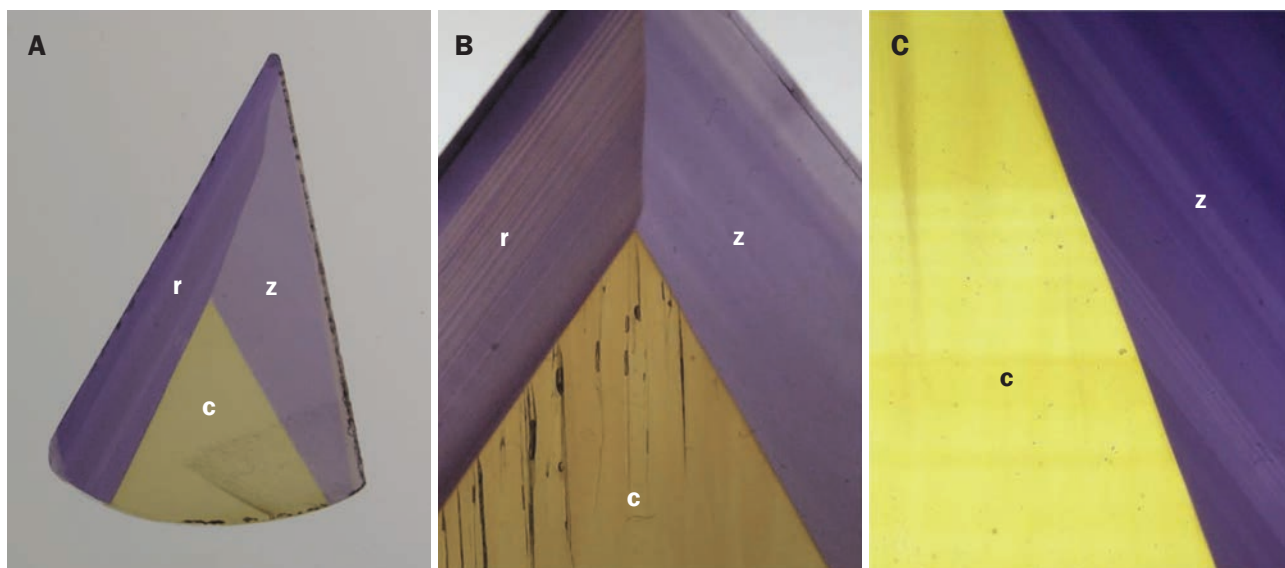
- In **r** zones, striations mostly tended to be parallel or almost parallel to the colour boundary, with angles smaller than 8° (Figure 26A,B), and only in samples grown with seeds interrupted by steel pins might this angle reach up to 18°.
- In **z** sectors, striations exhibited a broader range of angles, from slightly inclined to a maximum angle of 18° (i.e. in samples for which the angle between the violet/yellow boundary and the **c**-axis measured 20°; Figure 26C).

In some slices, fluid inclusions were observed that were elongated parallel to the **c**-axis and typically contained two-phase fillings (Figure 26B).

Synthetic Ametrine—Faceted Samples

Visual Appearance: The faceted synthetic ametrine samples studied here were typically cut to show a single colour boundary across the table of the gem (Figure 27), in keeping with normal trade practices. The colour boundary often appeared more pronounced when viewed from the pavilion side. In general, the colours displayed by the synthetics were of greater saturation than those exhibited by natural ametrine.

Figure 26: Growth striations in the rhombohedral **r** and **z** growth sectors of synthetic ametrine are always parallel to the external **r** and **z** crystal faces. In **r** growth zones, these striations are parallel or almost parallel to the violet/yellow colour boundary (A,B). In **z** growth zones, the striations are sometimes parallel or almost parallel to the violet/yellow boundary (B), but they also may be inclined up to 18° to this boundary (C). Note also the elongate two-phase inclusions in B. Photos by K. Schmetzer; (A) slice 25 × 16 × 3 mm, (B) field of view 20 × 15 mm and slice thickness 9 mm and (C) field of view 18.1 × 13.6 mm and slice thickness 10 mm.



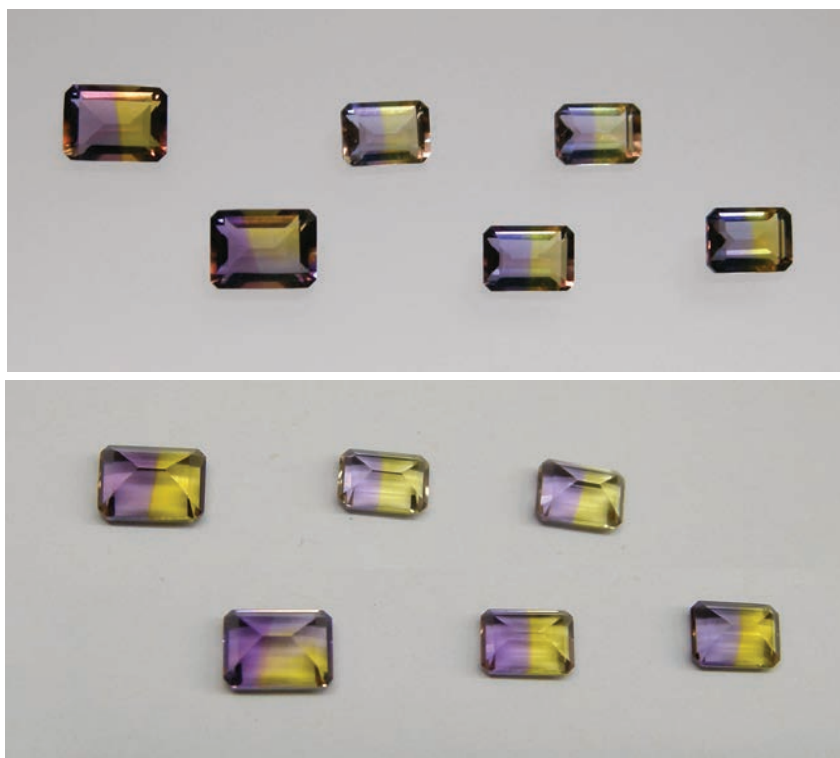


Figure 27: These faceted synthetic ametrines weigh from 1.67 ct (lower left, 8.1 × 6.1 mm) to 0.93 ct. They are viewed toward the table facets (top) and toward the pavilions of the same samples (bottom). Photos by K. Schmetzer.

Microscopic Examination: The optical properties of the faceted synthetics were consistent with those just described for complete crystals and oriented slices. Most faceted samples were un-twinned single crystals. They showed a simple interference pattern that consisted of coloured interference rings that moved toward the centre when the sample was tilted so that the optic axis was parallel to the microscope tube (Figure 28A). In addition, the rings were occasionally disturbed by triangular sectors twinned on the Brazil law (Figure 28B). The visual impression of these twinned areas, showing a so-called ‘flame structure’ appearance (Figure 28C,D), was quite distinctive and thus distinguishable from the various forms of Brewster fringes observed in natural samples (see again Figure 12). Rather, the appearance was consistent with the pattern observed for Dauphiné twins containing twin lamellae on the Brazil law (as described above for the slices; see again Figures 24C and 25).

The boundaries between violet and yellow growth zones were inclined to the c-axis by angles of 20°–38°. This range is analogous to that measured for the synthetic ametrine slices. Growth striations in the violet zones were observed in approximately half of the faceted samples. They were parallel or only slightly inclined to the violet/yellow boundary (Figure 29). Larg-

er inclinations (up to 18°) for such striations, as seen in some oriented slices, were not found in the faceted synthetics from the trade. For faceted material, orienting the rotation axis of the sample holder perpendicular to the colour zoning did not lead to a position enabling a view in the direction of the optic axis. Consequently, the typical interference pattern of an untwinned crystal could not be located using this orientation, on account of the angle of the violet/yellow boundary versus the c-axis in the synthetic samples.

Fluid inclusions were generally not observed in the faceted synthetic ametrines from the trade.

Discussion and Conclusions: Application of Optical Properties to Distinguish Between Natural and Synthetic Ametrine

Prior works have suggested distinguishing natural from synthetic ametrine based on two criteria: (1) the presence or absence of twinning and (2) the orientation of the violet/yellow boundary (Balitsky et al., 1999; Notari et al., 2001; Payette, 2013). The present study, in turn, has now yielded a third criterion: (3) the orientation of growth striations. In addition, it has revealed a more effective and practical approach for examining a sample of un-

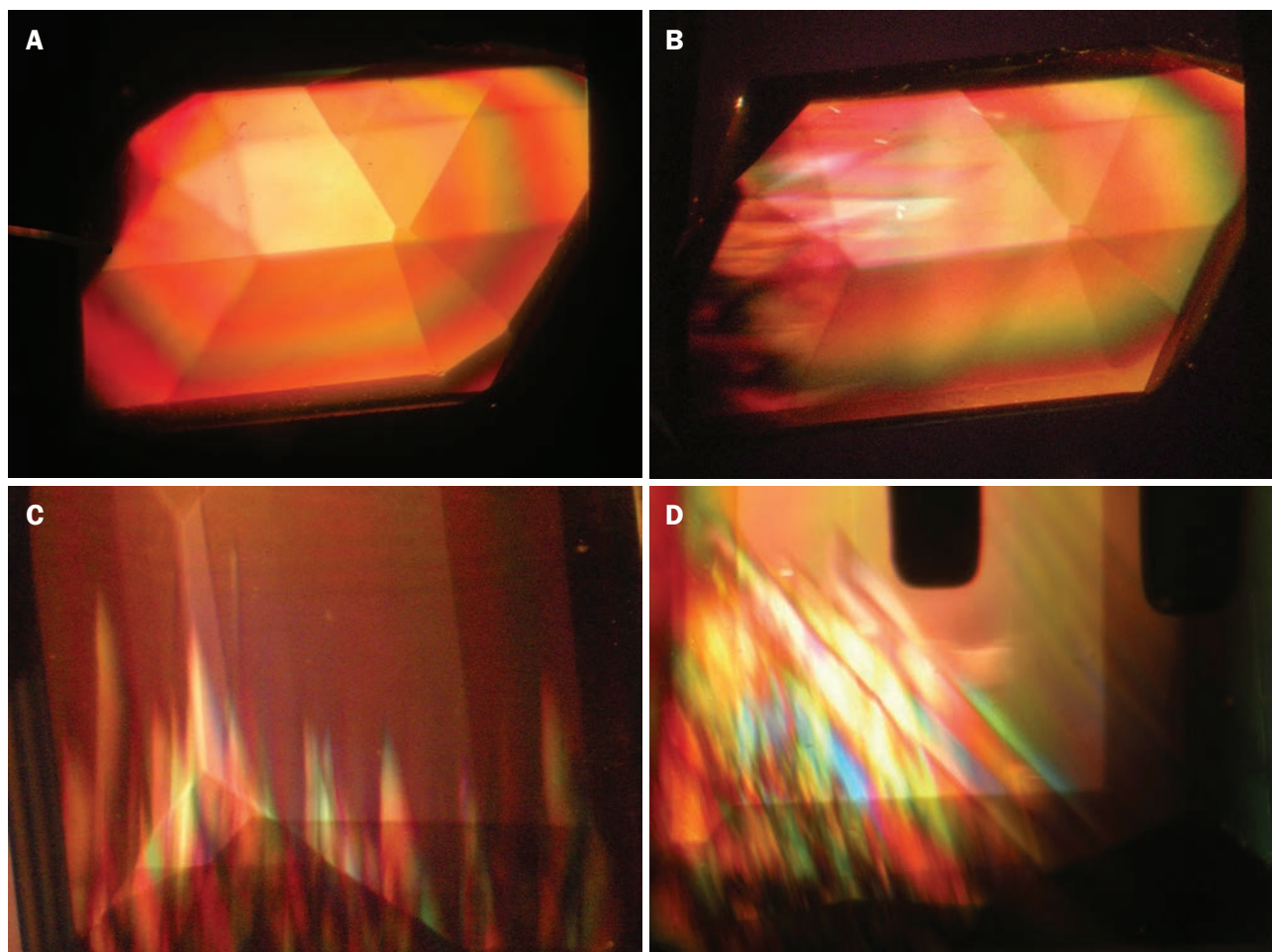


Figure 28: (A,B) In cross-polarized light, the interference patterns in faceted synthetic ametrine generally consist of interference rings, the sizes of which increase or decrease in diameter as the sample is tilted in the immersion microscope. (B–D) If the sample contains twinned areas, interference patterns related to twinning on the Brazil and Dauphiné laws are observed. Photomicrographs by K. Schmetzer, in immersion with crossed polarizers; field of view (A,B) 7.0 × 5.2 mm, (C) 4.7 × 3.5 mm and (D) 5.7 × 4.3 mm.

Figure 29: Growth striations are frequently seen in the violet zones of faceted synthetic ametrine. These striations are parallel or only slightly inclined to the violet/yellow boundary. Photomicrograph by K. Schmetzer; field of view 5.8 × 4.4 mm.



known origin in search of these three criteria. A microscopic observation procedure can be used in lieu of the previously employed combination of only refractometer and polariscope for determining the orientation of the growth boundaries. Doing so can reduce the uncertainty and risk for misinterpretation when faced with cut samples having an unfavourable orientation of the optic axis versus the table facet and with synthetic samples having a small inclination (only 20°) between the colour boundary and the c-axis. Furthermore, an erroneous interpretation of atypical twin patterns (interference patterns) can be avoided.

Table II provides an overview of the microscopic features seen with an immersion microscope for distinguishing between natural and synthetic ametrine.

Table II: Diagnostic features of natural and synthetic ametrine, seen with an immersion microscope.

Optical feature	Natural		Synthetic	
	Description	Relevant figures	Description	Relevant figures
Twinning	Violet growth sectors are intensely twinned on the Brazil law, showing various forms of Brewster fringes with crossed polarizers; yellow growth sectors are not polysynthetically twinned	8, 12	Violet and yellow growth sectors are primarily untwinned; small areas within the violet growth sectors may be twinned on the Dauphiné and/or the Brazil law	17D, 22D, 24, 25, 28B,C,D
Violet/yellow colour boundaries	Mostly parallel to the c-axis or only slightly inclined to the c-axis (up to about 10°)	6, 9, 13	Inclined between 20° and 38° to the c-axis	17, 18, 20, 21, 23, 24, 26, 29, B1
Growth striations	Violet growth sectors: inclined at about 67° or 38° to the violet/yellow boundary; yellow growth sectors: none observed	9, 13	Violet growth sectors: parallel or almost parallel to the violet/yellow boundary, mostly inclined at angles between 0° and 8°, with a maximum inclination of 18°; yellow growth sectors: very weak striations parallel to the basal face	26, 29
Fluid inclusions	Rare fluid inclusions, occasionally reflecting the polysynthetic twin pattern of the violet growth zones	14	Rare two-phase (liquid and gas) inclusions elongated parallel to the c-axis	24, 26B

First, with respect to twinning, as is well documented in the existing literature, the violet growth sectors of natural ametrine are polysynthetically twinned on the Brazil law and show Brewster fringes between crossed polarizers. In contrast, synthetic ametrine is typically untwinned, although it occasionally contains small conical twinned areas.

Second, pertaining to the dominant violet/yellow colour boundary, in natural ametrine it is approximately parallel to prism faces (i.e. parallel or almost parallel to the c-axis). In synthetic ametrine, the colour boundary varies at angles of 20°–38° relative to the optic axis, regardless of the cut orientation and elongation of the seed plate (amongst those currently known) used for growth. Note that the inclination angle of about 51° between the violet/yellow boundary and the c-axis mentioned by Balitsky et al. (1999) most likely refers to the complementary angle ($38^\circ + 51^\circ \approx 90^\circ$).

Third, growth striations in natural ametrine form two different angles of approximately 67° or 38° with the violet/yellow colour boundary. This contrasts markedly with the striations in synthetic ametrine, which are parallel to the dominant colour boundary or only slightly inclined, mostly at angles of up to 8° (rarely up to 18°).

In rare cases, the presence of typical inclusions might support a decision based upon the three main criteria described above.

Ametrine produced from natural amethyst by heat treatment (which is possible for samples from certain locations but, to the author's knowledge, not performed commercially) would show the same characteristic features of twinning, growth boundaries and growth striations described for natural unheated ametrine.

The microscopic procedure for identifying these key features can be summarized as follows. The examination of a faceted sample of unknown origin should begin by orienting the dominant colour boundary perpendicular to the rotation axis of the sample holder. If the stone is natural, the typical interference pattern with Brewster fringes will be revealed upon rotation of the sample. Furthermore, growth striations inclined at relatively large angles to the colour boundary will be observed in the violet portion of the stone after a rotation of about 40° versus the c-axis. If the sample is synthetic, rotating the sample generally will not bring the optic axis into view, and violet growth striations parallel or at a small angle to the violet/yellow colour boundary frequently will be present. It is possible to find the optic axis in a synthetic sample by moving

it to other orientations within the sample holder, in which case an untwinned interference figure normally will be seen.

Thus the present study demonstrates that parcels of faceted ametrine can be screened quickly to distinguish between natural and synthetic samples through use of an immersion microscope and the application of three criteria in combination (see again Table II):

- presence or absence of twinning
- orientation of the violet/yellow colour boundary
- orientation of growth striations relative to this colour boundary

To perform a full examination for all the criteria mentioned, unmounted samples are always preferred. Nonetheless, the examination process can be employed at least in part with mounted samples (e.g. Figure 1), revealing in jewellery pieces some of the noted properties.

The use of a standard gemmological microscope for such examinations is possible, but the observation of structural properties such as twinning and growth zoning, or optical phenomena such as interference patterns (e.g. details of Brewster fringes), is always limited and even finding the location of the optic axis might be problematic. Thus, the various patterns or structures observed without immersion often are of less diagnostic value.

References

- Balitsky V.S. and Balitskaya O.V., 1986. The amethyst-citrine dichromatism in quartz and its origin. *Physics and Chemistry of Minerals*, **13**(6), 415–421, <http://dx.doi.org/10.1007/BF00309187>.
- Balitsky V.S. and Balitskaya O.V., 2005. Some problems of natural and synthetic colored quartz identification. *GemmoBasel 2005*, Basel, Switzerland, 29 April–2 May, 68–70.
- Balitsky V.S. and Balitskaya O.V., 2009. The genetic approach for identification of varieties of crystalline and amorphous silica. *Australian Gemmologist*, **23**(11), 500–508.
- Balitsky V.S., Lu T., Rossman G.R., Makhina I.B., Mar'in A.A., Shigley J.E., Elen S. and Dorogovin B.A., 1999. Russian synthetic ametrine. *Gems & Gemology*, **35**(2), 122–134, <http://dx.doi.org/10.5741/gems.35.2.122>.
- Balitsky V.S., Machina I.B., Mar'in A.A., Shigley J.E., Rossman G.R. and Lu T., 2000. Industrial growth, morphology and some properties of bi-colored amethyst-citrine quartz (ametrine). *Journal of Crystal Growth*, **212**(1–2), 255–260, [http://dx.doi.org/10.1016/S0022-0248\(99\)00866-0](http://dx.doi.org/10.1016/S0022-0248(99)00866-0).
- Balitsky V.S., Makhina I.B., Marina E.A., Rossman G.R., Lu T. and Shigley J.E., 2001. Growth and characteristics of some new varieties of coloured quartz single crystals. *High Pressure Research*, **20**(1–6), 219–227, <http://dx.doi.org/10.1080/08957950108206169>.
- Balitsky V.S., Balitsky D.V., Bondarenko G.V. and Balitskaya O.V., 2004. The 3543 cm⁻¹ infrared absorption band in natural and synthetic amethyst and its value in identification. *Gems & Gemology*, **40**(2), 146–161, <http://dx.doi.org/10.5741/gems.40.2.146>.
- Biste M. and Burgoa A., 2002. Nuevos aspectos geológico-mineros sobre el yacimiento de bolivianita Anahi, ubicado en el Oriente Boliviano. *XV Congreso Geológico Boliviano*, Santa Cruz, Bolivia, October, 131–133.
- Collyer T., Fuzikawa K. and Schwarz D., 1994. Das Ametrin-Vorkommen von Anay, Santa Cruz, Bolivien. *Zeitschrift der Deutschen Gemmologischen Gesellschaft*, **43**(3–4), 117–126.
- Crowningshield R., Hurlbut C. and Fryer C.W., 1986. A simple procedure to separate natural from synthetic amethyst on the basis of twinning. *Gems & Gemology*, **22**(3), 130–139, <http://dx.doi.org/10.5741/gems.22.3.130>.
- Hainschwang T., 2009. The synthetic quartz problem. *GemGuide*, **28**(1), 1–5.
- Henn U. and Schultz-Güttler R., 2012. Review of some current coloured quartz varieties. *Journal of Gemmology*, **33**(1–4), 29–43, <http://dx.doi.org/10.15506/jog.2012.33.1.29>.
- Johnson M.L. and Koivula J.I., Eds., 1998. Gem News: First commercial synthetic ametrine from Russia. *Gems & Gemology*, **34**(1), 60–61.
- Karampelas S., Fritsch E., Zorba T., Paraskevopoulos K.M. and Sklavounos S., 2005. Distinguishing natural from synthetic amethyst: The presence and shape of the 3595 cm⁻¹ peak. *Mineralogy and Petrology*, **85**(1–2), 45–52, <http://dx.doi.org/10.1007/s00710-005-0101-9>.
- Karampelas S., Fritsch E., Zorba T. and Paraskevopoulos K.M., 2011. Infrared spectroscopy of natural vs. synthetic amethyst: An update. *Gems & Gemology*, **47**(3), 196–201, <http://dx.doi.org/10.5741/gems.47.3.196>.
- Kiefert L. and Schmetzer K., 1991a. The microscopic determination of structural properties for the characterization of optical uniaxial natural and synthetic gemstones. Part 1: General considerations and description of the methods. *Journal of Gemmology*, **22**(6), 344–354, <http://dx.doi.org/10.15506/JoG.1991.22.6.344>.
- Kiefert L. and Schmetzer K., 1991b. The microscopic determination of structural properties for the characterization of optical uniaxial natural and synthetic gemstones. Part 2: Examples for the applicability of structural features for the distinction of natural emerald from flux-grown and hydrothermal-grown synthetic emerald. *Journal of Gemmol-*

- ogy, **22**(7), 427–438, <http://dx.doi.org/10.15506/JoG.1991.22.7.427>.
- Kiefert L. and Schmetzer K., 1991c. The microscopic determination of structural properties for the characterization of optical uniaxial natural and synthetic gemstones. Part 3: Examples for the applicability of structural features for the distinction of natural and synthetic sapphire, ruby, amethyst and citrine. *Journal of Gemmology*, **22**(8), 471–482, <http://dx.doi.org/10.15506/JoG.1991.22.8.471>.
- Kitawaki H., 2002. Natural amethyst from the Caxarai mine, Brazil, with a spectrum containing an absorption peak at 3543 cm⁻¹. *Journal of Gemmology*, **28**(2), 101–108, <http://dx.doi.org/10.15506/JoG.2002.28.2.101>.
- Koivula J.I., 1980. Citrine-amethyst quartz—A gemologically new material. *Gems & Gemology*, **16**(9), 290–293.
- Laurs B., 2001. Gem News International: Update on amethyst, citrine, and ametrine from the Anahí mine, Bolivia. *Gems & Gemology*, **37**(4), 334–335.
- Lu T. and Shigley J.E., 1998. Optical characterization of synthetic faceted gem materials grown from hydrothermal solutions. *Optical Diagnostic Methods for Inorganic Transmissive Materials*, San Diego, California, USA, 19 July, 37–40.
- Lu T. and Sunagawa I., 1990. Structure of Brazil twin boundaries in amethyst showing Brewster fringes. *Physics and Chemistry of Minerals*, **17**(3), 207–211, <http://dx.doi.org/10.1007/bf00201451>.
- Lu T., Sunagawa I. and Balitsky V.S., 1990. Brazil twinning in natural and synthetic amethyst crystals. *Journal of Crystal Growth*, **99**(1–4), 1232–1237, [http://dx.doi.org/10.1016/s0022-0248\(08\)80114-5](http://dx.doi.org/10.1016/s0022-0248(08)80114-5).
- Neumann E. and Schmetzer K., 1984. Mechanism of thermal conversion of colour and colour centres by heat treatment of amethyst. *Neues Jahrbuch für Mineralogie, Monatshefte*, **1984**(6), 272–282.
- Notari F., Boillat P.-Y. and Caplan C., 2001. Quartz α -SiO₂: Discrimination des amethysts et des citrines naturelles et synthétiques. *Revue de Gemmologie AFG*, No. 141/142, 75–80.
- Payette F., 2013. A simple approach to separate natural from synthetic ametrine. *Australian Gemmologist*, **25**(4), 132–141.
- Schmetzer K., 1986. An improved sample holder and its use in the distinction of natural and synthetic ruby as well as natural and synthetic amethyst. *Journal of Gemmology*, **20**(1), 20–33, <http://dx.doi.org/10.15506/JoG.1986.20.1.20>.
- Schmetzer K., 1987. Microscopic observation of twinning structure in natural amethyst. *Neues Jahrbuch für Mineralogie, Monatshefte*, **1987**(1), 8–15.
- Schmetzer K., 1989. Methods for the distinction of natural and synthetic citrine and prasiolite. *Journal of Gemmology*, **21**(6), 368–391, <http://dx.doi.org/10.15506/JoG.1989.21.6.368>.
- Sunagawa I., Lu T. and Balitsky V.S., 1990. Generation of Brazil and Dauphiné twins in synthetic amethysts. *Physics and Chemistry of Minerals*, **17**(4), 320–325, <http://dx.doi.org/10.1007/bf00200127>.
- Vasconcelos P.M., Wenk H.-R. and Rossman G.R., 1994. The Anahí ametrine mine, Bolivia. *Gems & Gemology*, **30**(1), 4–23, <http://dx.doi.org/10.5741/gems.30.1.4>.
- Vasconcelos P., Cohen B. and Calos N., 2002. Colour in quartz: From atomic substitutions to nano-inclusions. *Australian Gemmologist*, **21**(8), 278.
- Weldon R., 2009. Gem News International: Anahí's "new" ametrine. *Gems & Gemology*, **45**(1), 63–64.
- Weldon R., 2013. From the Andes to the Pantanal: In Search of Ametrine. Gemological Institute of America, Carlsbad, California, USA, www.gia.edu/gia-news-research-In-Search-of-Ametrine.

The Author

Dr Karl Schmetzer

D-85238 Petershausen, Germany

Email: SchmetzerKarl@hotmail.com

Acknowledgements

Samples and photos for this study were kindly provided by the following: Dr Jaroslav Hyršl (Prague, Czech Republic), Dr Michael S. Krzemnicki (from the Henry A. Hänni collection of the Swiss Gemmological Institute SSEF, Basel, Switzerland), Francine Payette (Perth, Australia), Udo Reimann (Carat Co., Nürnberg, Germany), Dr George R. Rossman (California Institute of Technology, Pasadena, California, USA), Georg Sellmair (Kranzberg, Germany), Dr Yuri Shelementiev (Gemmological Center, Moscow State University, Moscow, Russia), Dr James E. Shigley (Gemological Institute of America, Carlsbad, California, USA) and Karl Egon Wild (Wild & Petsch Co., Kirschweiler, Germany).

Gemmological and Spectroscopic Features of Untreated vs. Heated Amber

Yamei Wang, Mingxing Yang, Shufang Nie and Fen Liu

Detailed testing of amber samples before and after heat treatment (i.e. clarifying, baking, decrepitating and 'beeswax ageing') was performed using standard gemmological instruments, as well as Fourier-transform infrared (FTIR) and FT-Raman spectroscopy. In general, the heated ambers were characterized by: (1) an increase in RI and a decrease in fluorescence; (2) the presence of discoidal stress fractures and red flow striations in the interior of some samples, as well as oxidation cracks, septarian cracks and ripples on the surface of amber treated by certain processes; (3) a significantly enhanced absorption in FTIR spectra of the carbonyl (C=O) stretching vibrations at 1732 and 1702 cm^{-1} , and of the C–O stretching vibration at 1260–1160 cm^{-1} ; and (4) an intensity ratio $I = 2932 \text{ cm}^{-1}/I = 1732 \text{ cm}^{-1}$ in FTIR spectra of >1.78 for untreated amber vs. ≤ 1.54 for clarified (golden) amber and ≤ 0.50 for baked (red) amber; intensity ratios of ~ 1.5 – 1.9 are not considered diagnostic.

The Journal of Gemmology, 35(6), 2017, pp. 530–542, <http://dx.doi.org/10.15506/JoG.2017.35.6.530>
© 2017 The Gemmological Association of Great Britain

Introduction

Amber is a fossilized organic gem material derived from Cretaceous–Tertiary ancient plant resin that has undergone devolatilization, polymerization and hardening through various geological processes. Because of its moderate price and warm colour appearance, and its status as one of the seven jewels embraced by Buddhists, amber is popular with many people and has profound cultural connotations. In recent years, the amber market has expanded rapidly in China. However, because heat-treated amber comprises a significant share of the market (e.g. Figure 1), distinguishing untreated from heat-treated amber has become a priority for some gem-testing institutions. The identification of heat-treated amber has been difficult, in part because knowledge of the heat-treatment processes and techniques used have long been kept confidential.

The main purposes of amber heat treatment are to improve or alter the colour, enhance the clarity and produce inclusions that have an appealing visual effect. Methods include clarifying, baking (oxidation), decrepitating and 'beeswax ageing'; see Wang et al. (2014) for a detailed description of the various processes and conditions used for each type of treatment. Clarification (or 'purification') removes bubbles from amber by heating it in an inert atmosphere under autoclave-controlled temperature and pressure. Baking involves adding an appropriate amount of oxygen gas to the autoclave to oxidize the amber surface and form a thin red to dark red layer, thus changing its colour appearance. Decrepitation involves the rapid release of gas from the autoclave after heating and pressurizing; this alters the pressure equilibrium of bubbles in amber so the internal pressure is greater than the external pressure, causing the



Figure 1: Various types of heat-treated amber are commonly encountered in the marketplace. Shown here are a golden amber pendant (upper left, 36.65 g), a bicoloured fire amber pendant (upper right, 22.59 g), a red amber necklace (96.27 g) and an aged beeswax bracelet (45.31 g). Photo by Y. Wang.

bubbles to expand and decrepitate into discoidal stress fractures. The purpose of decrepitation is to produce attractive inclusions called ‘sun spangles’ or ‘sun sparks’. In the beeswax ageing process, amber with low clarity (i.e. *beeswax* amber, which is sub-translucent or opaque due to abundant microscopic gas bubbles) is given an aged and darkened appearance by prolonged slow oxidation under low temperature at constant pressure, so that it resembles antique beeswax.

This article provides a detailed characterization of the amber samples that were treated in experiments by Wang et al. (2014). We used standard gemmological instruments and FTIR and Raman spectroscopy to document changes in the physical, optical and spectroscopic properties of the amber samples before and after heat treatment. The formation mechanisms of the features seen in heat-treated amber are discussed, and criteria for identifying heat-treated amber are presented.

Materials and Methods

Six blocks of Baltic amber originating from Kaliningrad, Russia, were sliced into pieces and subjected to heating experiments that were inferred to be representative of those performed by commercial treatment facilities; the treatment conditions and their outcomes were described by Wang et al. (2014). The samples from the six blocks are designated JA, JB, JC, JD, JE and JF (Figure 2), and they ranged from opaque to transparent, including some with a beeswax appearance (i.e. JC, JD, JE and JF). Of the 32 slices, one piece from each block was retained as an untreated reference sample (JA-1, JB-3, JC-5, JD-1, JE-1 and JF-4), three were preserved for future studies and the remaining 23 slices underwent clarifying, baking, decrepitating and/or beeswax-

ageing experiments, depending on the features present in each sample (see Figure 3 and Table I). The sawn surfaces of each sample were polished before any treatments were performed. After treatment, samples JA-5, JC-3, JC-4, JE-3 and JE-4 were repolished and JE-5 was partially repolished.

Detailed observations and testing of colour and clarity, RI, long-wave UV fluorescence and internal features were carried out on the samples before and after heat treatment using standard gemmological instruments, including a refractometer (GI-RZ6), UV lamp (GI-UVB) and microscope (GI-MPV), all manufactured by Shenzhen Baoguang Scientific Instruments Co. Ltd. In addition, SG was measured hydrostatically for all samples, but the values were all nearly identical (1.065–1.069) and therefore are not discussed further in this article.

A Bruker Tensor 27 FTIR spectrometer was used with a reflectance accessory to acquire FTIR absorption spectra of the samples before and after heat treatment, in the range of 4000–400 cm^{-1} with 32 scans at a resolution of 4 cm^{-1} . Analyses were performed at a temperature of 19°C and a relative humidity of 35%. Because specular reflectance FTIR was used to non-destructively analyse the samples, all the acquired spectra were subjected to a Kramers–Kronig transformation and baseline correction using OPUS software to eliminate the distortion of spectra caused by dispersion. FTIR spectroscopy was performed on the six untreated reference samples, as well as on all the other ambers before treatment. After heat treatment, FTIR spectra were collected on six golden ambers, one pearly beeswax sample, three golden fire ambers, three red fire ambers, seven red ambers, one bicoloured amber and two aged beeswax samples, and also on selected samples (JA-4, JB-4, JC-1,

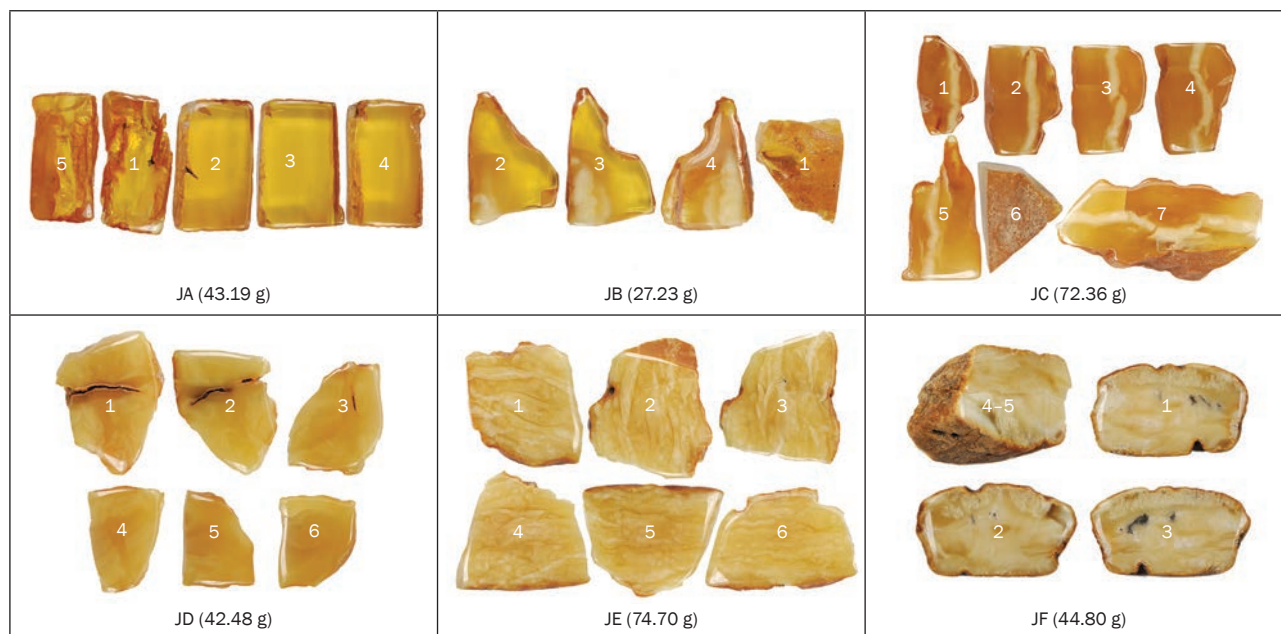


Figure 2: Untreated amber specimens from Kaliningrad, Russia, were sliced into multiple pieces for heating experiments. Each sample number is shown with the total weight of all the slices. Photos by Y. Wang.

JC-2, JD-6, JF-1 and JF-3) after clarifying and/or baking.

A Bruker Vertex 70 FT-Raman spectrometer was used to acquire Raman reflectance spectra with an excitation wavelength of 1064 nm, laser energy of 150 mW and 64 scans at a resolution of 4 cm⁻¹, at a temperature of 25°C and a relative humidity of 46%. Raman spectroscopy was performed on four representative untreated ambers (JA-1, JD-1, JE-1 and JF-4) and on three heated samples (bicoloured JA-5, golden JD-3 and red JD-6).

All spectroscopic measurements were performed on smooth flat faces that had been polished before heat treatment, except for those samples listed above that were repolished after treatment.

Results and Discussion

The colour and clarity, RI values, long-wave UV fluorescence and internal features of the amber samples before and after heat treatment are shown in Table I.

Colour and Clarity

Heat treatment effectively altered the colour and clarity of the amber. Yellow or light yellow beeswax amber was transformed into golden yellow, red or dark red-appearing material. The clarity of the entire sample changed in most cases from opaque or translucent to transparent, although a few of the treated ambers displayed a transparent surface and an opaque interior (e.g. the pearly beeswax sample JC-7).

Refractive Index

The RI of all samples was measured on flat-polished surfaces, and for each piece the refractometer displayed the shadow edge with a fairly clear boundary, so we consider the RI values to be accurate to two decimal places.

Table I and Figure 4 show that heat treatment increased the RI of the samples in most cases, and that variations in RI were closely related to heat treatment time and the amount of oxidation. Specifically, we found that: (1) the clarifying and baking processes increased the RI value; (2) the longer the clarifying time, the greater the increase in refractive index (e.g. the RI of sample JD-3 changed from 1.54 to 1.56 after three clarifying cycles); (3) the greater the oxidation amount (darker colour), the larger the increase in RI (e.g. sample JC-2 was oxidized to red in one baking cycle, yielding an RI of 1.56, while sample JC-1 underwent three baking cycles to turn dark red, with a resulting RI of 1.58); (4) prolonged (60–100 days) beeswax ageing at low temperature (60°C) did not significantly alter the refractive index (e.g. samples JD-2 and JE-6 had unchanged RIs of 1.54 before and after treatment); and (5) the increase in RI was limited to the near-surface, as no change in measurements compared to untreated amber was noted in practically all heated samples after they were repolished (e.g. samples JA-3, JC-4, JD-4, JE-5 and JF-2 underwent clarifying, decrepitating and/or baking followed by repolishing, and their measured RI values remained 1.54 before and after treatment).

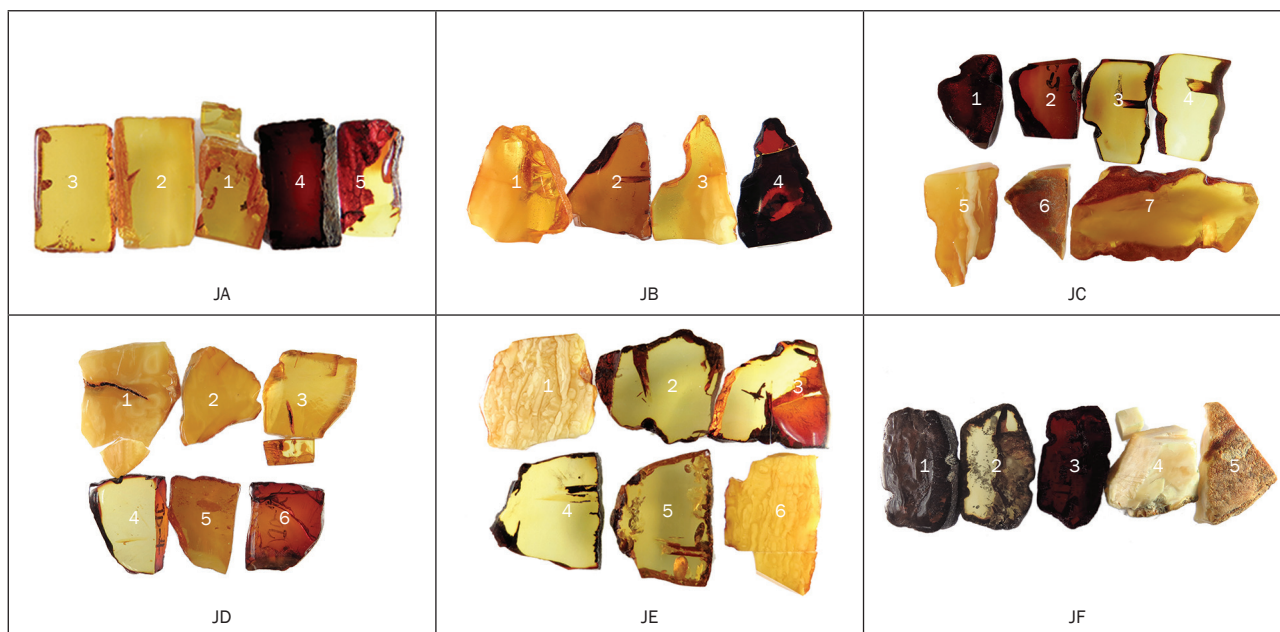
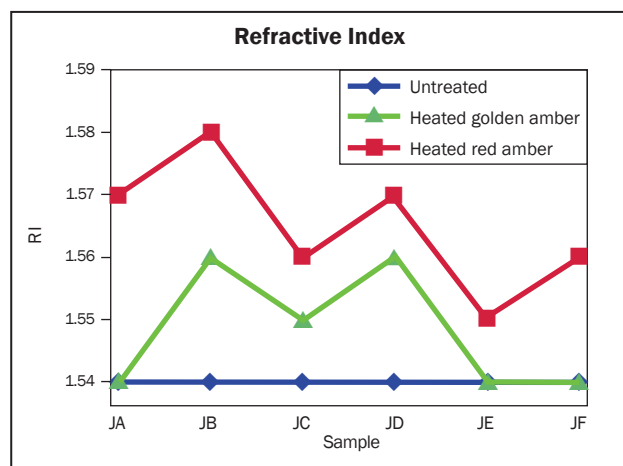


Figure 3: Pictured here are the same amber specimens in Figure 2 following various treatment processes, as described in the text and in Table I. Photos by Y. Wang.

Long-wave UV Fluorescence

Before treatment, all the samples showed similar moderate-to-strong yellow to yellowish white fluorescence (Table I), and their luminescence patterns mimicked the internal structure of the amber (e.g. flowed clouds of gaseous inclusions). Heat treatment significantly altered the UV fluorescence features of the amber, and the intensity, uniformity and colour of the luminescence closely corresponded with the heat-treatment process. Figure 5 shows the fluorescence of representative samples under

Figure 4: Compared to untreated samples, RI values were higher for some of the tested heat-treated golden ambers and all of the red ambers. While the golden ambers were clarified in an inert gas, the red ambers underwent oxidation during the baking process that was used to induce their surface coloration.



long-wave UV radiation, including untreated amber, clarified golden amber and baked red amber.

Our results indicate that: (1) the fluorescence intensity of our clarified golden amber samples decreased somewhat, exhibiting weak-to-moderate dull yellow or yellowish white fluorescence that was typically uniform in appearance; and (2) the fluorescence strength of our baked red ambers diminished significantly, becoming inert or showing only weak dull yellow fluorescence (with the exception of those samples that were repolished after treatment, which displayed moderate yellow or yellowish white luminescence). Therefore, such luminescence quenching provides important evidence of heat treatment.

The clarity of opaque Baltic amber can be improved with heat treatment under pressure. As supported by our experiments, an increased concentration of the carbonyl group ($C=O$; described below) acts as a chromophore because its $n-\pi^*$ transition absorbs visible light, leading to a darkened and reddened coloration and a quenching of fluorescence after heat treatment (Wu and Chen, 2000).

Internal Features

Discoidal Stress Fractures: After the beeswax-type samples were decrepitated, discoidal stress fractures appeared (i.e. ‘sun-spangle’ inclusions), and two varieties were noted. ‘Golden fire’ amber—containing golden yellow-coloured sun-spangle inclusions—resulted from decrepitation in an anaerobic environment (e.g. JE-5; Figure 6a), while

Table 1: Gemmological properties of amber samples before and after heat treatment.^a

Treatment method(s) ^a	Type	Sample no.	Treatment parameters	Colour		Clarity	
				Before	After	Before	After
Clarifying	Golden amber	JB-2	200 °C, 5 MPa, 5 hours, inert gas (N ₂)	Golden yellow – milky white	Brownish yellow	Transparent surface and opaque interior	Transparent
		JD-3	210 °C, 5.5 MPa, 5.5 hours, inert gas (N ₂)	Yellow	Brownish yellow	Translucent	Transparent
		JD-4	200 °C, 3 MPa, 3 hours, inert gas (N ₂)	Yellow	Bright yellow	Translucent	Transparent
		JE-2	210 °C, 5.5 MPa, 6 hours, inert gas (N ₂)	Yellow and light yellow	Bright golden yellow	Opaque	Transparent
		JF-2	200 °C, 5 MPa, 5 hours, inert gas (N ₂)	Milky white and yellow	Golden yellow	Opaque	Transparent
		JC-4	210 °C, 5.5 MPa, 6 hours, inert gas (N ₂)	Yellow and white	Bright yellow	Translucent	Transparent
	Pearly beeswax	JC-7	200 °C, 4.5 MPa, 5 hours, inert gas (N ₂)	Yellow and white	Yellow	Translucent	Transparent-translucent
Clarifying + baking	Red amber	JA-4	210 °C, 4.5 MPa, 3 hours, N ₂ +O ₂ gas	Golden yellow	Dark red	Transparent	Transparent
		JB-4	210 °C, 4.5 MPa, 3 hours, N ₂ +O ₂ gas	Yellow – milky white	Dark red	Transparent surface and opaque interior	Transparent
		JC-1	210 °C, 5.5 MPa, 6 hours, inert gas (N ₂) with residual air	Yellow and white	Dark red	Translucent	Transparent
		JC-2	210 °C, 4.5 MPa, 3 hours, N ₂ +O ₂ gas	Yellow and white	Red	Translucent	Transparent
		JD-6	210 °C, 4.5 MPa, 3 hours, N ₂ +O ₂ gas	Yellow	Orangey red	Translucent	Transparent
		JF-1	210 °C, 5.5 MPa, 6 hours, inert gas (N ₂) with residual air	Milky white	Dark red	Opaque	Translucent
	JF-3	210 °C, 4.5 MPa, 3 hours, N ₂ +O ₂ gas	Milky white	Dark red	Opaque	Transparent	
	Bicoloured amber	JA-5	210 °C, 4.5 MPa, 3 hours, N ₂ +O ₂ gas	Golden yellow	Yellow and red	Transparent	Transparent
Clarifying + decrepitating	Golden fire amber ^b	JA-3	200 °C, 3 MPa, 2.5 hours, inert gas (N ₂) with residual air	Golden yellow	Golden yellow	Transparent	Transparent
		JD-5	200 °C, 3 MPa, 2.5 hours, inert gas (N ₂)	Yellow	Brownish yellow	Translucent	Transparent
		JE-5	200 °C, 3 MPa, 2.5 hours, inert gas (N ₂)	Yellow and light yellow	Golden yellow	Opaque	Transparent
Clarifying + decrepitating + baking	Red fire amber ^b	JC-3	200 °C, 3 MPa, 3 hours, N ₂ +O ₂ gas	Yellow and white	Yellow	Translucent	Transparent
		JE-3	200 °C, 4 MPa, 3 hours, N ₂ +O ₂ gas	Yellow and light yellow	Golden yellow and red	Opaque	Transparent
		JE-4	200 °C, 4 MPa, 3 hours, N ₂ +O ₂ gas	Yellow and light yellow	Yellow	Opaque	Transparent
Beeswax ageing	Aged beeswax ^c	JD-2	60 °C, ambient pressure, 60 days, in air	Yellow	Brownish yellow	Translucent	Translucent
		JE-6	60 °C, ambient pressure, 90 days, in air	Yellow and light yellow	Brownish yellow	Opaque	Opaque

^a For detailed heat treatment procedures and results, see Wang et al. (2014). Samples shown in bold italics were repolished or partially polished after treatment.

^b 'Golden' and 'red' fire ambers are transparent and have golden and red discoidal fractures ('sun spangles'), respectively.

^c 'Aged beeswax' amber is slowly oxidized to show an aged and darkened-yellow appearance similar to antique beeswax.

RI		Long-wave UV fluorescence		Internal features	
Before	After	Before	After	Before	After
1.54	1.56	Moderate yellow to intense yellowish white	Weak orange	Flowed clouds of gaseous inclusions, bubbles, local cracks	Local red cracks
1.54	1.56	Strong yellow	Weak dull yellow	Flowed clouds of gaseous inclusions, small fissures	Small fissures
1.54	1.54	Strong yellow	Moderate yellowish white	Flowed clouds of gaseous inclusions	Small red striations
1.54	1.54	Strong yellowish white	Moderate-to-weak yellowish white	Flowed clouds of gaseous inclusions	Red cracks
1.54	1.54	Strong yellowish white	Moderate yellowish white	White flowed clouds of gaseous inclusions	Partial flowed clouds of gaseous inclusions
1.54	1.54	Strong yellowish white	Moderate yellow	Flowed clouds of gaseous inclusions	Clear with red microfissures on the rim
1.54	1.55	Strong yellowish white	Moderate dull yellow	Flowed clouds of gaseous inclusions	Flowed clouds of gaseous inclusions in the centre
1.54	1.57	Moderate yellowish white	Inert	Thin flowed clouds of gaseous inclusions	None
1.54	1.55	Strong yellowish white	Inert	Flowed clouds of gaseous inclusions	None
1.54	1.58	Strong yellowish white	Inert	Flowed clouds of gaseous inclusions	Partial flowed clouds of gaseous inclusions
1.54	1.56	Strong yellow to white	Inert	Flowed clouds of gaseous inclusions	Partial flowed clouds of gaseous inclusions
1.54	1.57	Strong yellow	Inert	Flowed clouds of gaseous inclusions	None
1.54	1.56	Strong yellowish white	Inert	Flowed clouds of gaseous inclusions	Red flow striations
1.54	1.56	Strong yellowish white	Inert	Flowed clouds of gaseous inclusions	Impurities and small fissures
1.54	Yellow: 1.54 Red: 1.56	Moderate yellowish white	Moderate yellowish white (yellow area) and inert (red area)	Thin flowed clouds of gaseous inclusions	None
1.54	1.54	Moderate yellowish white	Weak dull yellow	Bubbles, flowed clouds of gaseous inclusions	Golden and red discoidal stress fractures
1.54	1.55	Strong yellow	Weak dull yellow	Flowed clouds of gaseous inclusions	Golden discoidal stress fractures of variable size
1.54	1.54	Strong yellowish white	Weak yellow before repolishing; moderate yellowish white after repolishing	Flowed clouds of gaseous inclusions	Golden discoidal stress fractures
1.54	1.54	Strong yellow to white	Inert before repolishing; moderate yellow after repolishing	Flowed clouds of gaseous inclusions	Red discoidal stress fractures
1.54	Yellow: 1.54 Red: 1.55	Strong yellowish white	Inert before repolishing; moderate yellowish white after repolishing	Flowed clouds of gaseous inclusions	Red discoidal stress fractures
1.54	1.54	Strong yellowish white	Weak brownish yellow before repolishing; moderate yellowish white after repolishing	Flowed clouds of gaseous inclusions	Red discoidal stress fractures
1.54	1.54	Strong yellow	Moderate brownish yellow	Flowed clouds of gaseous inclusions, large cracks	Flowed clouds of gaseous inclusions
1.54	1.54	Strong yellowish white	Moderate yellow	Flowed clouds of gaseous inclusions	Flowed clouds of gaseous inclusions

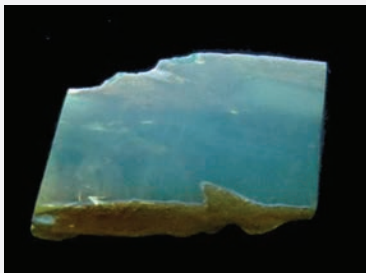


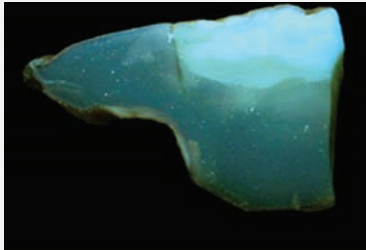
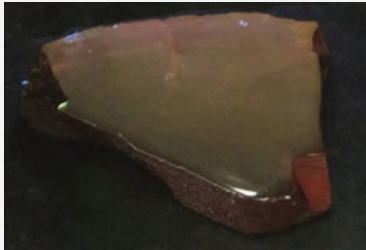
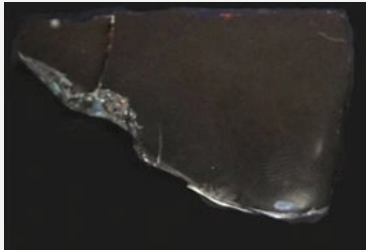
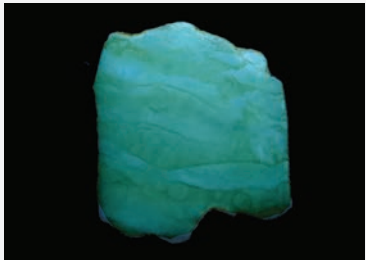
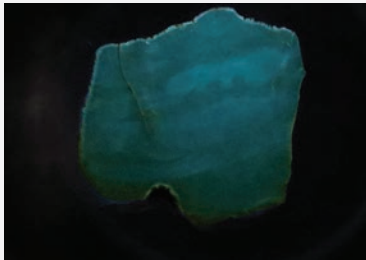
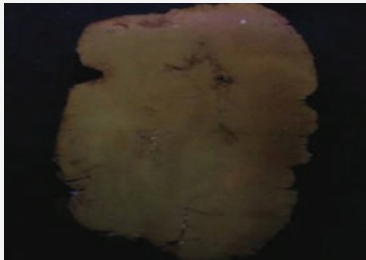
	Untreated	Clarified golden amber	Baked red amber
JA	 JA-1 (6.65 g): Moderate yellowish white	 JA-3 (9.44 g): Weak dull yellow	 JA-4 (8.94 g): Inert
JB	 JB-3 (6.25 g): Moderate yellow to intense yellowish white	 JB-2 (6.83 g): Weak orange	 JB-4 (5.42 g): Inert
JE	 JE-1 (13.54 g): Strong yellowish white	 JE-2 (11.50 g): Moderate-to-weak yellowish white	 JE-4 (13.87 g): Weak brownish yellow (before repolishing)

Figure 5: These images illustrate the typical long-wave UV fluorescence of the amber samples before and after heat treatment. The bluish hue seen in some of the images is a photographic artefact from the UV lamp. Photos by Y. Wang.

‘red fire’ amber showed sun-spangle inclusions that were red, ascribed to products of decrepitation combined with oxidation of the fissures (e.g. JC-3; Figure 6b).

Sun spangle-type inclusions are very rarely encountered within untreated amber, owing to the equilibrium of temperature and pressure during fossilization. In heat-treated amber, the discoidal stress fractures are produced by expansion and decrepitation after the pressure equilibrium of the bubbles within the amber has been abruptly broken (i.e. internal pressure exceeds external pressure). Therefore, the presence of large and numerous sun spangles within amber provides immediate evidence of heat treatment.

Red Flow Striations: Red flow striations were sometimes visible within heat-treated golden or red amber samples (e.g. Figure 7). These striations

were well defined, with a natural and fluid-like appearance, reflecting the primary textural features of beeswax amber. The original flow striations in the amber apparently were preferentially oxidized along the flow boundaries during heat treatment.

Surface Features

Various surface features were seen on the samples that had not undergone repolishing after treatment.

Oxidation Cracks: Narrow red oxidation cracks often were visible along fissures and defects in aged beeswax amber. The centrelines of such fissures were unoxidized with a light yellow colour, and both sides of the fissures were dark red with only minor ‘bleeding’ of colour (Figure 8a). This is dramatically different from the appearance of cracks that have undergone slow natural oxida-

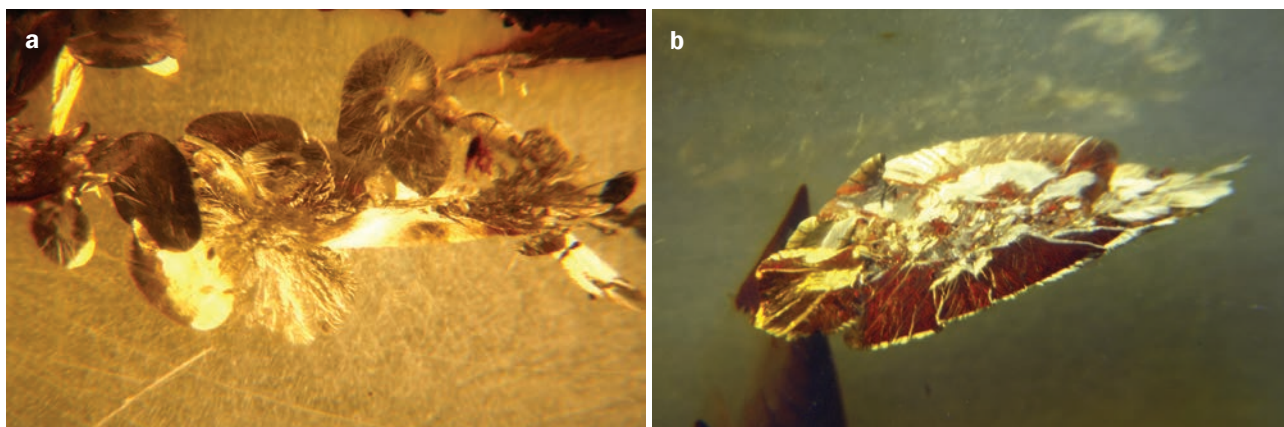


Figure 6: ‘Sun spangles’, or discoidal stress fractures, were exhibited by heat-treated amber samples that underwent decrepitation. They are shown here within: (a) golden fire amber JE-5 (magnified 15×) and (b) red fire amber JC-3 (20×; the red colour of this particular discoid fracture is partially obscured by yellow reflections from the surrounding amber). Photomicrographs by Y. Wang.



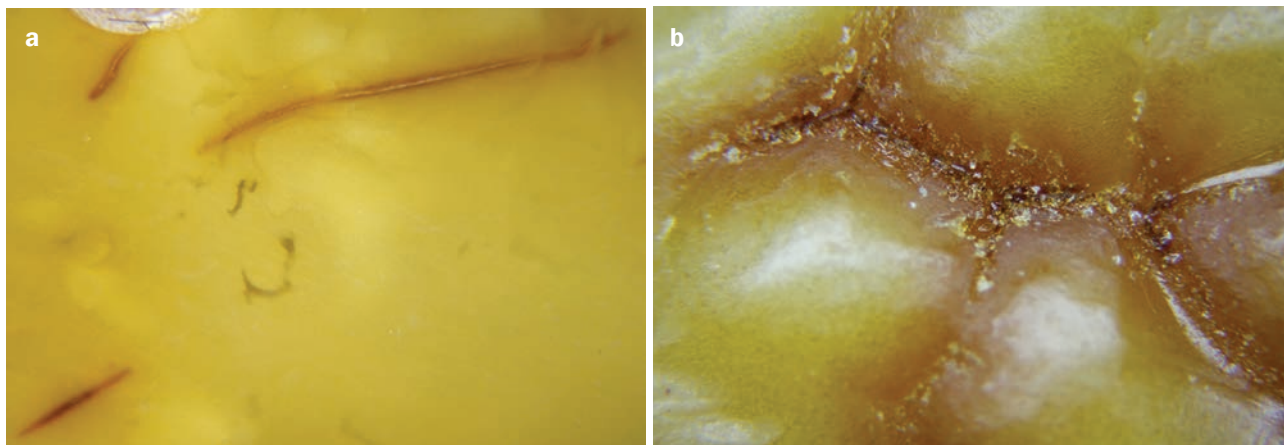
Figure 7: Red flow striations are seen within baked amber sample JF-1. Photomicrograph by Y. Wang; magnified 10×.

tion during geological weathering; they have dark centrelines and show progressively lighter coloration outward from the cracks (Figure 8b).

Septarian Cracks: Irregular networks of micro-cracks showing a mosaic-like appearance (i.e. ‘septarian cracks’) often were seen on the surface of red amber samples (Figure 9). They provide another indication of heat-treated amber, and appear to be caused by uneven contraction of the amber surface through rapid devolatilization resulting from improper temperature control during the heating process.

Surface Ripples: Wavy surface ripples were seen on some of the amber samples that had undergone treatment in an autoclave (e.g. Figure 10). These ripples probably formed when the surface of amber placed in the upper part of the autoclave softened during heat treatment and was slightly deformed by gas currents.

Figure 8: (a) Surface features of aged beeswax amber may include oxidation cracks, as shown here on sample JD-2; note the unoxidized centrelines and only minor ‘bleeding’ of adjacent colour. (b) By contrast, cracks formed in beeswax amber during natural weathering have dark centrelines with more extensive ‘bleeding’ of colour, as seen here on untreated amber JB-3. Photomicrographs by Y. Wang; magnified 20×.



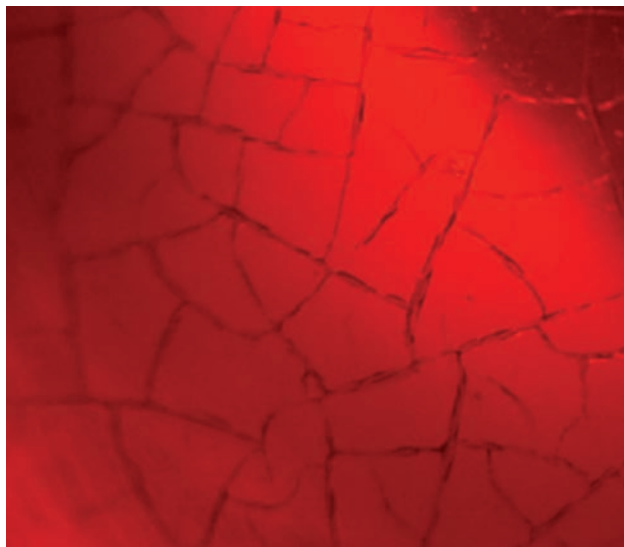


Figure 9: Septarian cracks (here, on the surface of red amber JA-4) display a mosaic-like appearance. Photomicrograph by Y. Wang; magnified 15 \times .



Figure 10: Ripples are seen on the surface of baked amber JF-1. Photomicrograph by Y. Wang; magnified 10 \times .

FTIR Spectra

Before Heat Treatment: FTIR spectroscopy of all 32 amber samples before treatment yielded largely the same results (see, e.g., the spectra of samples JA-4, JB-4 and JD-6 in Figure 11a). Strong IR absorption bands at 2932 and 2867 cm^{-1} corresponded to the asymmetric stretching vibration of the C–H saturated bond, and a pair of IR absorptions at 1732 and 1702 cm^{-1} resulted from the carbonyl stretching vibration $\nu(\text{C}=\text{O})$ (Abduriyim et al., 2009). Moderately strong IR absorptions from the $\delta(\text{CH}_2\text{--CH}_3)$ bending vibration occurred at 1452 and 1378 cm^{-1} , indicating that the basic structure of the amber is aliphatic (Qi et al., 2003; Guiliano et al., 2007). In addition, broad absorptions in the range 1260–1160 cm^{-1} are assigned to C–O stretching vibration; these features (known as the ‘Baltic shoulder’) are specific to Baltic amber and are related to the presence of succinic acid and succinate (Brody et al., 2001). (The features in the ~ 2300 cm^{-1} region are attributed to H_2O and CO_2 in the air.)

It is worth noting that almost all of our untreated Kaliningrad samples displayed absorptions at 1645 cm^{-1} related to unsaturated C=C double bonds and at 888 cm^{-1} due to C–H out-of-plane bending vibration of the exocyclic methylene group. These features also occur in other Baltic ambers from Poland, Ukraine and Lithuania, as well as in Dominican amber, as we have discovered during our routine analysis of amber. A previous study (Yang and Wang, 2010) also showed that, with natural resin polymerization and volatilization, the out-of-ring bonds (grouped absorptions at 3078, 1645 and 888 cm^{-1})

of unsaturated terpenoids existing in fossilized resin gradually broke down, and their relative intensities became weaker until they vanished. Nonetheless, weak absorptions at 1645 and 888 cm^{-1} suggest the presence of a small amount of terpenoid volatiles remaining in our amber samples. This is also one of the reasons why Baltic amber, after being rubbed or processed, gives off a more intense rosin smell than ambers from other localities.

After Heat Treatment: The FTIR spectra of the amber samples after heat treatment varied significantly with clarification and degree of oxidation (Figure 11b,c). Table II summarizes the intensity ratios of the two major bands—2932 cm^{-1} ($\nu[\text{CH}_2]$) and 1732 cm^{-1} ($\nu[\text{C}=\text{O}]$)—in the FTIR spectra of samples before and after heating and at different stages of treatment. The intensity ratio of these bands for golden amber ranged within 0.62–1.74, while the intensity ratio for red amber was <0.5 . As seen in Figure 11, the intensity ratio exhibits a distinct progressively decreasing trend from before heat treatment to clarification to oxidation.

The following FTIR spectral information of heat-treated amber can be obtained from Table II and Figure 11:

1. The intensities of the IR absorptions at 2932 and 2867 cm^{-1} —owing to the asymmetric stretching vibration of $\nu(\text{CH}_2)$ —tend to decrease progressively with clarification and oxidation, whereas the intensities of the bands at 1732 and 1702 cm^{-1} —owing to the carbonyl stretching vibra-

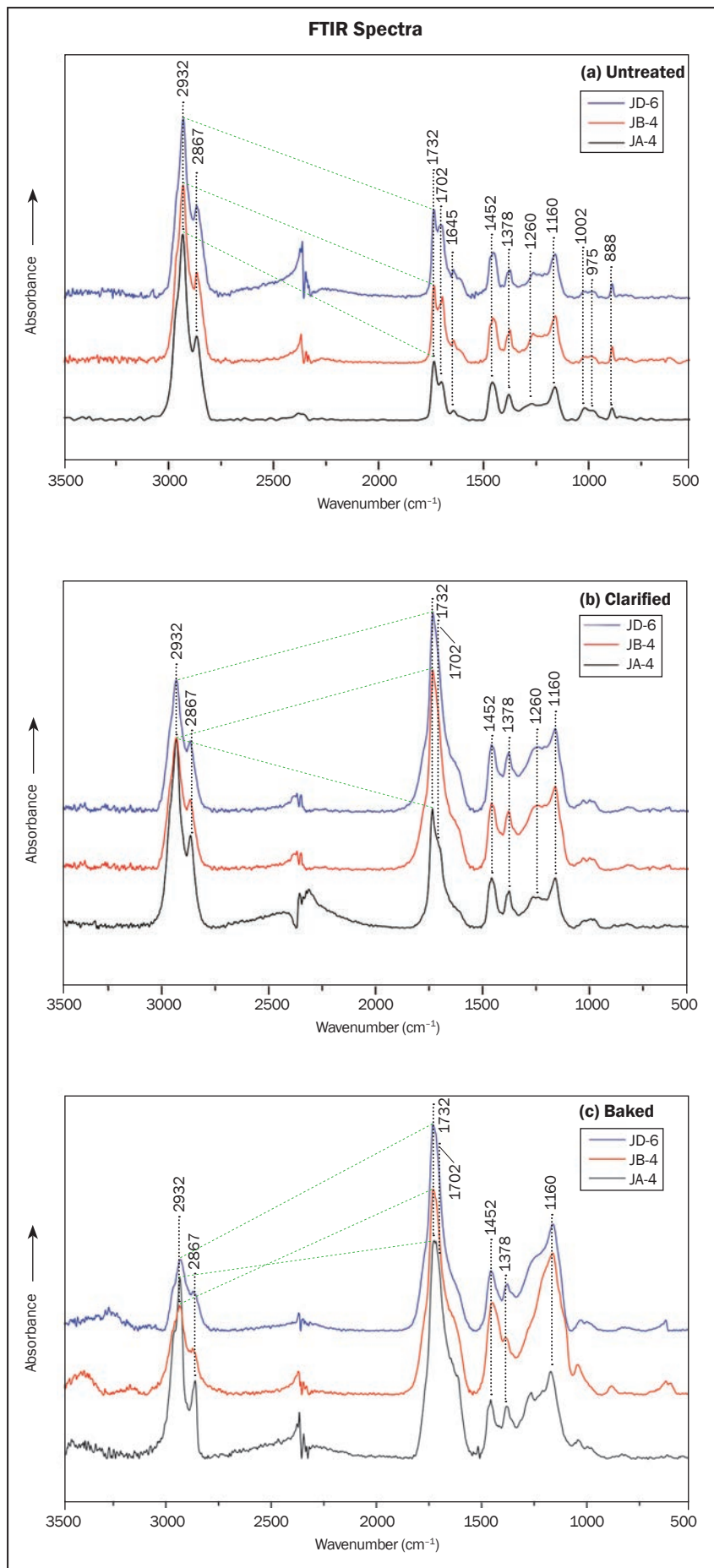


Figure 11: FTIR spectra of amber samples JA-4, JB-4 and JD-6 are shown (a) before heat treatment, (b) after clarification and (c) after oxidation. The clarification process increased the 1732 cm⁻¹ band in all three samples, although somewhat less in JA-4, probably because it was clarified only once whereas JB-4 and JD-6 were clarified twice.

Table II: Intensity ratios ($I = 2932\text{ cm}^{-1}/I = 1732\text{ cm}^{-1}$) in the FTIR spectra of the amber samples before and after heat treatment.*

Sample no.	Untreated	Heat treated		
		Golden amber and fire amber	Red amber	Aged beeswax
JA-3	2.94	1.00	—	—
JA-4	3.13	1.74	0.32	—
JB-2	2.28	0.62	—	—
JB-4	2.41	0.72	0.49	—
JC-1	2.41	0.82	0.50	—
JC-2	2.43	0.75	0.32	—
JC-3	2.08	0.92	—	—
JC-4	2.13	1.54	—	—
JC-7	2.05	0.92	—	—
JD-2	2.08	—	—	0.43
JD-3	2.15	0.79	—	—
JD-4	2.26	1.57	—	—
JD-5	2.52	0.72	—	—
JD-6	2.00	0.65	0.33	—
JE-2	2.00	1.21	—	—
JE-3	1.92	1.48	—	—
JE-4	1.96	1.26	—	—
JE-5	1.92	1.09	—	—
JE-6	1.94	—	—	0.48
JF-1	1.89	—	0.40	—
JF-2	1.78	1.08	—	—
JF-3	1.82	—	0.39	—

* Samples shown in bold italics were analysed on surfaces that were repolished after treatment.

tion of $\nu(\text{C}=\text{O})$ —tend to increase progressively with the overall peak shape, becoming sharper and steeper. In our samples, an intensity ratio of ≤ 1.54 for the 2932 and 1732 cm^{-1} bands is indicative of clarified amber, while ≤ 0.50 correlates to baked amber and the range of ~ 1.5 – 1.9 is not considered diagnostic.

2. During heat treatment, the weak absorptions at 1645 cm^{-1} (related to unsaturated C=C double bonds of the exocyclic methylene group) and at 888 cm^{-1} (related to C–H vibrations linked with the exocyclic methylene group) diminish until they disappear.
3. The relative intensity of the C–O stretching vibration features (Baltic shoulder at 1260 – 1160 cm^{-1}) generally increases progressively with clarification and oxidation.
4. With increasing absorption intensity of the carbonyl stretching vibration $\nu(\text{C}=\text{O})$, the appearance of heat-treated amber gradually darkens until it turns dark red. Therefore, it can be postulated that the carbonyl group is a chromophore that reddens amber.
5. Repolishing may remove the heat-treated surface, which has a higher degree of oxidation

than the interior, and thus may change the intensity of IR features. For example JC-4, JE-3, JE-4 and JE-5 have relatively high ratios of $I = 2932\text{ cm}^{-1}/I = 1732\text{ cm}^{-1}$ (i.e. 1.09–1.54). Depending on the extent of the treatment and the depth of repolishing, the intensity ratio may or may not be diagnostic.

A previous study (Abdurizim et al., 2009) also reported the diminishment of the unsaturated bonds at 3076 cm^{-1} , 1643 cm^{-1} (corresponding to 1645 cm^{-1} in this study) and 887 cm^{-1} (corresponding to 888 cm^{-1} in this study), and the increase of C=O carbonyl stretching vibration at 1732 cm^{-1} in Baltic amber during heat treatment. By combining the results of previous research with the conclusions of this study, we surmise that such variations in the FTIR spectra of amber represent proportional thermal oxidation. A decrease in the absorption of the major band at 2932 cm^{-1} suggests that the saturated C–H bond was broken down by heating. An increase in intensity of the absorption at 1732 cm^{-1} suggests that oxygen involvement enables a higher concentration of the C=O functional group. And the extinction of weak absorptions at 1645 and 888 cm^{-1} corresponds with the breaking of the unsaturated C=C double bond of the exocyclic methylene group. In summary, heat treatment eventually leads to fewer saturated C–H bonds and unsaturated C=C double bonds in amber, in correlation with more oxygen-bearing functional groups and a higher degree of polymerization.

Raman Spectroscopy

Before Heat Treatment: The untreated samples had a very strong fluorescent background, so a Fourier-transform technique was employed in this study to collect the signal followed by multiple accumulations to improve the signal-to-noise ratio. Samples also were illuminated by a near-IR laser at 1064 nm , which greatly mitigated the fluorescent background, and the spectra were baseline corrected.

Of the four untreated samples that were analysed, JA-1 was transparent whereas JD-1, JE-1 and JF-4 consisted of opaque beeswax types. Compared to the FTIR spectra, the FT-Raman spectra were simpler. As seen in Figure 12, they mainly consist of three regions:

1. Within the 3000 – 2800 cm^{-1} range is a group of multiple characteristic peaks related to the stretching vibration of the saturated C–H bond (Brody et al., 2001; Edwards et al., 2007), with the strongest Raman peak at around 2932 cm^{-1} .

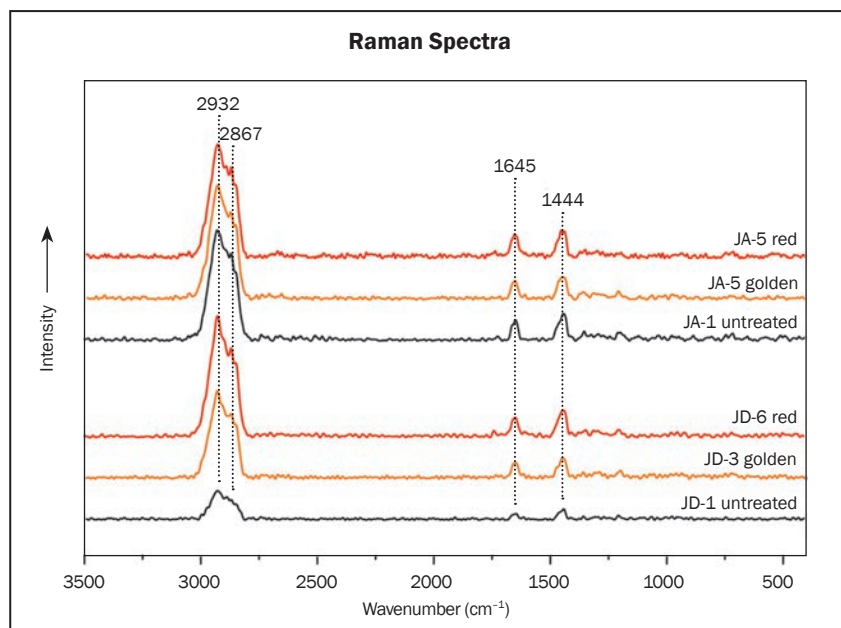


Figure 12: Representative FT-Raman spectra are shown for sample groups JA and JD, both before and after heat treatment.

2. The peak at $\sim 1444\text{ cm}^{-1}$ is due to the bending vibration of the C–H bond (Brody et al., 2001; Edwards et al., 2007). The peaks in the $3000\text{--}2800\text{ cm}^{-1}$ range and at 1444 cm^{-1} indicate the presence of a saturated aliphatic structure, which is consistent with the features shown by the FTIR spectra.
3. Significantly different from the FTIR spectra, the FT-Raman spectra had a strong peak at $\sim 1645\text{ cm}^{-1}$ related to the stretching vibration of the unsaturated C=C double bond (Brody et al., 2001; Edwards et al., 2007), whereas the feature at 1645 cm^{-1} in the FTIR spectrum resulting from the stretching vibration of the C=C double bond was extremely weak. This is related to the intense Raman activity of this group.

After Heat Treatment: Samples derived from the same original block of amber showed little variation in their Raman spectra before and after heat treatment (Figure 12). Previous Raman spectral studies of amber mainly focused on the intensity ratio $v(\text{C}=\text{C})/\delta(\text{CH}_2)$, or $I = 1645\text{ cm}^{-1}/I = 1444\text{ cm}^{-1}$, because during amber formation, as resin maturity increases, polymerization continuously alters unsaturated C=C double bonds into single bonds. As a result, the absorption intensity at 1645 cm^{-1} dwindles whereas that at 1444 cm^{-1} increases gradually, so the relative intensities of these two Raman peaks have been used to postulate the degree of amber polymerization (Brody et al., 2001; Vandenabeele et al., 2003; Guiliano et al., 2007). Table III reports

these intensity ratios for samples JA-1, JA-5, JD-1, JD-3 and JD-6 obtained through computation with the OPUS software.

Careful comparison indicated that: (1) for heat-treated amber, the Raman intensity ratios were still <1 , which is consistent with the ratio before treatment, and (2) after the samples had been heat treated, this ratio was slightly greater than before heat treatment. However, these minor changes are not considered diagnostic for heat treatment, and more data are needed for verification. Such changes might be related to oxidation during heat treatment, indicating that the number of saturated C–H bonds consumed by oxidation is more than that of unsaturated C=C double bonds consumed by oxidation.

Conclusions

Based on our experimental study of the heat treatment of amber (Wang et al., 2014), we performed a systematic comparison of the changes in gemmological features, FTIR spectra and FT-Raman spectra of samples before and after heating. We reached the following conclusions:

1. Heat treatment can alter the appearance of amber, clarifying inclusions and producing discoidal stress fractures and red flow striations internally as well as a red coloration (on baked amber) and cracking/ripples on the surface.
2. Heat treatment may cause the RI to increase according to the amount of clarification and oxidation. In this study, the RI of untreated

Table III: Intensity ratios ($I = 1645\text{ cm}^{-1}/I = 1444\text{ cm}^{-1}$) of FT-Raman spectra of amber before and after heat treatment.

Sample no.	Untreated	Heat treated	
		Golden amber	Red amber
JA-1	0.72	–	–
JA-5	–	0.81 (yellow zone)	0.93 (red zone)
JD-1	0.50	–	–
JD-3	–	0.78	–
JD-6	–	–	0.92

amber was 1.54, while that of clarified golden ambers ranged from 1.54 to 1.56 and oxidized red ambers yielded RIs of 1.55–1.58.

- Heat treatment weakened or completely quenched the long-wave UV fluorescence. The clarified golden ambers usually showed weak or moderate yellow-white or yellow fluorescence, while all the oxidized red ambers were inert.
- In FTIR spectra, the intensity ratio $I = 2932\text{ cm}^{-1}/I = 1732\text{ cm}^{-1}$ was >1.78 for untreated amber, compared to ≤ 1.54 for clarified amber and ≤ 0.50 for baked amber. The significant increase in absorption intensities of the C=O carbonyl stretching vibration at 1732 and 1702 cm^{-1} , and the C–O stretching vibration at 1260 – 1160 cm^{-1} , indicate the oxidation of the surface of heat-treated amber. An increase in carbonyl concentration is presumed to be the main cause of both the reddening of amber colour and the quenching of UV fluorescence in baked amber. In addition, thermal treatment promotes the decay or even extinction of the weak absorptions at 1645 cm^{-1} (related to unsaturated C=C double bonds of the exocyclic methylene group) and at 888 cm^{-1} (related to C–H out-of-plane bending vibrations linked with the exocyclic methylene group). Although the above-mentioned changes in the FTIR spectra of heat-treated amber are limited to only a thin layer, in most cases they should still be diagnostic for identifying heat treatment in amber that has been repolished after heating.
- FT-Raman spectra indicate that the number of saturated C–H bonds (1444 cm^{-1}) consumed by oxidation during amber heat treatment is greater than that of unsaturated C=C double bonds (1645 cm^{-1}) consumed during this process, and thus higher intensity ratios ($I = 1645\text{ cm}^{-1}/I = 1444\text{ cm}^{-1}$) indicate

a greater degree of oxidation. However, the minor changes recorded for this intensity ratio were not confirmed as being diagnostic for identifying heat treatment.

References

- Abduriyim A., Kimura H., Yokoyama Y., Nakazono H., Wakatsuki M., Shimizu T., Tansho M. and Ohki S., 2009. Characterization of “green amber” with infrared and nuclear magnetic resonance spectroscopy. *Gems & Gemology*, **45**(3), 158–177, <http://dx.doi.org/10.5741/gems.45.3.158>.
- Brody R.H., Edwards H.G.M. and Pollard A.M., 2001. A study of amber and copal samples using FT-Raman spectroscopy. *Spectrochimica Acta Part A: Molecular and Biomolecular Spectroscopy*, **57**(6), 1325–1338, [http://dx.doi.org/10.1016/s1386-1425\(01\)00387-0](http://dx.doi.org/10.1016/s1386-1425(01)00387-0).
- Edwards H.G.M., Farwell D.W. and Villar S.E.J., 2007. Raman microspectroscopic studies of amber resins with insect inclusions. *Spectrochimica Acta Part A: Molecular and Biomolecular Spectroscopy*, **68**(4), 1089–1095, <http://dx.doi.org/10.1016/j.saa.2006.11.037>.
- Guiliano M., Asia L., Onoratini G. and Mille G., 2007. Applications of diamond crystal ATR FTIR spectroscopy to the characterization of ambers. *Spectrochimica Acta Part A: Molecular and Biomolecular Spectroscopy*, **67**(5), 1407–1411, <http://dx.doi.org/10.1016/j.saa.2006.10.033>.
- Qi L., Yuan X., Chen M. and Lin S., 2003. ESR behavior and ^{13}C NMR representation of treated amber and resin. *Journal of Gems & Gemmology*, **5**(2), 1–6 (in Chinese with English abstract).
- Vandenabeele P., Grimaldi D.M., Edwards H.G.M. and Moens L., 2003. Raman spectroscopy of different types of Mexican copal resins. *Spectrochimica Acta Part A: Molecular and Biomolecular Spectroscopy*, **59**(10), 2221–2229, [http://dx.doi.org/10.1016/s1386-1425\(03\)00066-0](http://dx.doi.org/10.1016/s1386-1425(03)00066-0).
- Wang Y., Yang M. and Yang Y., 2014. Experimental studies on the heat treatment of Baltic amber. *Gems & Gemology*, **50**(2), 142–150, <http://dx.doi.org/10.5741/gems.50.2.142>.
- Wu Z. and Chen S., 2000. Study on oxidation mechanism of gum rosin under heat. *Chemistry and Industry of Forest Products*, **20**(3), 13–16.
- Yang Y. and Wang Y., 2010. Summary on organic components and relevant spectral characteristics of amber and copal. *Journal of Gems & Gemmology*, **12**(1), 16–22 (in Chinese with English abstract).

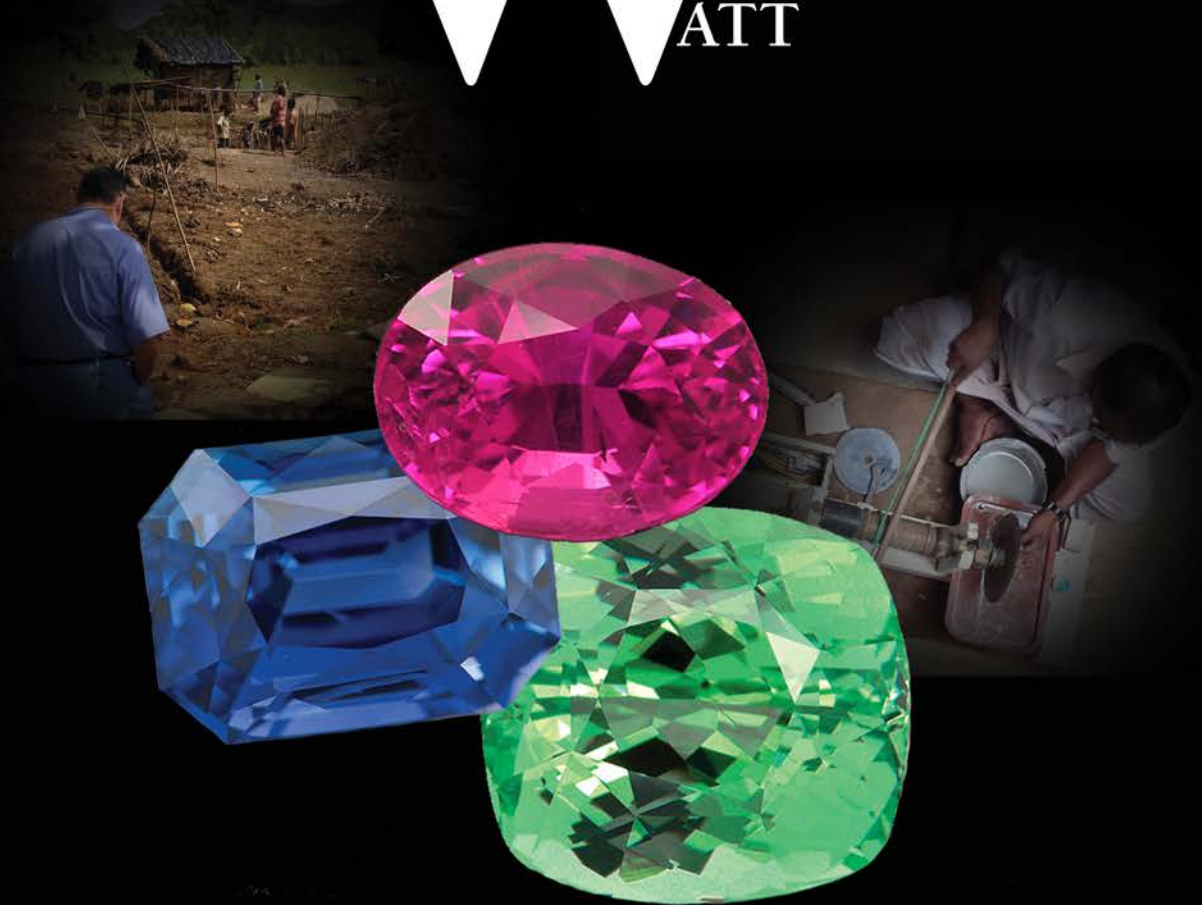
The Authors

**Yamei Wang, Dr Mingxing Yang*,
Shufang Nie and Fen Liu**

Gemological Institute, China University of
Geosciences, Wuhan 430074, China

*E-mail: mingxy@cug.edu.cn

MAYER & WATT



We Deal in inspiration...Naturally.

Download the Mayer and Watt
App for iOS/Droid.

US#: 606.564.3400



www.mayerandwatt.com

Sassolite- and CO₂-H₂O-bearing Fluid Inclusions in Yellow Danburite from Luc Yen, Vietnam

Le Thi-Thu Huong, Kurt Krenn and Christoph Hauzenberger

In 2015, gem-quality yellow danburite was discovered in placers of the Luc Yen mining area in northern Vietnam. Microscopic observations revealed ‘fingerprints’, hollow tubes and two types of fluid inclusions (two-phase and multiphase). Micro-Raman spectroscopy indicated that the two-phase inclusions consisted of CO₂ vapour and pure water, while the multiphase inclusions usually contained one or more crystalline phases in addition to CO₂ and H₂O. Most of the solid phases in the latter fluid inclusions were identified as sassolite (H₃BO₃) and, less commonly, calcite. The presence of sassolite associated with low-density CO₂-bearing fluid inclusions indicates a granitic pegmatite origin for Luc Yen danburite.

The Journal of Gemmology, **35**(6), 2017, pp. 544–550, <http://dx.doi.org/10.15506/JoG.2017.35.6.544>
© 2017 The Gemmological Association of Great Britain

Introduction

Danburite is a calcium borosilicate, CaB₂Si₂O₈, belonging to the orthorhombic crystal system. It is genetically associated with rocks of magmatic (granitic pegmatite), metasomatic (skarn) and sedimentary (evaporite) origins (Kurshakova, 1982; Anovitz and Grew, 1996). Gem-quality yellow danburite is known mainly from Tanzania, Madagascar and Myanmar (Kiefert, 2007; Chadwick and Laurs, 2008; Smith and Krzemnicki, 2017; Smith et al., 2017). In mid-2015, several gem-quality pieces of yellow danburite (1.0–2.5 cm) were discovered in the Bai Cat alluvial deposit, near An Phu in the Luc Yen mining area of northern Vietnam. The gemmological, chemical and spectroscopic properties, as well as inclusion characteristics, for this danburite were recently reported (Huong et al., 2016a). However, the original host-rock source remains unknown. The geology of Luc Yen is dominated by metamorphic rocks—mainly granulitic gneiss, mica schist,

and marble—that are locally intruded by granitic and pegmatitic dykes (Garnier et al., 2005; Huong et al., 2016a). The pieces of danburite were recovered together with minerals corresponding to both metamorphic (ruby, sapphire and spinel) and pegmatitic (tourmaline and topaz) host rocks.

Two-phase (liquid and gas) and ‘fingerprint’ inclusions were reported as the main internal features in Vietnamese danburite (Huong et al., 2016a), and similar inclusions also have been documented in yellow danburite from Tanzania and Myanmar (Kiefert, 2007; Chadwick and Laurs, 2008; Smith et al., 2017). In December 2015, a large broken piece of yellow danburite was recovered from the Bai Cat mine (Figure 1), and various types of liquid inclusions were present in the specimen. From a study of this and other recently found samples of Vietnamese danburite, the authors here provide an updated description of the inclusions in danburite from Luc Yen, which were characterized by opti-



Figure 1: This 31.6 g danburite specimen from the Bai Cat alluvial deposit in the Luc Yen mining area shows eye-visible hollow tubes and overlapping 'fingerprint' inclusions. Photo by L.T.-T. Huong.

cal means and by micro-Raman spectroscopy. The original source rock type for this alluvial danburite is then proposed, according to information provided by our study of the inclusions.

Materials and Methods

The large specimen (31.6 g) and four additional crystal fragments (0.7–1.0 g) of Vietnamese danburite were partially polished for optical observations and Raman measurements. Raman spectra of the inclusions were collected in confocal mode using a Jobin Yvon LabRAM HR800 spectrometer equipped with an Olympus BX41 optical microscope and an Si-based CCD (charged-coupled device) detector in the department of Petrology and Geochemistry, at the NAWI Graz Geocentre, University of Graz. The ability of micro-Raman spectroscopy to acquire data from aqueous solutions, together with the high spatial resolution of the Raman microprobe, make it well suited for non-destructive analysis of gas, liquid and solid phases within small ($\geq 5 \mu\text{m}$) fluid inclusions. The instrumentation used a 100 mW Nd-YAG laser (532 nm emission), a grating of 1,800 grooves/millimetre

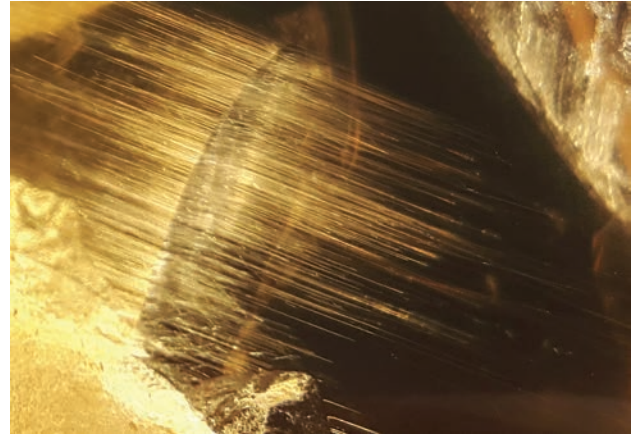


Figure 2: The hollow tubes in the danburite specimen shown in Figure 1 attain a length of 2.5 cm, and some of them nearly cross the host crystal. Photomicrograph by L.T.-T. Huong; field of view 2.5 cm.

and a slit width of $100 \mu\text{m}$. The spectral acquisition time was set to 20 seconds for all measurements in the range $150\text{--}4000 \text{ cm}^{-1}$. Peak analysis of CO_2 was performed with OriginLab software (OriginPro 9); peak-fitting used a Gauss-Lorentz function.

Results and Discussion

Optical Observations

Without magnification, the 31.6 g danburite specimen showed obvious hollow tubes and multiple overlapping fingerprint inclusions (Figure 1). The hollow tubes were up to 2.5 cm long and some of them crossed almost the entire specimen. With magnification, the tubes did not appear to be filled with any liquid or solid phases (Figure 2). The fingerprints appeared to contain liquid (one- or two-phase) inclusions. In addition, within the other danburite samples, primary fluid inclusions formed singly or were arranged along linear trails (Figure 3a) that were oriented both parallel and perpendicular to the c-axis of the host crystal. The individual fluid inclusions varied from $<1 \mu\text{m}$ to several hundred micrometres in size, and were composed of two-phase and multiphase assemblages (Figure 3a,b). The two-phase inclusions were typically composed of a liquid and a vapour bubble that showed various proportions, suggesting heterogeneous entrapment of the dominant fluid during crystal growth (Figure 3b). Most of the multiphase inclusions contained several crystals, a liquid phase and a vapour bubble (Figure 3c,d). In some cases, two vapour bubbles were seen (Figure 3e). The crystals in the multiphase inclusions

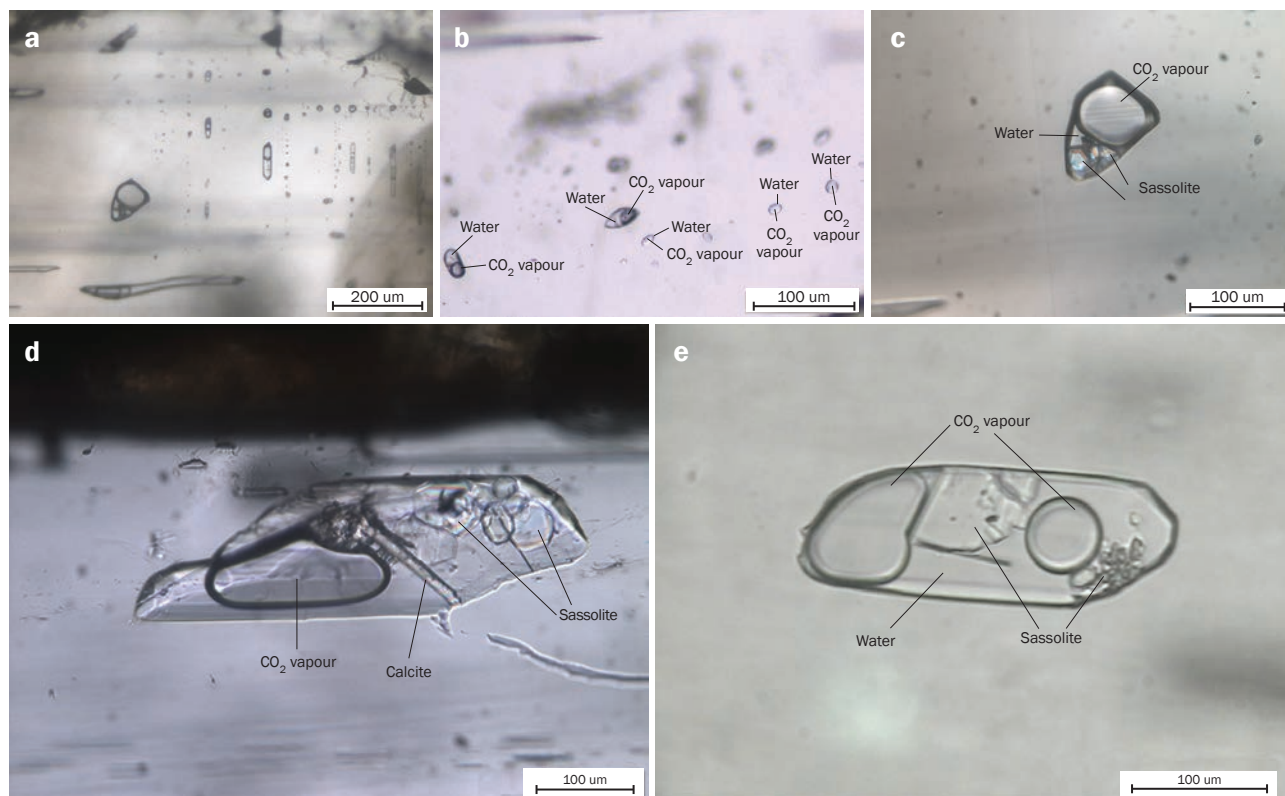


Figure 3: (a) Primary multiphase inclusions occur singly or are arranged along trails, both parallel and perpendicular to the *c*-axis of the host danburite crystal. (b) The CO₂ vapour bubbles in the two-phase inclusions vary in size, and in some cases only a thin layer of liquid is present along the inclusion walls. (c) Sassolite crystals in the multiphase inclusions appear as colourless, pseudo-hexagonal plates—sometimes displaying interference colours—with more-or-less perfect crystal faces. (d) Calcite crystals are occasionally associated with the sassolite plates in the multiphase inclusions. (e) This fluid inclusion contains multiple sassolite crystals accompanying two CO₂ vapour bubbles and a liquid (H₂O). Photomicrographs by K. Krenn.

typically formed colourless euhedral pseudo-hexagonal plates that varied from 5 to 50 µm in dimension; some of them displayed interference colours (again, see Figure 3c,d).

Micro-Raman Spectroscopy

Raman spectroscopy of the multiphase inclusions in all five samples revealed that most of the crystals were sassolite with occasional crystals of calcite (Figure 3d). The liquid and vapour phases were identified by Raman spectroscopy as H₂O and CO₂, respectively. All of these phases were unambiguously identified, as each one showed distinctive Raman bands. In the range 150–1500 cm⁻¹, we observed Raman bands of the host danburite in addition to characteristic bands of sassolite, calcite and CO₂ vapour (Figure 4a). Higher wavenumbers (1500–3000 cm⁻¹) yielded no evidence of additional gas phases, such as N₂ and/or CH₄, but only luminescence signals of the host danburite (Figure 4b). Between 3000 and 3800 cm⁻¹ were characteristic peaks for H₂O and sassolite (Figure 4c).

The sassolite showed two distinct bands at 500 and 880 cm⁻¹ (Figure 4a) and two additional bands at 3165 and 3247 cm⁻¹ (Figure 4c). The 500 and 880 cm⁻¹ bands are assigned to ν_sB³⁺-O species, where B³⁺-O denotes three-coordinated boron (Janda and Heller, 1980; Thomas, 2002).

The calcite was characterized by two strong bands at 1088 and 283 cm⁻¹ and a less-intense band at 714 cm⁻¹ (Figure 4a). The doublet at 270–300 cm⁻¹ in the Raman spectrum of the calcite might result from a combination of the intense calcite band at 283 cm⁻¹ with the two nearby danburite bands (~281 and 296 cm⁻¹).

Raman spectroscopy of the liquid phase gave no hint of the presence of organic matter, and showed only the characteristic peaks of the host danburite and some weakly resolved bands due to H₂O in the 3000–3800 cm⁻¹ range (Figure 4c). Some of the bands seen in the spectra of both sassolite and H₂O (i.e. above 3600 cm⁻¹) were probably generated by the luminescence of the host danburite.

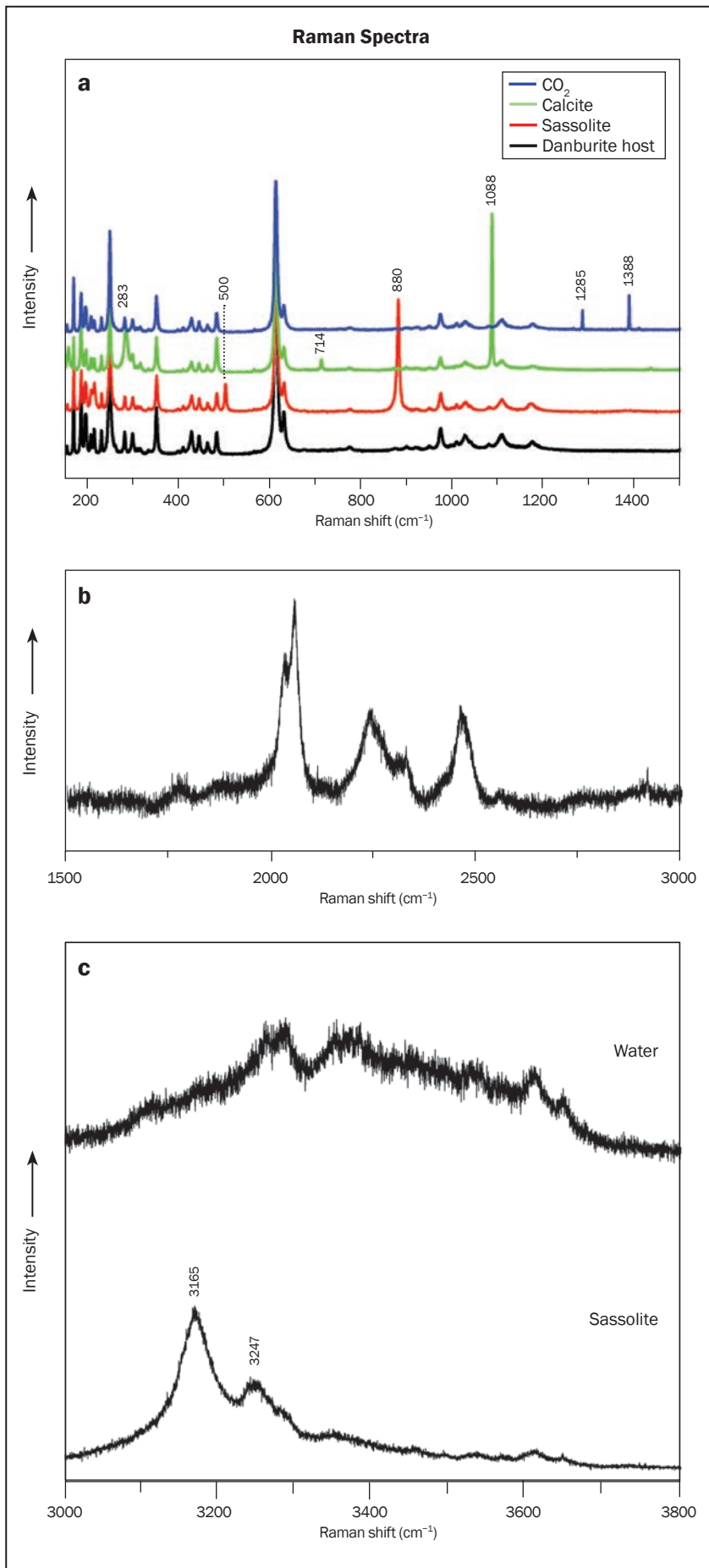
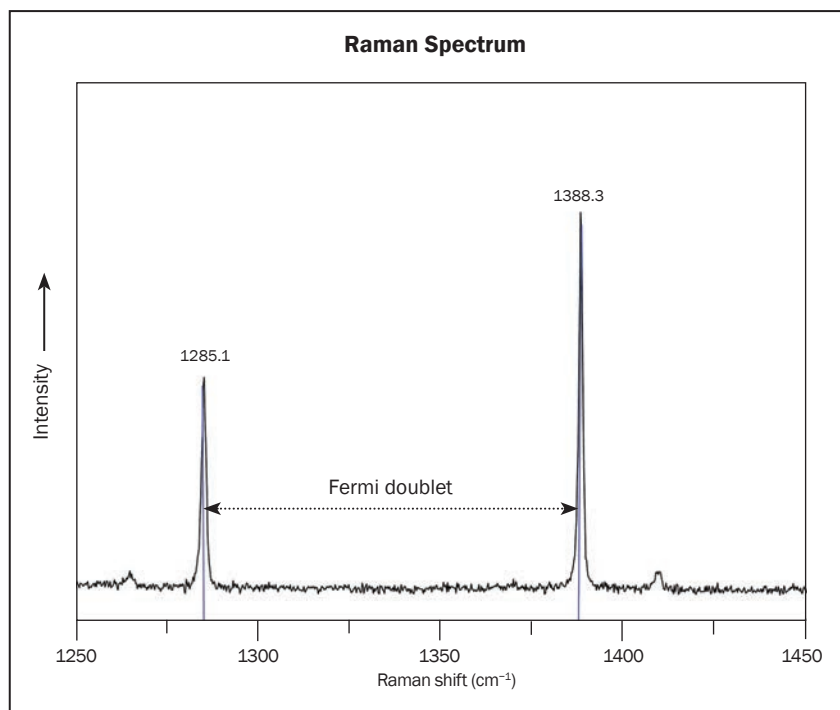


Figure 4: (a) Micro-Raman spectroscopy of the danburite fluid inclusions in the 150–1500 cm⁻¹ range shows the presence of sassolite, calcite and CO₂ vapour. The black trace shows only the bands of the host danburite. Labelled peaks are from the inclusion phases present. (b) Raman spectroscopy of the fluid inclusions in the 1500–3000 cm⁻¹ range shows no bands from additional gas phases (e.g. N₂ and/or CH₄), but only luminescence signals of the host. (c) In the 3000–3800 cm⁻¹ range, Raman spectroscopy of the fluid inclusions shows additional bands for sassolite (at 3165 and 3247 cm⁻¹) and characteristic bands of water.

Figure 5: This representative Raman spectrum of CO₂ in the danburite fluid inclusions shows two diad peaks positioned at 1285.1 and 1388.3 cm⁻¹. The diad split (known as the Fermi doublet) corresponds to low-density values, which points to a granitic pegmatite source rock for the danburite.



The Raman spectrum of CO₂ in the fluid inclusions showed two main bands at ~1388 and 1285 cm⁻¹, which are known as the Fermi diad (Gordon and McCubbin, 1966; see Figure 5). The separation between the Fermi diad bands (Fermi doublet Δ) is a function of CO₂ density in fluid inclusions, whereby the separation increases with increasing density of CO₂ (Song et al., 2009; Wang et al., 2011; Kobayashi et al., 2012). Thus, the density of CO₂ in primary-trapped inclusions is an excellent indicator for the formation conditions of the host mineral (i.e. lithostatic pressure, therefore providing an estimate of the depth of crystallization: Sirbescu and Nabelek, 2003; Yamamoto et al., 2007). According to Raman data for CO₂ in the Vietnamese danburite (Figure 5), Δ values fall in the range 102.7–103.1 cm⁻¹, which correspond to densities lower than 0.3 g/cm³ (Wang et al., 2011). The density of CO₂ in liquid inclusions in pegmatitic minerals (i.e. plagioclase, tourmaline and quartz) has been reported up to 0.65 g/cm³ (Smerekanicz and Dudás, 1999; Bakker and Schilli, 2016), whereas the CO₂ density in liquid inclusions in garnet of metamorphic origin is reportedly much higher: up to 1.13 g/cm³ (Santosh and Tsunogae, 2003; Lamadrid et al., 2014).

Origin of Luc Yen Danburite

The identification of sassolite in the fluid inclusions points to a pegmatite origin (cf. Anovitz and Grew, 1996) for the Luc Yen danburite, and this is

confirmed by the low-density values of the CO₂ (0.3 g/cm³) in the multiphase inclusions. Sassolite is a characteristic component of fluid inclusions in minerals from the majority of tourmaline-bearing and topaz-beryl miarolitic pegmatites worldwide (Peretyazhko et al., 1999, 2000; Smirnov et al., 2000; Bakker and Schilli, 2016).

Some pegmatites in the Luc Yen area of Vietnam have been exploited for tourmaline, green feldspar, topaz and lepidolite. These granitic pegmatites are of the relatively shallow miarolitic type, and are of Oligocene age (i.e. 30.58 million years according to K/Ar data for K-feldspar: Huong et al., 2016b). The presence of tourmaline and topaz with danburite in the alluvial sediments, combined with the inclusion data described above, suggests that the Luc Yen danburite is related to these pegmatites.

Conclusions

Internal features in Vietnamese danburite consist of fingerprints, hollow tubes, and two-phase and multiphase fluid inclusions. Micro-Raman spectroscopy was used to identify the various constituents of the multiphase inclusions. The solid phases consisted of sassolite—which was present in all of the analysed inclusions—and occasional calcite. The various proportions of a carbonic vapour phase (CO₂) compared to a liquid phase (H₂O) indicate a heterogeneous entrapment of

the fluid inclusions. This suggests that the associated sassolite and calcite precipitated as a result of decreasing temperature through hydration reactions with the host danburite. The presence of sassolite together with low-density H₂O–CO₂ fluid inclusions indicates the Luc Yen danburite originated from a granitic pegmatite source rock.

References

- Anovitz L.M. and Grew E.S., 1996. Mineralogy, petrology and geochemistry of boron: An introduction. In L.M. Anovitz and E.S. Grew, Eds., *Boron: Mineralogy, Petrology, and Geochemistry*, Reviews in Mineralogy, Vol. 33, Mineralogical Society of America, Washington DC, USA, 1–40.
- Bakker R.J. and Schilli S.E., 2016. Formation conditions of leucogranite dykes and aplite-pegmatite dykes in the eastern Mt. Capanne plutonic complex (Elba, Italy): Fluid inclusion studies in quartz, tourmaline, andalusite and plagioclase. *Mineralogy and Petrology*, **110**(1), 43–63, <http://dx.doi.org/10.1007/s00710-015-0417-z>.
- Chadwick K.M. and Laurs B.M., 2008. Gem News International: Yellow danburite from Tanzania. *Gems & Gemology*, **44**(2), 169–171.
- Garnier V., Ohnenstetter D., Giuliani G., Maluski H., Deloule E., Phan Trong T., Pham Van L. and Hoang Quang V., 2005. Age and significance of ruby-bearing marble from the Red River shear zone, northern Vietnam. *Canadian Mineralogist*, **43**(4), 1315–1329, <http://dx.doi.org/10.2113/gscanmin.43.4.1315>.
- Gordon H.R. and McCubbin Jr. T.K., 1966. The 2.8-micron bands of CO₂. *Journal of Molecular Spectroscopy*, **19**(1–4), 137–154, [http://dx.doi.org/10.1016/0022-2852\(66\)90237-2](http://dx.doi.org/10.1016/0022-2852(66)90237-2).
- Huong L.T.T., Otter L.M., Häger T., Ullmann T., Hofmeister W., Weis U. and Jochum K.P., 2016a. A new find of danburite in the Luc Yen mining area, Vietnam. *Gems & Gemology*, **52**(4), 393–401, <http://dx.doi.org/10.5741/gems.52.4.393>.
- Huong L.T.T., Nhung N.T., Kien N.D.T., Zubko M., Häger T. and Hofmeister W., 2016b. Structural investigation of K-feldspar KAlSi₃O₈ crystals by XRD and Raman spectroscopy: An application to petrological study of Luc Yen pegmatites, Yen Bai Province, Vietnam. *Acta Physica Polonica A*, **130**(4), 892–893, <http://dx.doi.org/10.12693/APhysPolA.130.892>.
- Janda R. and Heller G., 1980. IR- und Ramanspektren isotop markierter Tetra- und Pentaborate. *Spectrochimica Acta Part A*, **36**(11), 997–1001, [https://doi.org/10.1016/0584-8539\(80\)80179-6](https://doi.org/10.1016/0584-8539(80)80179-6).
- Kiefert L., 2007. Gem News International: Unusual danburite pair. *Gems & Gemology*, **43**(2), 167–168.
- Kobayashi T., Yamamoto J., Hirajima T., Ishibashi H., Hirano N., Lai Y., Prikhod'ko V.S. and Arai S., 2012. Conformity and precision of CO₂ densimetry in CO₂ inclusions: Microthermometry versus Raman microspectroscopic densimetry. *Journal of Raman Spectroscopy*, **43**(8), 1126–1133, <http://dx.doi.org/10.1002/jrs.3134>.
- Kurshakova L.D., 1982. Temperature regime and geochemical conditions of formation of danburite. *International Geology Review*, **24**(3), 367–371, <http://dx.doi.org/10.1080/00206818209452415>.
- Lamadrid H.M., Lamb W.M., Santosh M. and Bodnar R.J., 2014. Raman spectroscopic characterization of H₂O in CO₂-rich fluid inclusions in granulite facies metamorphic rocks. *Gondwana Research*, **26**(1), 301–310, <http://dx.doi.org/10.1016/j.gr.2013.07.003>.
- Peretyazhko I.S., Zagorsky V.Y., Prokof'ev V.Y. and Smirnov S., 1999. Boric acid as the most typical component of fluid inclusions in minerals from tourmaline-bearing and topaz-beryl miarolitic pegmatites. *Canadian Mineralogist*, **37**(3), 823–825.
- Peretyazhko I.S., Prokof'ev V.Y., Zagorsky V.Y. and Smirnov S., 2000. Role of boric acids in the formation of pegmatite and hydrothermal minerals: Petrologic consequences of sassolite (H₃BO₃) discovery in fluid inclusions. *Petrology*, **8**(3), 214–237.
- Santosh M. and Tsunogae T., 2003. Extremely high density pure CO₂ fluid inclusions in a garnet granulite from southern India. *Journal of Geology*, **111**(1), 1–16, <http://dx.doi.org/10.1086/344578>.
- Sirbescu M.-L.C. and Nabelek P.I., 2003. Crystallization conditions and evolution of magmatic fluids in the Harney Peak granite and associated pegmatites, Black Hills, South Dakota—Evidence from fluid inclusions. *Geochimica et Cosmochimica Acta*, **67**(13), 2443–2465, [http://dx.doi.org/10.1016/S0016-7037\(02\)01408-4](http://dx.doi.org/10.1016/S0016-7037(02)01408-4).
- Smerekanicz J.R. and Dudás F.Ö., 1999. Reconnaissance fluid inclusion study of the Morefield pegmatite, Amelia County, Virginia. *American Mineralogist*, **84**(5–6), 746–753, <http://dx.doi.org/10.2138/am-1999-5-606>.
- Smirnov S., Peretyazhko I.S., Prokof'ev V.Y. and Shebanin A.P., 2000. The first finding of sassolite (H₃BO₃) in fluid inclusions in minerals. *Geologiya i Geofizika*, **41**(2), 193–205.
- Smith C.P. and Krzemnicki M.S., 2017. Gem Notes: Yellow danburite from Namalulu, Tanzania and Myanmar: Origin of colour and its stability. *Journal of Gemmology*, **35**(5), 384–386.
- Smith C.P., Krzemnicki M.S. and Wang H., 2017. Gem Notes: Yellow danburite from Namalulu, Tanzania: Gemmological properties and chemical composition. *Journal of Gemmology*, **35**(5), 381–383.

Conferences

Fourteenth Annual Sinkankas Symposium—Sapphire

This sold-out conference was held on 8 April 2017 at the Gemological Institute of America (GIA) in Carlsbad, California, and was co-hosted by the Gemological Society of San Diego (GSSD). (See pp. 560–561 of this issue for a review of the accompanying proceedings volume.) The 12 speakers (Figure 1) covered a variety of topics related to sapphire, and a beautiful array of sapphire crystal specimens and polished stones was displayed during the event by Pala International of Fallbrook, California (Figure 2).

The symposium opened with brief introductions by **Donna Beers** of GSSD and **Robert Weldon** of GIA. Then **Richard Hughes** (Lotus Gemology, Bangkok, Thailand) gave a multimedia presentation that reviewed world sources and quality factors for blue and fancy-colour sapphires. He also looked at pricing and showed that, even though blue and padparadscha sapphires are the most valuable colours of sapphire, they are still much less expensive than ruby.

Alan Hart (Gem-A, London) reviewed sapphires in the British Crown Jewels, covering 1,200 years of history of the regalia, which is used particularly for coronation ceremonies. Interestingly, many of the sapphires and oth-

er gems mounted in various objects (e.g. crowns) were recycled into new versions of those pieces that were made for successive generations of kings and queens.

Nathan Renfro (GIA, Carlsbad) examined the microscopic internal and external features of sapphires. His attractive photomicrographs showed various mineral inclusions (rutile as silk and skeletal crystals, ilmenite, uraninite, zircon, apatite, spinel and metal sulphides) as well as colour zoning, thin films, fractures with epigenetic staining, negative crystals (with bubbles that appeared/disappeared upon cooling/heating) and surface textures.

Dr George Harlow and Rachelle Turnier (American Museum of Natural History, New York, New York) discussed syenite-hosted sapphires from the Baw Mar mine in Mogok, Myanmar, and compared their composition and oxygen isotope values to syenite-hosted sapphires from other localities. He concluded that there is no uniform formation environment for such sapphires, and that they are brought to the earth's surface as xenocrysts rather than phenocrysts.

Glenn Lehrer (Glenn Lehrer Designs, Larkspur, California) gave numerous tips for faceting and carv-

Figure 1: Sinkankas Symposium presenters and organizers gather for a group photo around a statue of Richard T. Liddicoat. From left to right: Edward Boehm, Lisbet Thoresen, Dr George Harlow, Richard Hughes, Dona Dirlam, Carl Larson, Robert Weldon (kneeling), Dr William 'Skip' Simmons, Glenn Lehrer (kneeling), Shane McClure, Dr George Rossman, Alan Hart, Nathan Renfro and Dr John Emmett. Photo by Jim Parrish.



Figure 2: This photo shows a few of the sapphire specimens that were displayed during the Sinkankas Symposium. Courtesy of Pala International; photo by Jim Parrish.



ing sapphire, as well as improving traditional-cut stones. In general, sapphires that contain 'silk' can benefit from fewer facets of larger size, while those that are free of silk should have numerous small facets. Also, he showed that when recutting the table and crown to improve a sapphire's appearance, dramatic results may be obtained with very little weight loss (only a few tenths of a point in some cases).

Dr John Emmett (Crystal Chemistry, Brush Prairie, Washington, USA) and co-authors covered the coloration mechanisms of sapphire, examining the strength of the chromophores (Cr^{3+} , Fe^{2+} - Ti^{4+} , V^{3+} , Fe^{3+} and trapped hole centres involving various ions) and how different combinations of them produce various colours. While the presence of Cr^{3+} alone causes pink coloration, it is the combination of Cr^{3+} with a trapped hole centre involving Cr^{3+} that causes the red colour of ruby (only about 1 ppm of trapped holes is needed).

Dr William 'Skip' Simmons (Maine Mineral & Gem Museum, Bethel, Maine, USA) reviewed the crystallography and mineralogy of sapphire. Although corundum is a trigonal mineral, its crystal structure is characterized by hexagonal close packing. It is commonly associated with spinel, phlogopite, calcite and olivine (in marbles); kyanite and sillimanite (in schists); and nepheline (in syenite).

Shane McClure (GIA, Carlsbad) provided a review of sapphire treatments, particularly heating. It has been estimated that 90–95% of sapphire on the market has undergone heat treatment, which takes place at temperatures ranging from ~800°C to 1,800°C and for periods of 1 hour to 3+ weeks. The main goals of heat treatment are to remove the blue tint from pink sapphires, deepen the colour of yellow sapphires, and create blue colour (while improving the transparency) of geuda material.

Carl Larson (Pala International, Fallbrook, California) discussed collecting sapphire crystals and

gemstones from worldwide localities. Generally it is best to have a particular focus when collecting; examples include locality, colour, crystal form or gemstone shape, and phenomena (e.g. star stones). Cut stones are more easily understood by consumers to have high value. Done correctly, collecting sapphires can be a good investment.

Lisbet Thoresen (Temecula, California) reviewed the archaeogemmology of sapphire, starting with the Hellenistic Era (323 BC). Studies of glyptic (carved or engraved) gems have shown that there are generally two categories of sapphires: small, heavily zoned dark blue stones and larger, lighter-coloured gems. All available evidence suggests that Sri Lanka (Ceylon) was the source of sapphires from the 3rd through the 6th century AD.

Edward Boehm (RareSource, Chattanooga, Tennessee, USA) explored the evolution of laboratory services for gemstones, which has shifted from basic gem identification to high-tech geographic origin determination—particularly for sapphires and other high-value coloured stones. Besides influencing a stone's pricing, origin reports are also important for traceability (e.g. separating gems associated with conflict from those that are mined sustainably).

Dr George Rossman (California Institute of Technology, Pasadena) performed experiments on a blue sapphire and a ruby to observe whether their colours are stable at temperatures that are at least as high as their formation conditions. The sapphire and ruby samples each were colourless when they were observed at high temperature (1,000°C), due to broadening of their absorption bands that occurred during the heating process. Therefore, Rossman postulated that sapphire and ruby are actually colourless when they crystallize, and only develop their colour upon cooling.

Brendan M. Laurs FGA

Presentations in Tucson, Arizona, USA

In April 2017, two presentations of interest to gemmologists took place in Tucson.

On 13 April, at the University of Arizona, **Prof. Lutz Nasdala** (University of Vienna, Austria) gave a presentation on new advances in Raman micro-spectroscopy. He described four case studies, two of which pertained to gemmology. The first study looked at natural radiation damage in gem-quality ekanite ($\text{Ca}_2\text{ThSi}_8\text{O}_{20}$), which occurs due to the decay of radioactive isotopes of Th and U. The resulting damage to the crystal structure may cause it to appear amorphous with no Raman peaks. Heat treatment of the metamict material causes recrystallization and the corresponding appearance of diagnostic Raman peaks. For the second case study, Nasdala explained that zircon samples for use as analytical reference material are best obtained from high-quality facetable material in pieces that are larger than 10 ct. The samples should be sliced into 100- μm -thick wafers and monitored for long periods of time to look for metamictization. Metamict gems with abundant radiation damage behave as amorphous material, and may not show the doubling of back facets that is commonly shown by faceted zircon. Annealing of zircon removes traces of helium, so analysis for He may provide a useful criterion for identifying heat treatment.

On 22 April, the Mineral Enthusiasts of the Tucson Area hosted **Mike Clow** (LightSource Industries, Sedona, Arizona), who discussed LED lighting for gem and mineral displays. LEDs are becoming the standard light sources for home, industry and now gem and mineral cases, as well as retail displays. Clow shared a few key facts we might not realize. For example, there is no such thing as a 'white' LED. Instead, apparent white light is achieved with a blue bulb that is coated with a yellow phosphor. Another example is that LEDs emit 50% of their energy as light and the remainder as heat; by comparison, incandescent bulbs produce 95% heat and only 5% light. Most gem and mineral displays respond well to having a mixture of 'warm' and 'cool' LEDs. Diamond merchants commonly prefer a colour temperature of 6,500 K because this cool light helps offset the slight yellow tint that can be seen in many diamonds. Overall, proper display lighting is dependent on the presence of other light sources as well as the background of a display. Black moves an object to the forefront while white gives more depth. Glare is never good, whereas side lighting can show textures effectively. Ultimately, proper lighting is subjective: What looks good, works.

*Eric Fritz
Gem-A, Tucson, Arizona*



Crown Color

Fine Rubies, Sapphires and Emeralds
Bangkok - Geneva - Hong Kong - New York



Head Office:

Crown Color Ltd.

14/F, Central Building, suite 1408, 1-3 Pedder Street

Central Hong Kong SAR

Tel: +852-2537-8986

New York Office: + 212-223-2363

Geneva Office: +41-22-8100540

Crown Color

is a proud supporter of the
Journal of Gemmology

Gem-A Notices

GIFTS TO THE ASSOCIATION

The Association is most grateful to the following for their gifts and donations for research and teaching purposes:

Gina Barnes, School of Oriental & African Studies, University of London, for two jade and jasper pebbles and a jasper fragment from Itoigawa, Niigata Prefecture, Japan.

Meg Berry, Megagem, Fallbrook, California, USA, for some fragments of tsavorite from Ethiopia.

Peter Dwyer-Hickey FGA DGA, South Croydon, Surrey, for copies of the following books: *The Diamond Underworld* by F. Kamil; *English Medieval Lapidaries* by J. Evans and M. Serjeantson; *Gems, Minerals and Rocks in Southern Africa* by J. R. McIver; *Jewellery* by the National Museum of Ireland; *Gold* by S. La Niece/British Museum; and *Medieval Goldsmiths* by J. Cherry/British Museum.

Melvyn Gallagher, Upminster, Essex, for a scrapbook of diamond sales at Debenhams Store Auction House, 1871–1872.

William Hasselrot, Stockholm, Sweden, for a monetary donation.

Marcus McCallum FGA, Hatton Garden, London, for a monetary donation.

Antony Shih, Taipei City, Taiwan, RO China, for one large piece of rough 'blue' amber and a carved 'blue' amber Buddha.

Beth West, Reading, Berkshire, for a large cubic zirconia set in a ring.

ANNUAL GENERAL MEETING

The 2017 Gem-A Annual General Meeting will be held on 27 July at 18:30 at The Goldsmiths' Centre, London.

Gem-A
INSTRUMENTS

NEW IN! CZ Colour Comparison Set: N-Z

- + Grade fancy coloured diamonds with ease
- + Hand-graded for accurate colour comparisons
- + Individually laser inscribed on the girdle for easy differentiation between colour grades
- + The ideal companion for professional diamond graders

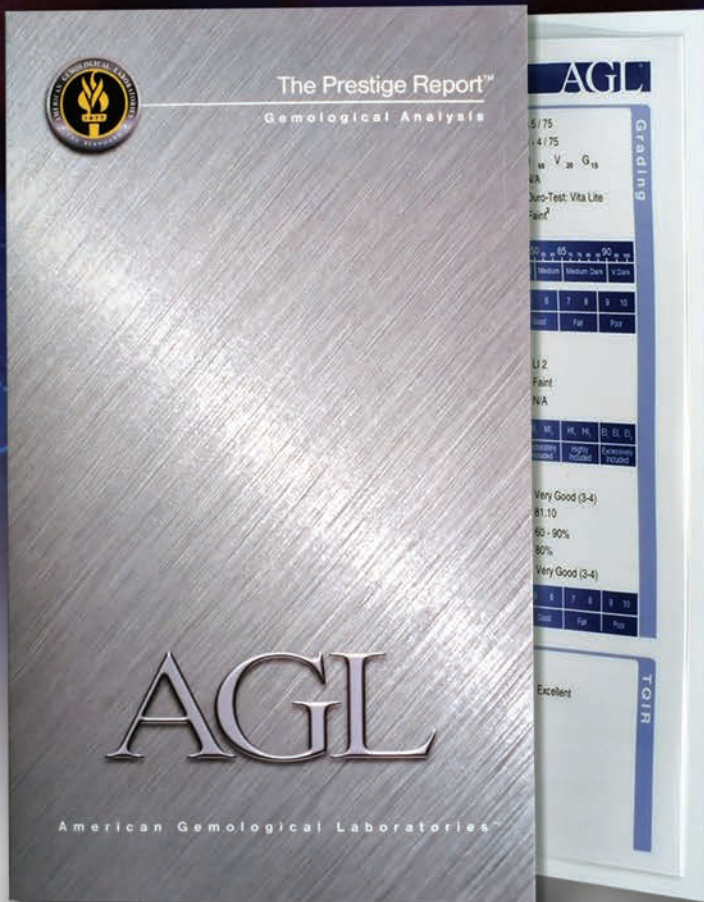
Get 15% off!
When you quote 'The Journal of Gemmology'

£380^{+VAT}
£323
^{+VAT}
with offer*

Postage and packaging fee applies. 20% VAT applies to UK and European countries, except companies with a valid VAT registration number. Gemmological Instruments Ltd. is a company limited by guarantee and registered in England No. 838324.
*Offer ends 23 August

An innovator in gemstone reporting

- Identification of colored gemstones • Country of origin determination • Full quality and color grading analysis



AMERICAN GEMOLOGICAL LABORATORIES

AGIL

580 5th Ave • Suite 706 • New York, NY 10036, USA
www.agilgemlab.com • +1 (212) 704 - 0727

Learning Opportunities

CONFERENCES AND SEMINARS

Swiss Gemmological Society Conference and European Gemmological Symposium 2017

29 June–1 July 2017
Zermatt, Switzerland
<http://gemmologie.ch/en>

International Conference in Geology, Mining, Mineral and Groundwater Resources of the Sub-Saharan Africa

11–13 July 2017
Livingstone, Zambia
www.mines.unza.zm/conference
Theme of interest: Gemstones Mining

East Coast Gem, Mineral & Fossil Show

11–13 August 2017
West Springfield, Massachusetts, USA
www.mzexpos.com/east-coast-show
Note: Includes a seminar programme.

Northwest Jewelry Conference

11–13 August 2017
Seattle, Washington, USA
www.nwjcon.com

48th ACE® IT Annual Mid-Year Conference

12–15 August 2017
Indianapolis, Indiana, USA
www.najaappraisers.com/html/conferences.html

Dallas Mineral Collecting Symposium

25–27 August 2017
Dallas, Texas, USA
www.dallassymposium.org

28th International Conference on Diamond and Carbon Materials (DCM 2017)

3–7 September 2017
Gothenburg, Sweden
www.diamond-conference.elsevier.com

Hong Kong Jewellery & Gem Fair

13–19 September 2017
Hong Kong
www.tinyurl.com/hbn8y56
Note: Includes a seminar programme.

Denver Gem & Mineral Show

15–17 September 2017
Denver, Colorado, USA
www.denvermineralshow.com
Note: Includes a seminar programme.

IRV Loughborough Conference

16–18 September 2017

Loughborough
www.jewelleryvaluers.org/Loughborough-Conference

11th International Kimberlite Conference

18–22 September 2017
Gaborone, Botswana
www.11ikc.com
Note: Pre- and post-conference field trips will visit diamond deposits in Botswana and neighbouring countries.

World of Gems Conference V

23–24 September 2017
Rosemont, Illinois, USA
<http://gemguide.com/events/world-of-gems-conference>
Note: Will include a poster session.

ASA 2017 International Appraisers Conference

7–10 October 2017
Houston, Texas, USA
www.appraisers.org/education/conferences/asa-joint-conferences

35th International Gemmological Conference

11–15 October 2017
Windhoek, Namibia
www.igc-gemmology.org

200th Anniversary Meeting of the Russian Mineralogical Society

10–13 October 2017
Saint Petersburg, Russia
www.minsoc.ru/2017
Session of interest: Natural Stone in History of Civilization (Including Gemology)

Friends of Mineralogy Pacific Northwest Chapter 43rd Annual Symposium: Minerals of the Pacific Northwest

13–15 October 2017
Kelso, Washington, USA
www.pnwfm.org/symposium

Canadian Gemmological Association Conference

20–22 October 2017
Toronto, Ontario, Canada
www.canadiangemmological.com/index.php/com-virtuemart-menu-configuration/conferences-and-special-events

ICA Congress

21–24 October 2017
Jaipur, India
www.gemstone.org/events/2017-congress

Compiled by Angharad Kolator Baldwin and Brendan Laurs

Geological Society of America Annual Meeting

22–25 October 2017
Seattle, Washington, USA
<http://community.geosociety.org/gsa2017/home>
Session of interest: Gemological Research in the 21st Century: Characterization, Exploration, and Geological Significance of Diamonds and Other Gem Minerals

9th International Congress on the Application of Raman Spectroscopy in Art and Archaeology

24–28 October 2017
Évora, Portugal
www.raa2017.uevora.pt

The Munich Show

27–29 October 2017
Munich, Germany
www.munichshow.com/en
Note: Includes a seminar programme.

Inaugural Conference on Applied Earth Sciences in Myanmar and Neighboring Regions

2–3 November 2017
Yangon, Myanmar

www.maesa.org/info.html
Session of interest: Applied Mineralogy and Gem Deposits

World Ruby Forum 2017

4 November 2017
Bangkok, Thailand
www.worldrubyforum.com

Gem-A Conference

4–5 November 2017
London
www.gem-a.com

CIBJO Congress 2017

5–7 November 2017
Bangkok, Thailand
www.cibjo.org/2017-cibjo-congress-take-place-bangkok-thailand-november-5-7

Swiss Geoscience Meeting

17–18 November 2017
Davos, Switzerland
<https://geoscience-meeting.ch/sgm2017>
Session of interest: Gemmology

EXHIBITIONS

Asia

Imperial Splendours: The Art of Jewellery Since the 18th Century

Until 2 July 2017
The Palace Museum, Beijing, China
<http://en.dpm.org.cn/exhibitions/current/2017-03-02/2602.html>

Europe

Stone of Heaven. HRH Prince Henrik's Collection of Oriental Jade

Until 27 August 2017
Musée på Koldinghus, Kolding, Denmark
www.koldinghus.dk/uk/exhibitions-2017/stone-of-heaven.aspx

Authentically Inauthentic?—Jewellery from Pforzheim's Industrial Production

Until 10 September 2017
Municipal Museum, Pforzheim, Germany
www.schmuckmuseum.de/flash/SMP_en.html

Must-haves—Jewellery Created by Greats of the Craft and Must-Sees—Jewellery in the Arts

Until 10 September 2017
Schmuckmuseum, Pforzheim, Germany
www.schmuckmuseum.de/flash/SMP_en.html

Amber and Form

Amber Room in Saint Petersburg Jewels of the Baltic in Novo Mesto

Until 30 September 2017
Dolenjski muzej Novo mesto, Slovenia
www.dolenjskimuzej.si/en/amber

Liv Blåvarp: Jewellery

Until 29 October 2017
Lillehammer Kunstmuseum, Lillehammer, Norway
<http://lillehammerartmuseum.com/utstilling/liv-blavarp-smykker-17-juni-24-september-2017/?lang=en>

Jewellery—Materials Craft Art

Until 22 October 2017
Swiss National Museum, Landesmuseum Zürich, Switzerland
www.nationalmuseum.ch/e/microsites/2017/Zuerich/Schmuck.php

Vanity: Stories of Jewelry in the Cyclades

Until 31 October 2017
Archaeological Museum of Mykonos, Greece
<http://news.gtp.gr/2016/08/18/ancient-cyclades-jewelry-mykonos>

Pretty on Pink—Éminences Grises in Jewellery

27 October–mid-February 2018
Schmuckmuseum, Pforzheim, Germany
www.schmuckmuseum.de/flash/SMP_en.html

Smycken: Jewellery—From Decorative to Practical

Ongoing
Nordiska Museet, Stockholm, Sweden
www.nordiskamuseet.se/en/utställningar/jewellery

North America

Jeweled Splendors of the Art Deco Era: The Prince and Princess Sadruddin Aga Khan Collection

Until 27 August 2017
Cooper Hewitt, New York, New York, USA
www.cooperhewitt.org/events/current-exhibitions/jeweled-splendors

Linda MacNeil: Jewels of Glass

Until 1 October 2017
Museum of Glass, Tacoma, Washington, USA
<https://museumofglass.org/mog/exhibition/linda-macneil-jewels-of-glass>

Spectacular! Gems and Jewelry from the Merriweather Post Collection

Until 1 January 2018

Hillwood Estate, Museum & Gardens, Washington DC, USA
www.hillwoodmuseum.org/Spectacular-Gems-and-Jewelry

Past is Present: Revival Jewelry

Until 19 August 2018
Museum of Fine Arts, Boston, Massachusetts, USA
www.mfa.org/news/past-is-present-revival-jewelry

Australasia

Australian Opal Exhibition

3–4 August 2017
Surfers Paradise, Queensland, Australia
www.austopalexpo.com.au

The House of Dior: Seventy Years of Haute Couture

27 August–7 November 2017
The National Gallery of Victoria, Melbourne, Australia
www.ngv.vic.gov.au/exhibition/the-house-of-dior

OTHER EDUCATIONAL OPPORTUNITIES

Gem-A Workshops and Courses

Gem-A, London
www.gem-a.com/education/courses

Sri Lanka Trip with Gem-A and The National Association of Jewellers

16–30 October 2017
Visit mines, markets and cutting centres in Sri Lanka
<http://tinyurl.com/kujwh72>
Note: Open to members of Gem-A and NAJ.

DUG Advanced Gemology Program (in English)

6 November–8 December 2017
Nantes, France
www.gemnantes.fr/en

Gemstone Safari to Tanzania

8–25 January 2018
Visit Morogoro, Umba, Arusha, Longido, Merelani and Lake Manyara in Tanzania
www.free-form.ch/tanzania/gemstonesafari.html
Note: Includes options for a lapidary class and/or a private trip to visit ruby mines near Morogoro and Mpwapwa (including Winza).

Lectures with Gem-A's Midlands Branch

Fellows Auctioneers, Birmingham

Email Georgina@fellows.co.uk

- 29 September 2017
Geoff Whitefield—Valuation Practice
- 27 October 2017
Stephen Alabaster—The History of Alabaster & Wilson

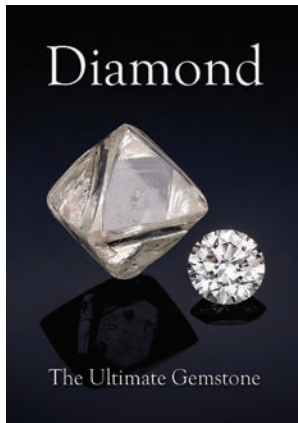
Lectures with The Society of Jewellery Historians

Society of Antiquaries of London, Burlington House, London
www.societyofjewelleryhistorians.ac.uk/current_lectures

- 26 September 2017
(*40th Anniversary Lecture*)
Mag. Paulus Rainer—Benvenuto Cellini's Salt Cellar: Some New Thoughts, Some New Discoveries
- 3 October 2017
Raymond Sancroft-Baker—Hidden Gems – Jewellery Stories from the Salesroom
- 24 October 2017
Lynne Bartlett—The Rise and Fall of the Chatelaine
- 28 November 2017
Judy Rudoe—Cartier Gold Boxes: A Visionary Patron and a Bet with Ian Fleming

New Media

Diamond—The Ultimate Gemstone



Ed. by Jeff W. Harris and Gloria A. Staebler, 2017. MINERAL Monograph No. 19, Lithographie Ltd., Arvada, Colorado, USA, www.lithographie.org/bookshop/diamond_the_ultimate.htm, 152 pages, illus., ISBN 978-0983632351. US\$40.00 softcover.

Did you know that the first experiments to ‘vaporize’ diamond with focused sunlight were conducted in 1694 in Florence, Italy, by Giuseppe Averani and Cipriano Targioni, and in 1772 Antoine Lavoisier was able to prove that diamonds consisted of carbon? And did you know that the impact of the huge meteorite that created the Nördlinger Ries crater in Bavaria, Germany, also turned a nearby graphite deposit into the rock suevite, which contains about 72,000 tonnes of tiny (less than 0.2 mm) impact-origin diamonds? And that the largest CVD-grown synthetic diamond identified by the GIA laboratory so far (2016) is a J-VS₂ cushion cut of 5.19 ct? Or that the production of HPHT-grown synthetic diamonds currently exceeds 300 tonnes per year? These and many more facts can be found in this volume.

The editors have brought together a group of authors who are well-known experts in their fields, and their papers comprise a wide range of topics. ‘Lands Immemorial’ by G. A. Staebler and C. Mitchell summarizes the history of diamonds from the oldest known jewels of Roman times to the discovery of diamonds in South Africa, their mining and trade, and their role as symbols of wealth and power. India and Brazil are treated in more detail. As an example of a historic Indian stone, B. Janse briefly depicts the history of the Hope Diamond from its discovery to its current home in the Smithsonian Institution.

Janse is also the author of the chapter ‘Geology of Diamond’. The geological conditions of diamond formation are described comprehensively, as are the classification, distribution and prospection of diamondiferous rocks and indicator minerals; secondary deposits (alluvial and marine); the age dating and world production of diamonds; and where diamond prospecting is taking place today.

In ‘The Magnificent Mineralogy of Diamond’, J. A. Jaszczak and K. Dunnell first explain the differences

between the structures of diamond and graphite. Then they describe the most interesting aspects of diamond morphology (e.g. for monocrystalline, twinned and fibrous diamonds), surface features, lustre, refraction, dispersion, inclusions, hardness and thermal conductivity. The chapter closes with a description of diamond types based on the presence/absence of nitrogen and boron.

‘Diamond Studies’ is mainly an abbreviated version of an article by the late M. Glas published in *extraLapis* No. 18 (2000). Glas presents diamond crystal drawings from Fersman and Goldschmidt’s *Der Diamant, eine Studie* (1911), and also the detailed drawings of a complicated multiple diamond twin made in 1942 by Berend George Escher, the half-brother of the famous graphic artist M. C. Escher. In a separate box, J. Rakovan, A. G. Schauss and R. P. Richards discuss ‘The Puzzle of Re-Entrant Cube Morphology’.

With the title ‘On the Beauty of Defects’, E. Gailou and G. R. Rossman do not refer to the clarity of diamond, but to various ‘imperfections’ that cause the different colours, such as trace elements (e.g. nitrogen, boron and hydrogen), effects of radiation, lattice defects, etc. Then they discuss the specific causes for each colour, as well as for phenomena such as luminescence and ‘chameleon’ colour behaviour.

In ‘Diamond: Intimate Portraits’, J. I. Koivula and E. A. Skälwold offer a gallery of breathtakingly beautiful photomicrographs of structures and inclusions. They also give accompanying explanations, but frankly speaking, you may also skip them and just enjoy the beauty of the incredible images.

J. Shigley then covers ‘Diamonds as Gemstones’. Starting with quality criteria for faceted diamonds (the famous 4Cs), he describes modern gem diamond manufacturing, in which computers play an ever-increasing role, and the identification of diamond treatments, synthetics and simulants, in which high-tech analytical methods are needed where the naked eye and loupe are not sufficient. In a separate box, Robert M. Shipley Sr. (1887–1978) is portrayed as one of the fathers of modern gemmology.

The following five chapters deal with selected diamond sources, ranging from a continent to a single pipe. ‘Diamonds in Africa – A Tribute to Tom Clifford’, by N. Norman, gives a comprehensive description of the African diamond industry since the discovery of the first diamonds in South Africa in the 19th century, with a focus on this part of the continent. This is followed by a brief review of 10 major diamond-producing countries in Africa.

In 'Crater of Diamonds—The Natural State's Gem of a Park', M. Howard traces the history of this unique deposit in Arkansas, USA, from its discovery in 1906 and several failed attempts to operate a mine, to 1972, when it became a state park. The chapter not only contains images of some of the named diamonds from this source, but also a table of the 24 largest diamonds.

Diamonds were discovered in Russia on 4 July 1829 when 14-year-old Pavel Popov found a 0.52 ct stone while panning for gold in the Ural Mountains. In 'Diamonds in Russia', V. K. Garanin and G. Y. Kriulina give a comprehensive historical outline from this discovery to the prospecting efforts that led to the discovery of numerous deposits in Siberia and more recently in the Arkhangelsk region, and the development of the Russian diamond industry.

In 'Argyle Diamonds', J. Chapman describes the geology and future prospects of the Argyle mine and the extraordinary diamonds it produces.

T. C. Wallace Jr. relates the history of 'Colorado Diamonds'. A series of kimberlites, some of them diamondiferous, are known along the Front Range, but only a little mining has taken place, and with little success. The most important enterprise was the Kelsey Lake mine, which was operated in the 1990s and yielded the 28.3 ct yellow Colorado Diamond, the largest found in that state.

'Laboratory-Grown Diamonds' by J. E. Butler and B. N. Feigelson is the most technical chapter in this monograph. The authors give a detailed description of the problems of diamond synthesis and how they were solved through the development of various HPHT and CVD methods. To conclude, they describe the different applications and uses of both techniques and their growing importance, including in the gem industry.

In 'Diamonds in the Sky', E. Bullock shows that diamonds are not only created deep in the earth, but also near its surface by meteorite impacts. And there are also extraterrestrial diamonds that are hosted by meteorites. Conditions favourable for diamond growth may be found on Jupiter, Saturn, Uranus and Neptune. Some researchers believe that certain planets in other solar systems may even be completely composed of diamond.

In the last chapter of this volume, T. Funk discusses some of the most spectacular 'Diamond Heists', mainly in this century, and why diamonds and jewels are so attractive to thieves. A box in this chapter (by J. H. Betts) briefly outlines 'The Kimberley Process for Collectors'.

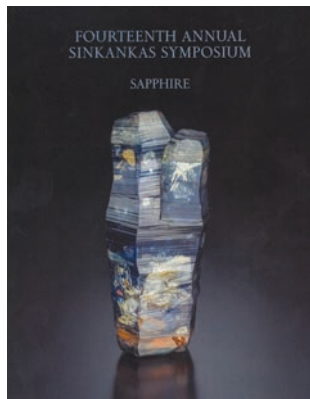
All texts in this volume are well written, concise and offer an abundance of up-to-date information. The monograph contains a number of maps, graphics and tables, and is lavishly illustrated. The only flaw I found is on page 80, where the diamond production of Sierra Leone is given as "roughly 300,000 carats per annum (...) more than either Brazil or Australia". While this is possibly true for Brazil, Australia produced 13,570,000 carats in 2015 (see table on page 20).

Considering the vastness of the field, the choice of topics is necessarily incomplete. There is little, for example, about the history of diamond cutting or about the role of diamonds in jewellery throughout history, and one might also desire a description of additional source countries such as Canada. Nevertheless, one can say that the subjects chosen for this volume provide a good survey of all important aspects.

All in all, reading *Diamond—The Ultimate Gemstone* was pleasant and informative, and if it was to be certified like a real diamond, it would certainly get a very good colour grade and VVS₁ clarity.

Dr Rolf Tatje
Duisburg, Germany

Fourteenth Annual Sinkankas Symposium—Sapphire



Ed. by Stuart Overlin, 2017. Pala International, Fallbrook, California, USA, 136 pages, illus., ISBN 978-0991532025. US\$45.00 softcover.

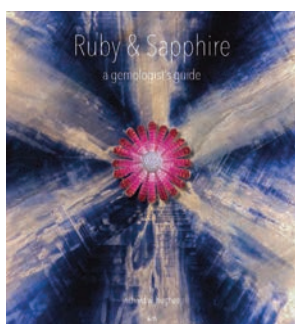
Gemological Society of San Diego (see pp. 551–552 of this issue for a report on this conference). As for other Sinkankas Symposia, each attendee received a copy of an attractive proceedings volume that serves as a record of the conference, as well as a detailed reference on the various topics covered by most of the speakers.

The volume begins with a listing of the symposium programme, speaker biographies and abstracts. These are followed by speaker contributions covering a range of topics pertaining to sapphire: world sources and quality factors (Richard Hughes); microscopic features (Nathan Renfro); geochemistry and oxygen isotope values of syenite-hosted sapphires from the Baw Mar mine in Mogok, Myanmar, compared to those from other localities (Rachelle Turnier and Dr George Harlow); the art and science of faceting and

The Fourteenth Annual Sinkankas Symposium, featuring sapphire, was held in April 2017 at the Gemological Institute of America in Carlsbad and was co-hosted by the

carving sapphire, as well as improving traditional-cut stones and the process of developing the TorusRing cut (Glenn Lehrer); coloration mechanisms, focusing on the chromophores Cr^{3+} , $\text{Fe}^{2+}\text{-Ti}^{4+}$, V^{3+} , Fe^{3+} and trapped hole centres involving various ions (Dr John Emmet and Emily V. Dubinsky, with Richard Hughes); mineralogy and crystallography (Dr William 'Skip' Simmons); archaeogemmology (Lisbet Thoresen); collecting rough and cut stones from worldwide localities (Carl Larson); treatments and their detection (Shane McClure); evolution of laboratory services, culminating in origin determination (Edward Boehm); and a bibliography covering both rubies and sapphires (Richard Hughes).

Ruby & Sapphire—A Gemologist's Guide



By Richard Hughes with Wimon Manorotkul and E. Billie Hughes, 2017. RWH Publishing/Lotus Publishing, Bangkok, Thailand, www.lotusgemology.com, 816 pages, illus., ISBN 978-0964509719. US\$200.00 hardcover.

In the 20 years since Richard Hughes' book *Ruby & Sapphire* was published, many new mines have been discovered and different treatments have appeared, requiring an extensive update. Together with his wife Wimon Manorotkul and daughter E. Billie Hughes, he has managed this task in a grand way, with hundreds of pages that are packed with information. While working on a book chapter of my own about gem treatments and synthetics, I referred to Hughes' book numerous times and never failed to get an answer.

The book starts with some personal information about the author, as well as an exhaustive list of people who helped him during the compilation of this work. This is followed by Chapter 1, a 20-page historical outline, starting with ancient China, moving west to ancient India, and then on to the Arab world and into Europe.

Chapter 2 covers chemical and crystallographic data, including two pages of trace-element contents for corundum from all important origins (compiled by K. Scarratt), as well as a useful table giving the angles between crystal faces of corundum, drawings of known crystal shapes and listings of the major morphologies for different deposits. This is followed by Chapter 3 on physical and optical properties and phenomena, including cleavage/parting/fracture, hardness, thermal properties, melting point, density, electrical and optical properties, lustre, asterism, colour change and trapiche corundum.

The volume is attractively laid out, with many colour images and even a full-page photo to mark the beginning of each article. The various diagrams and spectra have mostly been redrafted into a consistent and easy-to-read format, although headings are missing from some of them and one heading is incorrect (the spectrum on p. 53 refers to the $\text{Fe}^{2+}\text{-Ti}^{4+}$ chromophore, rather than Cr^{3+}).

Every sapphire enthusiast should have this volume in his or her library. Not only does it provide useful reviews of several important aspects of sapphire, but in some cases the information is not available anywhere else in the literature.

Brendan M. Laurs FGA

At nearly 60 pages, Chapter 4 covers colour, spectra and luminescence, and is co-authored by J. L. Emmett, E. V. Dubinsky and K. Scarratt. The authors go into detail about colour causes from trace elements, charge-transfer effects, band gaps, hole defects, impurity effects, and absorption and transmission. This is accompanied by explanatory graphs and spectra. All colours of corundum are covered, not only taking into consideration the colours themselves but also the connection to their geological origin. A sub-section is dedicated to FTIR spectra, which gives information about the presence or absence of contaminants or treatments. Another important aspect which is covered brilliantly in this chapter is luminescence and fluorescence, with many illustrations and explanations of how these properties can be used to determine origin and treatment. The chapter ends with some observations about pleochroism.

Chapter 5 is dedicated to inclusions and photomicrography. In addition to a multitude of beautiful images, the chapter covers the history of inclusion photography, explains how these inclusions formed, and provides an extensive listing of inclusions observed in corundum.

Chapter 6, with co-authors J. L. Emmett and T. R. Douthit, covers corundum treatments, reaching as far back as 2,000 years. Heat treatment is covered in great detail, from traditional heating to modern high-temperature methodology. The chapter gives information on furnaces, the gases used during heating and the resulting effects on corundum coloration (summarized in a table). Flux-healing of fractures, Ti-diffusion and Be-diffusion are described, as well as fissure and cavity filling. Inclusion photos give detailed information about ways to detect such treatments. The chapter ends with the description of irradiation effects on corundum, as well as oiling and dyeing.

Chapter 7 provides a thorough review of synthetic corundum, starting from the first attempts in the mid-1800s, to the Verneuil, Czochralski and floating-zone

processes, as well as hydrothermal and flux-grown synthetic rubies from various producers. The chapter outlines the history of the methods, but also gives tables with properties of the various synthetics available. Images of inclusions help identify such synthetics. The chapter also shows how synthetics can be treated to induce asterism or make them appear more natural. This is followed by a chapter describing assembled stones such as various doublets and triplets, as well as coatings and foiling.

The next two chapters are valuable tools mostly for buyers and appraisers, but they are interesting for gemmologists as well. Chapter 9 gives a short summary of cutting styles and what to look for when buying stones, while Chapter 10 is about judging the quality of corundum, including colour, inclusions and facet geometry, leading us back to the chapter on gem cutting. Hughes summarizes how these factors influence prices, and then goes into other properties that are sometimes even more important than cut and colour. For example, he lists the most sought-after geographic origins for ruby and sapphire, with an explanation why they are so much more valued than others, and includes guidelines for how to judge star, trapiche, colour-change and fancy-colour corundum. Also provided is a summary of market tastes according to various nations all over the world, and a description of colour types. This is followed by an extensive section covering famous rubies and sapphires (including spinel, which was often mistaken for ruby) with historical background information, lists of significant rubies and sapphires with prices obtained for them at auction, and notable rough and carved stones.

Chapter 11 is dedicated to the geological formation of corundum, starting with a short introduction about the formation of the earth and its components before going into specific geological settings. Hughes, together with R. M. Allen, divide these into igneous, metamorphic and sedimentary deposits, followed by case studies of the most important corundum deposits and their mining methods. A useful table of all deposits lists the mode of occurrence as well as the colours found at each location.

The last chapter, on world sources, is most exhaustive (over 270 pages), describing ruby and sapphire from nearly every known deposit according to geological setting, history and gemmological characteristics (providing that Hughes had study samples available). Maps, mining photos, and images of stones and their inclusions are complemented by tables summarizing the properties of corundum from the described areas. Beautiful images of the countryside and its people are also included. This aspect makes it a pleasure just to scan through, and is a welcome addition to all the

information collected and compiled in this chapter. The amount of information for each of the deposits in 52 countries is related to their importance, allowing Burmese rubies and sapphires the most coverage with about 40 pages. Great effort is also spent describing the Kashmir deposit as well as those of Afghanistan, Tajikistan, Madagascar, Kenya, Mozambique, Tanzania, Malawi, Sri Lanka, Australia and Thailand/Cambodia.

The book is completed by two appendices. Appendix A is a reprint of portions of Tagore's *Mani-Málá* (1879, 1881). Appendix B is a pricing chart, compiled together with R. Drucker, along with identification flow charts for ruby and sapphire. The last pages contain a very complete and helpful subject index.

Worth highlighting is the extensive bibliography compiled by Hughes: The 3,500 references go back 2,000 years and span all centuries up to the newest literature from 2015. These references are invaluable for every gemmologist. They are listed at the end of each chapter (for those from 1 to 11), and also at the end of each description of the various localities in Chapter 12. While I usually prefer to have all references in one place, I appreciate the ease of finding relevant literature according to the subject covered by the corresponding chapter.

Of course, in such a fundamental work there is always room for criticism, and I have two. The first one is the sheer volume and weight of the book (nearly 10 lb or 4.5 kg), which makes it hard to handle in everyday work. The second one concerns errors in the Table of Contents. The introduction starts on page 35, not on page 39 as stated in the Contents. This inconsistency continues all the way to Chapter 4 (which indeed starts at page 107). The problem happens again with the geology chapter, which starts on page 403 (rather than page 383 as given in the Contents), and this shifts all subsequent page numbers so that the reader needs to search a little bit unless the Index is used, where page numbers are correct. Fortunately, readers can download a corrected version of the Contents (along with a listing of several errata) at www.lotusgemology.com/files/pdf/RS-Errata.pdf.

In summary, this book is a must for all gemmologists working in laboratories or as appraisers. It also contains helpful information for those dealing in ruby and sapphire. It is the most comprehensive reference on corundum that I have seen, but also a great source of information for anyone interested in gems. Although some may find the many quotes unnecessary, they do brighten the text. The beautiful images are a delight for the eyes. This is a very well-balanced work that offers the reader both beauty and valuable information.

*Dr Lore Kiefert FGA
Gübelin Gem Lab, Lucerne, Switzerland*

OTHER BOOK TITLES

Coloured Stones**Agates—The Pat McMahan Collection**

By Pat McMahan, 2016. Self-published at McMahan Press, Cottonwood, Arizona, USA, 496 pages, ISBN 978-0692651384. US\$129.99 hardcover.

Bursztynowe przemiiany—Amber**Metamorphoses** [exhibition catalogue]

By Anna Sobiecka, 2016. International Amber Association, Gdańsk, Poland, 82 pages, ISBN 978-8391289426 (in English and Polish). zł25.00 softcover.

Diamond**Diamond Deposits: Origin, Exploration & History of Discovery**

Ed. by Minh Chi Ngo, 2017. Scitus Academics, Valley Cottage, New York, USA, 302 pages, ISBN 978-1681175737. US\$169.00 hardcover.

The Great Diamond Heist—The True Story of the Hatton Garden Robbery

By Gordon Bowers, 2016. John Blake Publishing Ltd., London, 288 pages, ISBN 978-1784189785. £7.99 softcover.

Rocks, Ice and Dirty Stones: Diamond Histories

By Marcia Pointon, 2017. Reaktion Books, London, 256 pages, ISBN 978-1780237527. £18.00 softcover.

Gem Localities**Australian Gemstones Series**

By Trudy Toohill, 2016. CreateSpace Independent Publishing Platform, 168 pages, ISBN 978-1541209664. US\$79.99 softcover.

Mines of the American West – San Diego County, California

By Ivan Herring, 2017. Self-published, 364 pages, ISBN 978-1520658520. \$38.99 softcover.

Rockhounding Colorado: A Guide to the State's Best Rockhounding Sites, 3rd edn.

By William A. Kappeler and Gary Warren, 2017. FalconGuides, Guilford, Connecticut, USA, 256 pages, ISBN 978-1493017393. US\$19.95 softcover.

General Reference**Mineral Collections in the American Northeast**

By Joseph Polityka and Wendell E. Wilson, 2016. Mineralogical Record Inc., Tucson, Arizona, USA, 460 pages. US\$35.00 softcover.

Minerals and Gemstones—300 of the Earth's Natural Treasures

By David Cook and Wendy Kirk, 2017. Amber Books

Ltd., London, 320 pages, ISBN 978-1782742593. £9.99 flexibound.

Jewellery History**Arts of the Hellenized East: Precious Metalwork and Gems of the Pre-Islamic Era**

By Martha L. Carter, 2017. Thames and Hudson, New York, New York, USA, 424 pages, ISBN 978-0500970706. US\$29.95 softcover.

Gemstones in the First Millennium AD—Mines, Trade, Workshops and Symbolism

Ed. by Alexandra Hilgner, Susanne Greiff and Dieter Quast, 2017. Römisch-Germanisches Zentralmuseum, Mainz, Germany, RGZM – Conferences, Vol. 30, 332 pages, ISBN 978-3884672716. €44.00 softcover.

Jewellery and Objets d'Art**Fabergé in London: The British Branch of the Imperial Russian Goldsmith**

By Kieran McCarthy, 2017. ACC Publishing Group, Suffolk, 240 pages. ISBN 978-1851498284. £55.00 hardcover.

Flora: The Art of Jewellery

By Patrick Mauriès and Évelyne Possémé, 2017. Thames and Hudson, New York, New York, USA, 128 pages, ISBN 978-0500519424. US\$24.95 hardcover.

Hidden Gems: Jewellery Stories from the Saleroom

By Sarah Hue-Williams and Raymond Sancroft-Baker, 2016. Unicorn Publishing Group, London, 312 pages, ISBN 978-1910065990. £28.00 hardcover.

Italian Jewelry of the 20th Century

By Melissa Gabardi, 2017. Silvana Editoriale, Milan, Italy, 338 pages, ISBN 978-8836635078. €45.00 hardcover.

Jeweled Splendors of the Art Deco Era: The Prince and Princess Sadruddin Aga Khan Collection

By Catherine Aga Khan, Pierre Rainero, Évelyne Possémé, Stephen Harrison, Sarah D. Coffin and Sarah Davis, 2017. Thames and Hudson, New York, New York, USA, 256 pages, ISBN 978-0500519479. US\$75.00 hardcover.

DVDs**AGTA GemFair Tucson Seminar DVD**

2017. American Gem Trade Association, Dallas, Texas, USA. US\$50.00.

Mineral Explorers: Season 2

2017. Crystal Springs Mining & Jewelry Co. Inc., Hot Springs, Arkansas, USA, 3-DVD set, 300 minutes. US\$39.99.

Compiled by Angharad Kolator Baldwin and Brendan Laurs



Gem-A

THE GEMMOLOGICAL ASSOCIATION
OF GREAT BRITAIN



BOOK

NOW!

Gem-A Conference 2017

Saturday 4
and Sunday 5
November

**NEW VENUE
ANNOUNCED:**

etc.venues
County Hall,
Westminster,
London

**THE £50
STUDENT
RATE IS
BACK!**

SOME OF OUR SPEAKERS:

Vladyslav Yavorsky, IVY/Yavorskyy

Klemens Link, Gübelin Gem Lab

Dr Ulrika D'Haenens-Johansson, GIA

Dr John Rakovan, Miami University

Reena Ahluwalia, Creator of Jewelry & Paintings

Booking is now open on Eventbrite:
<https://gemaconference.eventbrite.com>

Literature of Interest

Coloured Stones

Causes of iridescence in natural quartz. X. Lin and P.J. Heaney, *Gems & Gemology*, **53**(1), 2017, 68–81, <http://dx.doi.org/10.5741/GEMS.53.1.68>.*

Ciel pommel  dans une opale mexicaine d stabilis e [Dappled sky in a destabilized Mexican opal]. J.-P. Gauthier and E.J. Fereire, *Revue de Gemmologie A.F.G.*, No. 198, 2016, 12 (in French).

Coloration of natural zircon. U. Kempe, M. Trinkler, A. P ppl and C. Himcinschi, *Canadian Mineralogist*, **54**(3), 2016, 635–660, <http://dx.doi.org/10.3749/canmin.1500093>.

Cuprian liddicoatite tourmaline. Y. Katsurada and Z. Sun, *Gems & Gemology*, **53**(1), 2017, 34–41, <http://dx.doi.org/10.5741/GemS.53.1.34>.*

Emerald eyes [imitation, synthetic and treated emeralds]. *Gemmology Today*, May 2017, 34–41, www.worldgemfoundation.com/GTMay2017DV.*

Gemmological characteristics of the “Eilat” stone. H. Zhu, T. Li and X. Zhao, *Superhard Material Engineering*, **28**(4), 2016, 60–62 (in Chinese with English abstract).

Gemmological characteristics & significance of “ink & wash” and “black rooster” fei cui. M.C.M. Ouyang, H. Yen and K. Cheung, *Journal of the Gemmological Association of Hong Kong*, **37**, 2016, 78–81, www.gahk.org/journal/2016/a13.pdf (in Chinese with English abstract).*

Gemmological features & colouration of red jasper from Qinghai Province, China. Z. Lu, X. Yu, X. He, S. Wang and Y. Lin, *Journal of the Gemmological Association of Hong Kong*, **37**, 2016, 67–71, www.gahk.org/journal/2016/a11b.pdf (in Chinese with English abstract).*

Gemmological and mineralogical characteristic of jade from Kunlun, Xinjiang, China. K. Yin, Y. Pan, J. Yu, T. Li and W. Han, *Journal of Gems & Gemology*, **18**(5), 2016, 15–19 (in Chinese with English abstract).

Gr ne undurchsichtige Quarze mit besonderer Ber cksichtigung bestrahlter Achate und aventurisiertem Quarzit aus Brasilien [Green opaque quartz with special attention to irradiated agates and aventurescent quartzite from Brazil]. U. Henn, R. Schultz-G ttler and T. Stephan, *Gemmologie: Zeitschrift der Deutschen Gemmologischen Gesellschaft*, **65**(1–2), 2016, 9–22 (in German with English abstract).

The influence of the Fe₂O₃ content on the Raman spectra of sapphires. D.T.M. Phan, T. H ger and W. Hofmeister, *Journal of Raman Spectroscopy*, **48**(3), 2016, 453–457, <http://dx.doi.org/10.1002/jrs.5043>.

Mineralogical characteristics and cause of color of a red fire opal. J. Li, K. Yin, W. Han and H. Hong, *Journal of Computational and Theoretical Nanoscience*, **13**(3), 2016, 2082–2086, <http://dx.doi.org/10.1166/jctn.2016.5159>.

Name, Kristallstruktur, Kristallchemie, Kristallmorphologie und physikalische Eigenschaften von Turmalinen. [Name, crystal structure, crystal chemistry, crystal morphology and physical properties of tourmalines]. U. Henn and F. Schmitz, *Gemmologie: Zeitschrift der Deutschen Gemmologischen Gesellschaft*, **65**(3–4), 2016, 3–18 (in German with English abstract).

New data on “kerolite-pimelite” series and the colouring agent of Szklary chrysoprase, Poland. Z.  erm kov , D. Hradil, P. Bezdi ka and J. Hradilov , *Physics and Chemistry of Minerals*, **44**(3), 2016, 193–202, <http://dx.doi.org/10.1007/s00269-016-0848-z>.

Origin of petrified wood color. G. Mustoe and M. Acosta, *Geosciences*, **6**(2), 2016, 1–24, <http://dx.doi.org/10.3390/geosciences6020025>.*

Origin of sapphires from a lamprophyre dike at Yogo Gulch, Montana, USA: Clues from their melt inclusions. A.C. Palke, N.D. Renfro and R.B. Berg, *Lithos*, **260**, 2016, 339–344, <http://dx.doi.org/10.1016/j.lithos.2016.06.004>.

Para ba-Tourmaline [Para ba tourmaline]. C.C. Milisenda, S. M ller, S. Koch, J. Guo and C. Stoffel, *Gemmologie: Zeitschrift der Deutschen Gemmologischen Gesellschaft*, **65**(3–4), 2016, 41–56 (in German with English abstract).

Raman, FT-IR and XRD investigation of natural opals. A. Sodo, A.C. Municchia, S. Barucca, F. Belatreccia, G.D. Ventura, F. Butini and M.A. Ricci, *Journal of Raman Spectroscopy*, **47**(12), 2016, 1444–1451, <http://dx.doi.org/10.1002/jrs.4972>.

The research on color grading of green jade images based on HSL chromaticity analysis. L. Zhang and X. Yuan, *MATEC Web of Conferences*, **82**, 2016, article 03002, 6 pp., <http://dx.doi.org/10.1051/mateconf/20168203002>.*

The role of silicon in the color of gem corundum. J.L. Emmett, J. Stone-Sundberg, Y. Guan and Z. Sun, *Gems & Gemology*, **53**(1), 2017, 42–47, <http://dx.doi.org/10.5741/GEMS.53.1.42>.*

Spektrentypen und Farben von Turmalinen [Spectra types and colours of tourmalines]. Th. Lind and T. Stephan, *Gemmologie: Zeitschrift der Deutschen Gemmologischen Gesellschaft*, **65**(3–4), 2016, 19–40 (in German with English abstract).

* Article freely available online, as of press time

That old black magic - jet. S. Steele, *Gemmology Today*, May 2017, 62–66, www.worldgemfoundation.com/GTMay2017DV.*

Cultural Heritage

The ring monstrance from the Loreto treasury in Prague: Handheld Raman spectrometer for identification of gemstones. J. Jehlička, A. Culka, M. Baštová, P. Bašta and J. Kuntoš, *Philosophical Transactions of the Royal Society A*, **374**(2082), 2016, article 20160042, <http://dx.doi.org/10.1098/rsta.2016.0042>.

The sights of Spain [study of Cruz de los Ángeles (Angel's Cross)]. C. Garcia-Carballido, *Gems&Jewellery*, **26**(1), 2017, 32–35.

Diamonds

Appraising and insuring chipped diamonds. V. Rundhaug, *GemGuide*, **36**(3), 2017, 17–18.

Brazilian diamonds: A historical and recent perspective. D. Svisero, J.E. Shigley and R. Weldon, *Gems & Gemology*, **53**(1), 2–33, <http://dx.doi.org/10.5741/GEMS.53.1.2>.*

Carbon and nitrogen isotope systematics in diamond: Different sensitivities to isotopic fractionation or a decoupled origin? K. Hogberg, T. Stachel and R.A. Stern, *Lithos*, **265**, 2016, 16–30, <http://dx.doi.org/10.1016/j.lithos.2016.06.020>.

Coesite inclusions in diamonds of Yakutia. L.D. Bardukhinov, Z.V. Spetsius and R.V. Monkhorov, *Doklady Earth Sciences*, **470**(2), 2016, 1059–1062, <http://dx.doi.org/10.1134/S1028334X16100093>.

Crystallographic orientations of olivine inclusions in diamonds. S. Milani, F. Nestola, R.J. Angel, P. Nimis and J.W. Harris, *Lithos*, **265**, 2016, 312–316, <http://dx.doi.org/10.1016/j.lithos.2016.06.010>.

Diamond growth from C–H–N–O recycled fluids in the lithosphere: Evidence from CH₄ micro-inclusions and δ¹³C–δ¹⁵N–N content in Marange mixed-habit diamonds. K.V. Smit, S.B. Shirey, R.A. Stern, A. Steele and W. Wang, *Lithos*, **265**, 2016, 68–81, <http://dx.doi.org/10.1016/j.lithos.2016.03.015>.

Early Permian diamond-bearing proximal eskers in the Lichtenburg/Ventersdorp area of the North West Province, South Africa. M.C.J. de Wit, *South African Journal of Geology*, **119**(4), 2016, 585–606, <http://dx.doi.org/10.2113/gssajg.119.4.585>.

First evidence of hydrous silicic fluid films around solid inclusions in gem-quality diamonds. P. Nimis, M. Alvaro, F. Nestola, R.J. Angel, K. Marquardt, G. Rustioni, J.W. Harris and F. Marone, *Lithos*, **260**, 2016, 384–389, <http://dx.doi.org/10.1016/j.lithos.2016.05.019>.

The first finding of graphite inclusion in diamond from mantle rocks: The result of the study of eclogite xenolith from Udachnaya pipe (Siberian craton). D.S. Mikhailenko, A.V. Korsakov,

A.V. Golovin, P.S. Zelenovskiy and N.P. Pohilenko, *Doklady Earth Sciences*, **469**(2), 2016, 870–873, <http://dx.doi.org/10.1134/S1028334X16080250>.

FTIR thermochronometry of natural diamonds: A closer look. S.C. Kohn, L. Speich, C.B. Smith and G.P. Bulanova, *Lithos*, **265**, 2016, 148–158, <http://dx.doi.org/10.1016/j.lithos.2016.09.021>.

Fundamentals of the mantle carbonatite concept of diamond genesis. Y.A. Litvin, A.V. Spivak and A.V. Kuzyura, *Geochemistry International*, **54**(10), 2016, 839–857, <http://dx.doi.org/10.1134/S0016702916100086>.

The last mile toward a universal diamond grading standard? Y. Almor, *World Diamond Magazine*, December 2016, 47–49.

Micro- and nano-inclusions in a superdeep diamond from São Luiz, Brazil. H. Kagi, D.A. Zedgenizov, H. Ohfuji and H. Ishibashi, *Geochemistry International*, **54**(10), 2016, 834–838, <http://dx.doi.org/10.1134/S0016702916100062>.

Mineralogical characterization of diamonds from Roosevelt Indigenous Reserve, Brazil, using non-destructive methods. M.P.A.C. Borges, M.A. Moura, S.L.R. Lenharo, C.B. Smith and D.P. Araujo, *Lithos*, **265**, 2016, 182–198, <http://dx.doi.org/10.1016/j.lithos.2016.08.003>.

Nitrogen nano-inclusions in milky diamonds from Juína area, Mato Grosso State, Brazil. J. Rudloff-Grund, F.E. Brenker, K. Marquardt, D. Howella, A. Schreiber, S.Y. O'Reilly, W.L. Griffin and F.V. Kaminsky, *Lithos*, **265**, 2016, 54–67, <http://dx.doi.org/10.1016/j.lithos.2016.09.022>.

Selling fancy coloured diamonds. D. Siskin, *World Diamond Magazine*, December 2016, 63–64.

Shaping an industry - The genesis of diamond cutting. J. Asplund, *Gemmology Today*, May 2017, 5–9, www.worldgemfoundation.com/GTMay2017DV.*

Source assemblage types for cratonic diamonds from X-ray synchrotron diffraction. F. Nestola, M. Alvaro, M.N. Casati, H. Wilhelm, A.K. Kleppe, A.P. Jephcoat, M.C. Domeneghetti and J.W. Harris, *Lithos*, **265**, 2016, 334–338, <http://dx.doi.org/10.1016/j.lithos.2016.07.037>.

A spectrum of diamonds [Aurora Pyramid of Hope collection]. A. Bronstein, *Gems&Jewellery*, **26**(1), 2017, 18–20.

Synchrotron Mössbauer source technique for *in situ* measurement of iron-bearing inclusions in natural diamonds. F. Nestola, V. Cerantola, S. Milani, C. Anzolini, C. McCammon, D. Novella, I. Kuppenko, A. Chumakov, R. Ruffer and J.W. Harris, *Lithos*, **265**, 2016, 328–333, <http://dx.doi.org/10.1016/j.lithos.2016.06.016>.

Tracing the depositional history of Kalimantan diamonds by zircon provenance and diamond morphology studies. N. Kueter, J. Soesilo, Y. Fe-

dortchouk, F. Nestola, L. Belluco, J. Troch, M. Wälle, M. Guillong, A. Von Quadt and T. Driesner, *Lithos*, **265**, 2016, 159–176, <http://dx.doi.org/10.1016/j.lithos.2016.05.003>.

Unusual paired pattern of radiohaloes on a diamond crystal from Guaniamo (Venezuela).

D.J. Schulze and L. Nasdala, *Lithos*, **265**, 2016, 177–181, <http://dx.doi.org/10.1016/j.lithos.2016.09.024>.

Various growth environments of cloudy diamonds from the Malobotubia kimberlite field (Siberian craton).

S. Skuzovatov, D. Zedgenizov, D. Howell and W.L. Griffin, *Lithos*, **265**, 2016, 96–107, <http://dx.doi.org/10.1016/j.lithos.2016.04.013>.

Gem Localities

Age of the emerald mineralization from the Itabira-Nova Era District, Minas Gerais, Brazil, based on LA-ICP-MS geochronology of co-genetic titanite.

H. Jordt-Evangelista, C. Lana, C.E.R. Delgado and D.J. Viana, *Brazilian Journal of Geology*, **46**(3), 2016, 427–437, <http://dx.doi.org/10.1590/2317-4889201620150074>.*

Can gemstones bring prosperity to Malawi?

D. Craig, *Gems&Jewellery*, **26**(1), 2017, 10–12.

Characteristics of the gem and jade mineral resources in Guangxi and the discussion of its industrial development.

R. Zhang, W. Yang, H. Zhang and H. Zhang, *Superhard Material Engineering*, **28**(4), 2016, 56–59 (in Chinese with English abstract).

Japanese jadeite: History, characteristics, and comparison with other sources.

A. Abduriyim, K. Saruwatari and Y. Katsura, *Gems & Gemology*, **53**(1), 2017, 48–67, <http://dx.doi.org/10.5741/GEMS.53.1.48>.*

Major zircon megacryst suites of the Indo-Pacific lithospheric margin (ZIP) and their petrogenetic and regional implications.

L. Sutherland, I. Graham, G. Yaxley, R. Armstrong, G. Giuliani, P. Hoskin, V. Nechaev and J. Woodhead, *Mineralogy and Petrology*, **110**(2–3), 2016, 399–420, <http://dx.doi.org/10.1007/s00710-015-0421-3>.

Mineralogical signs of rare-metal and semi-precious ore mineralization in the Murzinskaya-Aduyskaya beryllium (gemstone) subprovince.

M.P. Popov, *News of the Ural State Mining University*, **3**(43), 2016, 59–63, <http://dx.doi.org/10.21440/2307-2091-2016-3-54-63>.*

Tanzanite processing in Tanzania: Challenges and opportunities.

W.E.N. Mbowe, N. Yabu and M. Lugobi, *Applied Economics and Finance*, **3**(3), 2016, 236–257, <http://dx.doi.org/10.11114/aef.v3i3.1640>.*

Visit to Mogok, Myanmar. Chan Wai Ching Joanne, Lee Tak Yan Ann and Lee Fung Mei Miranda, *Journal of the Gemmological Association of Hong Kong*, **37**, 2016, 16–21, www.gahk.org/journal/2016/a6.pdf (in Chinese with English abstract).*

Instrumentation

Development of a new multi-spectral induced luminescence imaging system (GV5000) and its application in screening melee-sized near-colorless synthetic diamonds and natural diamonds.

Lan Y., Lu T., Zhang C., Liang R., Ding T., Chen H., Ke J. and Bi L., *Rock and Mineral Analysis*, **35**(5), 2016, 505–512, <http://dx.doi.org/10.15898/j.cnki.11-2131/td.2016.05.009> (in Chinese with English abstract).

Gem and mineral identification using GL Gem Raman and comparison with other portable instruments.

A. Culka, J. Hyršl and J. Jehlička, *Applied Physics A*, **122**(11), 2016, article 959, <http://dx.doi.org/10.1007/s00339-016-0500-2>.

Miscellaneous

Bargaining powers of buyers and sellers on the online diamond market: A double perspective non-parametric analysis.

F.-C. Wolff, *Annals of Operations Research*, **244**(2), 2016, 697–718, <http://dx.doi.org/10.1007/s10479-016-2160-1>.

Grand opening of the David Friend Mineral Hall & Yale Peabody Museum of Natural History's 150th anniversary celebration.

G.C. Spann, *Rocks & Minerals*, **92**(3), 2017, 238–243, <http://dx.doi.org/10.1080/00357529.2017.1283659>.

“Treasures of the Earth”, the new exhibit at the Paris National Museum of Natural History.

C. Ferraris, C. Noyes and J.-M. Fourcault, *Mineral Observer*, **22**(1), 2017, 42–56.

News Press

Battling for blood jade: Inside one of the world's most dangerous industries.

H. Beech, *Time*, 9 March 2017, <http://time.com/4696417/myanmar-blood-jade-hpakant>.*

Big diamonds are big business.

R. Taylor, *Financial Times*, 22 March 2017, www.ft.com/content/ea9d6340-e795-11e6-967b-c88452263daf.*

England's pearls are going EXTINCT: Fresh-water mussels and the gems they produce are dying out due to pollution.

P. Weston, *Daily Mail*, 10 April 2017, www.dailymail.co.uk/sciencetech/article-4397084/Freshwater-pearl-mussels-England-stopped-reproducing.html.*

For world's super-rich, a pink diamond is forever.

S. Hemrajani, *Reuters*, 10 May 2017, www.reuters.com/article/us-global-diamond-idUSKBN18613X.*

Gemfields tests nanotechnology at Kagem mine to trace Zambian emeralds.

Mining Review Africa, 28 March 2017, www.miningreview.com/news/gemfields-tests-nanotechnology-kagem-mine-trace-zambian-emeralds.*

Into the green land: Emerald mining in Colombia. J. Corso, Aljazeera, 20 March 2017, www.aljazeera.com/indepth/inpictures/2017/03/green-land-emerald-mining-colombia-170306110821882.html.*

Pearls

Chemical composition analysis of *Pinctada martensii* pearls from Japan by synchrotron radiation micro X-ray fluorescence. J. Zhang, S. Huang, B. Tang, J. Dong, D. Chen and X. Wu, *Acta Petrologica et Mineralogica*, **35**(4), 2016, 729–734 (in Chinese with English abstract).

Fukui unveils South Sea pearls with Metakaku [RFID] nuclei. *Jewellery News Asia*, No. 392, 2017, 66–67.

Mono- and polychromatic inner shell phenotype diversity in *Pinctada margaritifera* donor pearl oysters and its relation with cultured pearl colour. C.-L. Ky, C. Lo and S. Planes, *Aquaculture*, **468**(Part 1), 2017, 199–205, <http://dx.doi.org/10.1016/j.aquaculture.2016.10.017>.

Synthetics

Behavior of crystal defects in synthetic type-IIa single-crystalline diamond at high temperatures under normal pressure. N. Tatsumia, K. Tamasakub, T. Itoc and H. Sumiya, *Journal of Crystal Growth*, **458**, 2017, 27–30, <https://doi.org/10.1016/j.jcrysgro.2016.10.033>.

Characteristics of gem-quality by-product synthetic zincite. J. Zhang, Y. Gao and G. Shi, *Gems & Gemology*, **53**(1), 2017, 82–89, <http://dx.doi.org/10.5741/GEMS.53.1.82>.*

Diamond crystallization and growth in N–H enriched environment under HPHT conditions. X. Liu, X. Jia, C. Fang and H.-A. Ma, *CrystEngComm*, **18**(43), 2016, 8506–8515, <http://dx.doi.org/10.1039/C6CE02034H>.

HPHT type 2b synthetic diamond with trigons. M. Chauhan, *Gemmology Today*, May 2017, 10–13, www.worldgemfoundation.com/GTMay2017DV.*

Synthesis of diamonds with mineral, fluid and melt inclusions. Y.V. Bataleva, Y.N. Palyanov, Y.M. Borzdov, I.N. Kupriyanov and A.G. Sokol, *Lithos*, **265**, 2016, 292–303, <http://dx.doi.org/10.1016/j.lithos.2016.07.005>.

Treatments

Analysis and modification of natural red spinel by ion beam techniques for jewelry applications. D. Bootkul, T. Tengchaisri, U. Tippawan and S. Intarasiri, *Surface and Coatings Technology*, **306**(Part A), 2016, 211–217, <http://dx.doi.org/10.1016/j.surfcoat.2016.05.084>.

Cleaning, washing and waxing in the processing of fei cui. Lai Yat Lung Francis, *Journal of the Gemmological Association of Hong Kong*, **37**, 2016, 64–65, www.gahk.org/journal/2016/a11.pdf (in Chinese with English abstract).*

Natural vs enhanced: Navigating lapidary materials. H. Serras-Herman, *Gems&Jewellery*, **26**(1), 2017, 14–17.

Spectroscopic investigation and colour change of natural topaz exposed to PbO and CrO₃ vapour. P.P. Rout, R.K. Sahoo, S.K. Singh and B.K. Mishra, *Vibrational Spectroscopy*, **88**, 2017, 1–8, <http://dx.doi.org/10.1016/j.vibspec.2016.10.005>.

Compilations

G&G Micro-World. Optical dishes in ametrine • Astrophyllite in bastnäsite • Flashes and flames in Ethiopian opal • Cat's-eye imitation pen pearls • Negative crystals in sapphire • Mystery inclusion in topaz. *Gems & Gemology*, **53**(1), 2017, 102–108, <http://tinyurl.com/kesj77w>.*

Gem News International. Tucson 2017 • New Ethiopian emeralds • Myanmar gems • Gemfields activities • New Mozambique ruby mine • Canaan emerald mine in Brazil • Secondary market for colored stones • Cultured pearl update • Moroccan amethyst • Emerald dealing in Afghanistan • Notable Montana sapphires • Magnesio-axinite from Tanzania • Sustainable vertical integration in sapphires • Freeform tanzanite and sunstone • Gem paintings • Paula Crevoshay designs • Nigerian tourmaline and sapphire • Turquoise Starship Enterprise • Rutilated quartz mining community • Jewelry Industry Summit • Pyrope-spessartine from Sri Lanka • Plastic imitation of amber • Mixed-type treated red HPHT synthetic diamond • Filled calcite with strong phosphorescence. *Gems & Gemology*, **53**(1), 2017, 112–142, <http://tinyurl.com/m8kwe4r>.*

Lab Notes. Faceted wagnerite, thaumasite and strontianite • Orangy red cordierite • Cape diamond with yellow phosphorescence • Sapphire filled with bismuth-based glass • H4 defect in CVD synthetic diamond • HPHT synthetic melee • Intense green HPHT synthetic diamond • Ti-diffused synthetic sapphire • Coated Paraíba tourmaline • Rubellite with strong 'pink sleeves'. *Gems & Gemology*, **53**(1), 2017, 90–101, <http://tinyurl.com/ku7xxjj>.*

Conference Proceedings

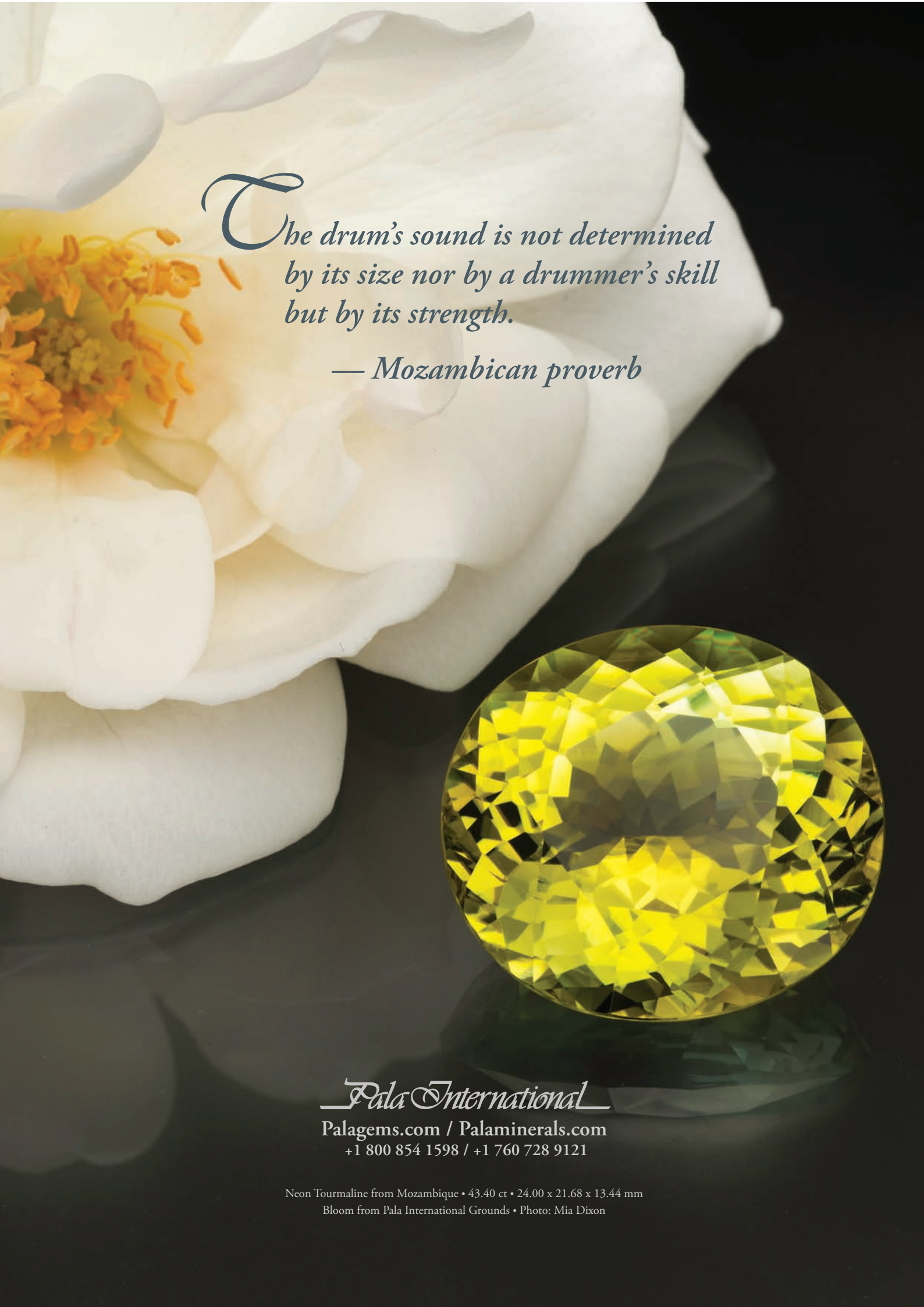
The Amber Roads—Ancient Cultural and Commercial Communication Between the Peoples. Ed. by P.L. Cellarosi, R. Chellini, F. Martini, A.C. Montanaro, L. Sarti and R.M. Capozzi, 2016. Proceedings of the 1st International Conference on Ancient Roads, San Marino, Italy, 3–4 April 2014, 452 pages, <http://tinyurl.com/khw543e> (in English and Italian).*



A Story in Every Gemstone

Passion, Protection, Prosperity
Responsibly sourced Mozambican rubies by Gemfields
www.gemfields.co.uk

GEMFIELDS

A large, close-up photograph of a white flower with a vibrant yellow center, set against a dark background. In the lower right foreground, a large, faceted yellow gemstone, likely a tourmaline, is prominently displayed, reflecting light and casting a shadow on the surface below it.

*The drum's sound is not determined
by its size nor by a drummer's skill
but by its strength.*

— Mozambican proverb

Pala International
Palagems.com / Palaminerals.com
+1 800 854 1598 / +1 760 728 9121

Neon Tourmaline from Mozambique • 43.40 ct • 24.00 x 21.68 x 13.44 mm
Bloom from Pala International Grounds • Photo: Mia Dixon